INVESTIGATING THE PRODUCTS FROM DIFFERENT MODES OF PARTICLE BREAKAGE TESTING

M. VAN ECK
SEPTEMBER 2007

SUBMITTED TO THE UNIVERSITY OF CAPE TOWN IN FULFILMENT FOR THE DEGREE OF MASTER OF SCIENCE IN ENGINEERING

STATEMENT OF ORIGINALITY

I, Melanie van Eck, submit this thesis in fulfilment of the requirements for the degree of Master of Science in Engineering. I know the meaning of plagiarism and claim that this is my original work, except as acknowledged in the text and to the best of my knowledge has not been submitted in similar form for a degree at any University.

ACKNOWLEDGEMENTS

- The support of MINTEK for all equipment and funding is acknowledged with gratitude.
- Special thanks to my supervisors, Dr Aubrey N Mainza and Prof. Malcolm S Powell for their assistance and technical discussions.
- To Adrian and Johnny, my dear colleagues in the Minerals Processing Division at MINTEK, thank you.

ABSTRACT

The development of realistic comminution models is dependent on the accuracy with which ore breakage can be predicted. This hinges on our understanding of the basic concepts of breakage and the different modes in which it manifests in the comminution environment. Three distinctly different modes of breakage were identified and investigated as the elementary processes that govern comminution.

Impact breakage was investigated as the first mode of breakage. Drop weight tests were performed to determine the influence of different energy intensities on the product particle size distribution. The drop weight tests were carried out on UG2 platinum and Target gold ore. The particles were broken over a range of six size classes ranging from 13 to 106mm. It was observed that the product size distribution becomes finer with increasing energies and that the sub 400μm fraction may contain valuable information for some ore types.

The second mode that was investigated was abrasion. Abrasion experiments were performed in a 1.68x0.597m pilot mill and a 0.57x0.485m torque mill. This was done in order to see how the breakage changes when the size and aspect ratio of the mill changes. It was observed that fewer impact breakage events occur in a mill with a smaller diameter. For angular rocks it was observed that after the initial chipping phase, abrasion takes over as the primary mode of breakage and the rate of mass lost out of the mill becomes lower. With angular rocks the rate of discharge of fines increases rapidly when the test is started. Then it slows down and becomes constant. The rate of fines production is fast when the corners and edges of the rocks are chipped off. When the rocks in the mill take on a more rounded shape, the production of fines slows down and abrasion becomes the primary mode of breakage.

Bed breakage in a laboratory scale High Pressure Grinding Roll (HPGR) was investigated. UG2 ore was used to conduct a comparative study on the Autogenous mill and the HPGR. A Mineral Liberation Analyser (MLA) was used to determine the liberation of the product samples. The AG mill gave better liberation of the sub 38μm size class than the HPGR. The MLA results showed that for the sub 38μm AG

mill sample a bigger volume percent and more particles per hundred were properly liberated in comparison with the sub 38µm HPGR sample. However the deportment (and recoverability) of the valuable minerals within the sub 38µm fractions of both samples is unknown.

The effects of various operating conditions were investigated on the HPGR with another platinum ore, a Merensky reef sample. It was found that the energy consumption of the HPGR increases with specific press force, but the reduction ratio does not increase beyond a certain specific press force. This threshold was found to be $4N/mm^2$ for the Merensky ore. When the specific press force is increased, the energy consumption increases accordingly. But once a certain threshold is reached, the reduction ratio no longer increases with increasing specific press force. Therefore optimum operating conditions must be found in order to avoid energy inefficiencies.

The liberation of an HPGR sample broken under High Pressure and Low Pressure was also determined by MLA. It was observed from the MLA data that the HPGR operated at a higher pressure gave better liberation in the sub 38µm size class than that operated at a lower pressure. The deportment (and recoverability) of the valuable minerals in the sub 38µm fractions of both samples is unknown. However the HPGR operated at a lower pressure gave better liberation in the -75+38µm size class compared to that operated at a higher pressure. The lower pressure gave better liberation in the -75+38µm fraction and therefore operating at the lowest pressure that will still produce the required grind is beneficial.

The different modes of breakage were compared and it was found that with bed breakage from the HPGR there will not be a build up of a critical size that is difficult to break. Critical size build up is commonly associated with run of mine mills (AG/SAG) and negatively impacts throughput. The product particle size distributions of UG2 ore and Target Gold ore were compared for the various modes of breakage. It was found that UG2 ore is much more fragile and that it produces a distinct bimodal product size distribution, whereas Target Gold ore produces a normal Rosin-Rammler distribution.

TABLE OF CONTENTS

LIST OF TABLES

LIST OF FIGURES

1. INTRODUCTION

The complexity of the comminution process has been fascinating and frustrating modellers of AG/SAG mills and other comminution equipment for several decades. Much progress has been made and better equipment and models are constantly being developed. The high incentive that is placed on energy efficiency encourages this. However, the comminution process is still governed by a large number of factors that influence the liberation of the valuable components in the ore. A better understanding of these basic factors will provide more certainty about the design of equipment in order to achieve the best liberation and energy efficiency.

Much of the modelling and simulation of comminution processes is largely dependant on the researcher's understanding of ore breakage. Information about ore breakage properties obtained from well structured experiments performed using sound experimental techniques is therefore essential.

1.1 THE FRACTURE THEORY

The breakage of ore, like that of any other material, depends on how it responds to the applied load. When the applied load is lower than the yield stress of the rock, it undergoes elastic deformation proportional to the load. In this region, no permanent deformation will take place. This means that repeated impacts at that load will have no effect on the particle.

If the applied load to the particle is increased further it enters the ductile zone. The particle would still posses the ability to resist the load, but micro fractures like crack initiation and propagation will take place. Therefore cumulative damage results, but the effect of repeated impacts would not be seen until the threshold is reached, where it will take just one last impact to cause fracture (Tavares and King, 1998). When more strain energy is applied, the brittle zone is reached and sudden failure of the material is encountered. This is when the available energy is sufficient to cause unstable crack propagation and only one impact is required to fracture the rock. The

energy intensity (or strain rate) at which a particle will be broken must be carefully selected because it has an influence on the progeny particle size distribution (Tavares and King, 1998).

The strength of a particle also depends on its orientation and it may take several impacts before a favourable orientation (comparative to pre-existing flaws or weaknesses) is found (Tavares and King, 2002). Tavares and King also observed that the other factors that influence a particle's response to repeated impacting are the strength of the particles, the intensity of the impacts and the amenability of the particle's microstructure to withstand the applied stresses.

All naturally occurring rocks contain zones of weakness like cracks and flaws. In these zones, the inter-atomic distances are greater and irregular and therefore make it weaker than a perfect lattice structure. These cracks and flaws may have been caused by explosives, shear and fault zones, bedding planes, grain and crystal boundaries and atomic lattice discontinuities. When these are concentrated at any particular size range it is called a natural grain size (Bond, 1962).

The distribution of cracks varies from particle to particle and this makes it difficult to determine the energy needed to break a rock sample. The geometry of the particle also has an influence on the probability of breakage. Rounded particles have a greater probability of fracture because they tend to absorb more of the impact energy in comparison to angular specimens. A similar observation was made from cumulative impact tests performed by Bbosa *et al.* (2006) using the Split Hopkinson Pressure Bar (SHPB). A detailed discussion of micro-fracture mechanisms (crack initiation and propagation) and macro measures of response (ultimate strength and the means to describe its response to loading) is presented by Napier-Munn *et al.*, (1999). A discussion of the basics of the fracture theory and a procedure of determining the fracture probability was described by Bwalya *et al.*, (2001).

In 1980, Kiss and Schonert made their own two phase composite material from quartz particles and cement. After allowing this material to undergo single particle compression and impact crushing, they found that the method of breakage had no effect on the liberation at all (Kiss and Schonert, 1980). Only the degree of breakage

was found to influence the degree of liberation. This may not be true for a real ore as it is in contradiction with some recent statements in literature about the significant advantages that packed bed breakage has on liberation (Knecht and Patzelt, 2004). Packed bed breakage may also offer improved energy efficiency in downstream process units (Tavares, 2005). These are key issues that will be investigated in this study.

1.2 RESEARCH FOCUS AND OBJECTIVES

1.2.1 RESEARCH FOCUS

The focus of this project is on two traditionally separate fields: Comminution and Process Mineralogy. The primary focus will be on comminution, but liberation studies will be performed on some of the samples from the comminution test work.

Comminution: In section 2.1 the main methods of breakage are highlighted and the industrial applications of these methods are also discussed. The three distinctly different basic modes of breakage that are identified are impact, abrasion, and bed breakage. Some of the valuable contributions to the knowledge in this field are discussed.

Liberation studies: The various techniques with which the liberation of a valuable component can be determined are given in section 2.2 and the developments in this field are discussed.

In the literature it is sometimes seen that the comminution-liberation relationship is not yet fully understood due to difficulties such as the estimation of the liberation distribution of ore textures. This has been studied by numerous researchers reviewed by Gay, (1999). All the studies performed to relate liberation to comminution appear to be equipment specific, and not derived from breakage tests (King and Schneider, 1998, Hsih *et al.,* 1995, Gay, 2004). Most of the research done to date seems to be focussed on either of the two fields. The aim of this project is to develop a

methodology that would link these two fields and make an attempt to incorporate liberation into particle breakage testing.

The aim is therefore to improve our understanding of the influence that breakage and the intensity of breakage has on the particle size distribution and the liberation of the valuable minerals.

1.2.2 HYPOTHYSES

1. **There is a relationship between the energy intensity of the breakage event and the size distribution of the product.**

   Breaking rocks at different energy intensities results in different progeny particles and these differences can be quantified. Increasing the energy intensity at which the breakage event takes place may produce a finer product. However this trend may stop once it reaches a certain threshold.

2. **There is a relationship between the mode of breakage and the size distribution of the product.**

   The method that was used to break the ore may determine the particle size distribution of the final product. Impact, Abrasion and Bed breakage are three distinctly different modes of breakage that my produce different products. A suitable mode of breakage may therefore be selected in order to achieve certain product size distributions.

3. **In the operation of the HPGR there is an optimum specific press force where there will be no advantage in operating at higher specific press forces.**

   When the HPGR is operated over a wide range of specific press forces the reduction ratios will indicate conditions that consume the least energy but still provide the required grind. Comparable product size distributions may be obtained at different operating conditions. Therefore, the operating conditions

that consume the least energy can be determined and used in order to save energy without compromising significantly on the grind.

4. **The state of liberation for the samples broken by different modes of breakage and intensities of breakage is different.**

Certain rock breakage devices may promote breakage around grain boundaries of base metal sulphides and therefore increase the amount of liberated particles. Numerous rock breakage techniques are available today and the influence that the mode or manner of breakage has on liberation has not been fully quantified.

1.2.3 OBJECTIVES

The following objectives form the work plan to test the hypotheses formulated for this thesis:

- To investigate the relationship between the amounts of energy applied per mass of ore and the size distribution of the product. This will be done by the application of different energies to similar rock samples and the investigation of the product size distributions.
- To investigate the relationship between the modes of breakage that are used in the breakage events and the size distribution of the products. This will be done by applying different modes of breakage to similar rock samples. Impact, abrasion and bed breakage will be investigated. The impact breakage tests will be conducted with a drop weight tester, the abrasion experiments will be conducted in mills and the bed breakage tests will be done with a HPGR.
- The HPGR will be operated with various operating conditions and the energy consumptions will be recorded and evaluated together with the reduction ratios of the products to determine an optimum specific press force. When the HPGR is operated over a wide range of specific press forces, the reduction ratios may indicate conditions that consume the least energy but still provide the required grind.

- Analyse samples from specific size fractions using a Mineral Liberation Analyser (a process mineralogy tool) in order to determine whether the liberation status of the products from the various modes or intensities of breakage differs.

2. LITERATURE SURVEY

In this chapter the most popular ore breakage methods and the progress made by researchers over the years are discussed. The techniques available for mineralogical analysis as well as the development of research in quantifying liberation in minerals processing are discussed.

2.1. COMMINUTION

Comminution is the essential step in minerals processing where the run of mine ore is broken in order to expose the valuable particles for recovering using different down stream processes. In this section ore breakage characterisation and the most widely used comminution machines will be discussed.

There are three distinctly different modes of breakage that are described in this section. With each of these modes, some of the equipment that is most commonly used in industry to achieve that mode of breakage is described. But before attention can be given to various modes of breakage or equipment, the basics of a breakage event are discussed.

In 1962, Bond identified three principles of energy required for comminution:

- The specific energy input equals the energy index of the product minus the energy index of the feed.
- The energy input is directly proportional to the new crack length produced and is therefore inversely proportional to the square root of the product size minus the square root of the feed size. The work index is the proportionality constant.
- The work input, exposure of fines and variations of the work index at different product sizes are governed by the flaw structures of the material.

The Bond Work Index is calculated from the formula:

$$WI_{test} = \frac{(1.10)(44.5)}{\left\{(p_1^{0.23})(G_{bp})^{0.82} \times \left[\frac{10}{\sqrt{x_Q}} - \frac{10}{\sqrt{x_G}}\right]\right\}}$$

Where p_1 = the opening of the classifying screen

G_{bp} = net grams of undersize produced per mill revolution

x_Q = 80% passing size of the product (μm)

x_G = 80% passing size of the feed (μm)

His tests showed that the specific grinding energy E in kWh/t was empirically related to the make-up feed and circuit product sizes by

$$E = WI\left(\frac{10}{\sqrt{x_Q}} - \frac{10}{\sqrt{x_G}}\right)$$

He also developed equations in order to scale these results up to other mill dimensions:

$$WI = (WI_{test})\left(\frac{2.44}{D}\right)^{0.2} \qquad D \le 3.81m$$

$$WI = (WI_{test})(0.914) \qquad D \ge 3.81m$$

Where D = the diameter of the mill

In 1963 he presented equations for calculating product sizes from surface area approximations as well as equations for calculating the power requirements and the capacity of grinding equipment (Bond, 1963). These equations are useful, but limited in terms of SAG mill operations. The Bond Crushability test is still being used, but it is not particularly accurate for predicting crushability in intermediate crushers and fine crushers. It also shows large variation in individual rock breakage and does not provide any estimation of crusher product size. It also requires the operator to make subjective judgments about the breakage of rocks (Mular and Jergensen, 1982).

Breakage is caused when the ore is stressed above the breaking strength limit (E_{crit}), which leads to cracking of the ore particles (Napier-Munn *et al.*, 1999). When ore particles are crushed by direct hits from a ball or a bigger rock in AG or SAG mills, impact breakage occurs. Abrasion is caused by the sliding and rolling action between particles in the moving charge. Abrasion also takes place where individual grains are removed from the surface of a rock by frictional forces. A low inter-particle pressure will result in a fine abrasion product and the frictional forces are proportional to the pressure (Loveday, 2004). According to Digre (1969) abrasion is usually the main reduction mechanism.

Preferential breakage often occurs when crack branching occurs more frequently in one mineral than in the others. This causes the preferentially broken mineral to occur more abundantly in the finer sizes after each fracture event than the other minerals (King and Schneider, 1998). It is an example of non-random breakage and it often occurs in the form of breakage around grain boundaries. This results in particles of a particular size fraction (or more) in a particle size distribution to be more abundant than would be expected. This may probably result in preferential liberation. One of the common causes of preferential breakage is confined particle bed breakage (King and Schneider, 1998).

Another form of non-random breakage is interfacial breakage. If there is a loss of particle interfacial surface area between feed and product, interfacial breakage or grain boundary fracture has taken place (Frandrich *et al.*, 1997).

In 1988 Pauw experimented with different energy intensities in the breakage of single ore particles of different sizes. He showed that the application of excessive amounts of energy to particles close to the required product size leads to over-breakage. This is when particles are broken to a size finer than the required product size. He also showed that over-breakage is a potential source of over-grinding in tumbling mills. Another reason for inefficient energy usage is when insufficient energy (lower than the fracture energy) is applied in an impact event (this is referred to as the elastic zone). The applied energy is converted to heat or sound energy, but a fracture event does not occur. The ratio of stress to strain in the elastic zone in its simplest form gives Young's modulus (Napier-Munn *et al.*, 1999). When more stress and strain

energy is applied, the ductile zone is entered. The material will lose the ability to resist the applied load and will deform. After the ductile zone, the brittle zone is entered and sudden failure of the material occurs (Napier-Munn *et al.*, 1999). This sudden failure is never exactly simultaneous over the whole new surfaces. It starts at the weakest place in the strained matrix. This failure concentrates the surrounding stress and strain at the newly formed crack tip and this is rapidly propagated across the rock (Bond, 1962). The physical properties of the particle and the grinding media will affect the value of the optimum input energy. In mills, the density of the slurry as well as the slurry hold up, mill speed and lifter configuration can determine the extent to which breakage takes place (Loveday and Naidoo, 1997).

2.1.1. IMPACT

Impact breakage in AG/SAG mills is caused by steel balls or bigger particles that break smaller particles against the mill liner or charge, or when a dropping particle breaks itself against the liner or the charge. Often rocks don't break with a single impact but repeated softer blows may cause cumulative damage up to a point where one final hit causes breakage. Multiple hit breakages will result in fewer, larger fragments of progeny rocks in comparison with the finer particle size distribution associated with single impact breakage (Digre 1969). Specific breakage energy is dependant on the size of the rocks, which means that smaller rocks are more likely to break than the bigger rocks when the same energy is applied to each rock. The probability that a rock will break from a single impact decreases with increasing rock size. In AG mills, this can cause a depletion of pebbles in certain size classes and the critical sized rocks will remain unbroken. Chipping also occurs as a kind of impact breakage. It can be described as the mass lost from the mother particle when particles collide with other particles or the mill liner.

Reliable particle breakage data is important in the development of breakage functions that are needed for a population balance model to reasonably predict the performance of industrial comminution machines. Single particle impact breakage is one of the key areas in ore breakage characterisation. There are a large number of different

impact breakage devices and the most commonly used devices are discussed hereafter.

2.1.1.1. Twin pendulum

The twin pendulum device employs an input pendulum that is released from a known height that breaks the rock specimen against a rebound pendulum as demonstrated in Figure 2.1 (Napier-Munn *et al.* 1999).

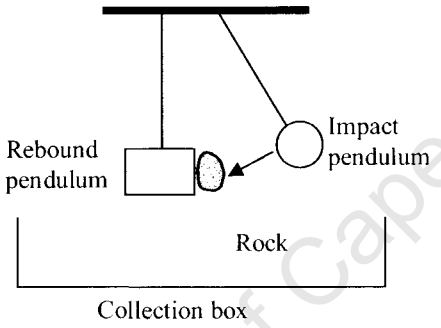

Figure 2.1: A schematic of the twin pendulum rock breakage device (Napier-Munn *et al.* 1999)

The rebound pendulum swings between a laser source and a detector. The motion of the rebound pendulum is monitored with a computer which records the time it takes to pass through the laser beam. The twin pendulum comes in two sizes to break different particle sizes. The smaller unit is used to relate the energy consumption in single particle breakage to industrial rod and ball mills and the bigger unit is used to relate the energy consumption in single particle breakage to industrial crushers and AG/SAG mills (Napier-Munn *et al.* 1999). In spite of this, the Twin pendulum is still limited in the particle sizes that it can take and the energy inputs that it can achieve and the operation is time consuming. In addition to this, the energy calculation is not always accurate and it can be observed from the secondary movement that occurs when the rebound pendulum follows the collision. This lack of restraint in the motion of the rebound pendulum after the collision and the high energy inputs that are

typically used in the pendulum experiments result in the low energy transfer efficiencies of this device (Tavares, 1999). Therefore, in recent years the JK drop weight apparatus largely replaced the pendulum at the JKMRC (Briggs and Bearman, 1996).

2.1.1.2. Drop weight tester

In the drop weight test, a particle is placed on a steel anvil and is broken by a steel drop weight of a specific mass, falling from a specific height. By changing the release height and the mass of the drop weight, a wide range of input energies can be achieved (Napier-Munn *et al.,* 1999). The weights are mounted on two guide rails (see Figure 2.2) in an attempt to get a uniform impact across the weight. The device is built on a strong steel frame and enclosed in Perspex to avoid the loss of product sample as a result of the impact. It has some advantages such as extended energy inputs, large particle size ranges, short time span of operations and greater precision than the twin pendulum. The remaining gap (the space between the anvil and the drop weight) is used to calculate the amount of energy that was not transferred into the rock. Still, the greatest limitation of the drop weight test is that it does not allow the direct measurement of the fraction of the input energy that is used in particle breakage (Tavares, 1999). It is assumed that all the potential energy that is applied goes into the rock when some of the energy may still be transferred to the concrete surface, but not in a way that can be easily observed. The drop weight tester produces quantitative information about the relationship between input energy and size distributions of the broken specimens, when screened after the impact (Banini, 2000). The drop weight tester has been widely used for determining the so called A and B parameters that are used in the design of industrial AG/SAG mills.

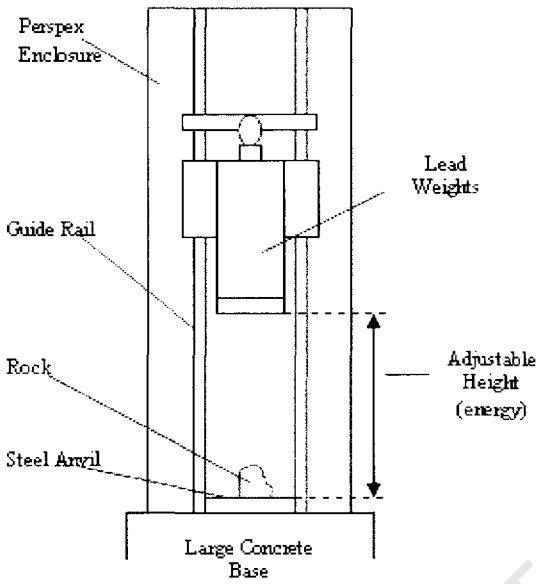

Figure 2.2: A schematic of the JKMRC drop weight rock breakage device (Napier-Munn *et al.* 1999)

The drop weight test is the most commonly used method of investigating breakage characteristics of materials and also the simplest in design. It is can be operated over an extended input energy range (Tavares, 1999).

Dukino *et al.* (1997) investigated the strength of Australian iron ores in different tumble and drop tests. They found that the tumbling process causes surface breakage and the drop tower causes volume breakage. The extent of breakage that occurs when a particle is dropped (in a mill or drop weight tester) depends on the degree of stabilisation (see Figure 2.3), the drop height and the rock density, volume, elastic modulus and geometry (Dukino *et al.*, 1997).

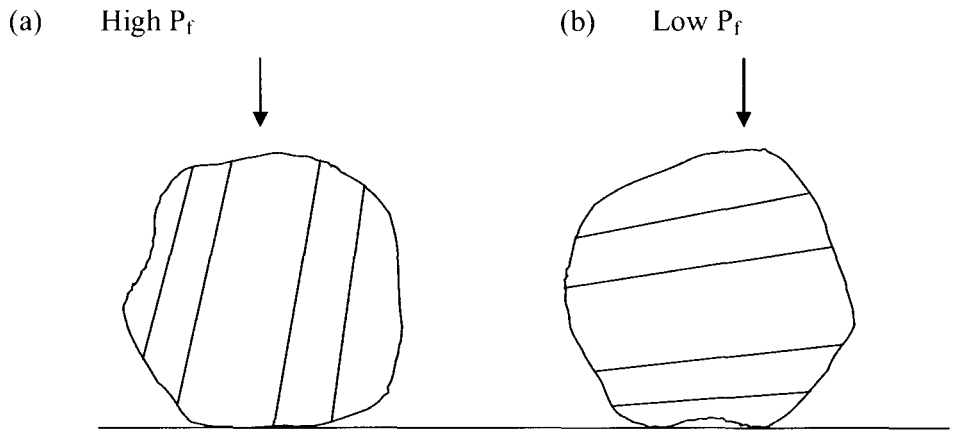

Figure 2.3: Effect of different loading configurations on probability of fracture Pf (Dukino *et al.*, 1997)

The loading geometry, (the profile of the rock that contacts the plate) affects the probability of fracture. In Figure 2.3, two different loading configurations can be seen (a) will have a higher probability of fracture (Pf) than (b). The loading configuration illustrated in (a) will promote breakage along the natural mineral planes and that in configuration (b) will tend to cause compression. Higher energy inputs will therefore be required to break a rock specimen in configuration (b). The problem arising from this is that the natural mineral planes may not always be visible with the naked eye and produce inconsistent results.

2.1.1.3. Impact load cell

The impact load cell was invented by Weichert (Bourgeois & Banini, 2002). It is, in principle, just another type of drop-weight testing machine, but also incorporates principles of the Hopkinson bar (see section 2.1.1.4). Detailed energy aspects of single-particle breakage can be obtained with impact load cells. These devices can also be used to measure particle compression, compressive force and energy absorbed by the particle (Bourgeois & Banini, 2002). The use of impact load cells are limited to specialised laboratories as a result of their physical dimensions and the sensitivity of its electronic measuring devices (Bourgeois & Banini, 2002).

It was also only after the development of the Ultra Fast Load Cell (UFLC) that it became possible to measure particle fracture energy directly (Tavares & King, 1998). This apparatus employs a long steel rod equipped with strain gauges. The rock specimen(s) are placed on this rod and impacted by a falling steel ball. The impact causes a compressive wave that progresses down the rod and is recorded by the strain gauges. A digital oscilloscope is used to record the voltage change in a Wheatstone bridge (bridge circuit) as a function of time, which facilitates the calculation of force-time data (Tavares & King, 1998). These accurate measurements permit calculation of other fundamental properties of the specimen including the energy absorbed by the particle prior to initial fracture and the relationship between this energy and the breakage function.

The UFLC is an accurate, fast and inexpensive device that can be used to study the breakage of particles subject to impact fracture (Tavares and King, 1998). However, the accuracy of these measurements depends on the precision of measurement of the material properties of the sphere and the rod, because it is calibrated according to these (King and Bourgeois, 1993). The mass specific fracture energy distributions of the material tested represents log-normal distributions and consistent variance with size. A correspondence between the probability of fracture and fracture energy was observed (King and Bourgeois, 1993). The schematic representation of the UFLC can be seen in Figure 2.4.

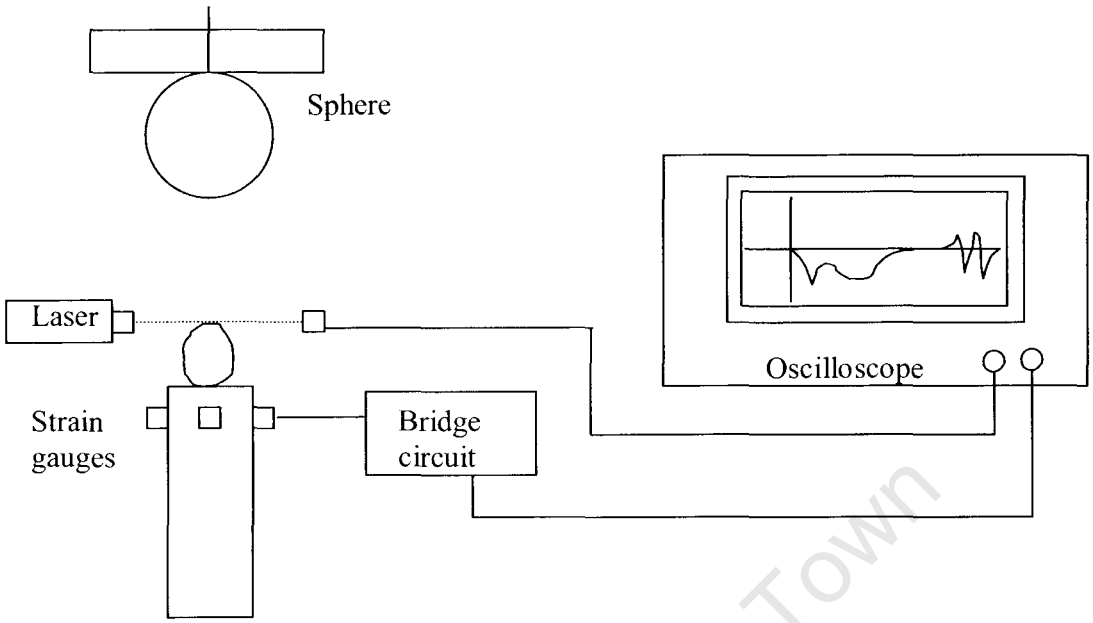

Figure 2.4: Schematic outline of the ultra-fast load cell (King and Bourgeois, 1993)

The UFLC measures two important parameters: the specific particle fracture energy, and the particle stiffness. The specific particle fracture energy refers to the minimum amount of energy that is needed to fracture a particle, while the particle stiffness is the rate at which strain energy is stored in the specimen before fracture. It can be used to classify materials on their resistance to comminution (Tavares & King, 1998). From these experiments it was found that fracture characteristics are independent of the rate of strain at rates expected to be found in industrial comminution equipment.

2.1.1.4. Split Hopkinson Pressure bar

Breakage of single particles depends on the rate sensitivity of the different materials (Yang, & Shim, 2005). The Split Hopkinson Pressure Bar (SHPB) is a device that can be used to accurately determine rate dependent tensile or compressive properties of different materials. The SHPB has been used extensively to study the dynamic behaviour of plastics, metals, rubber and concrete (Yang, & Shim, 2005).

The force and the energy that is required to cause complete fracture of materials can be measured with this apparatus. It consists of two horizontally suspended steel bars and the specimen being tested is wedged between the ends of these two bars as seen in Figure 2.5.

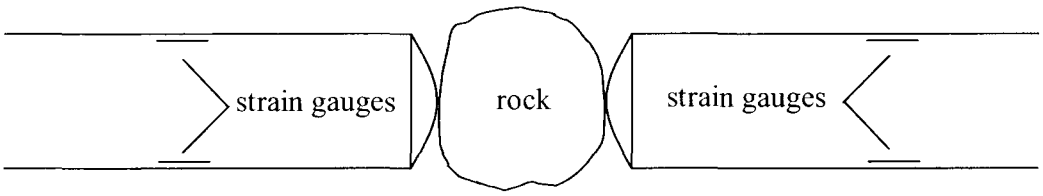

Figure 2.5: Experimental setup of the Split Hopkinson Pressure Bar

A striker bar is fired with a blast of nitrogen gas to hit the incident bar. The input energy is calculated from the initial velocity of the striker that is determined with an optical sensor. A rectangular compression wave of well-defined amplitude and length is generated in the incident bar when the striker bar strikes it. When the wave reaches the particle, some of it transmits through the particle, some of it reflects back through the incident bar, and some is absorbed. High stress-strain curves are then obtained from measurements of strain with the strain gauges on the incident and output bars. Therefore, lost strain energy can be subtracted from the input energy and the energy that is actually responsible for breakage can be calculated (Bbosa *et al.*, 2006). The SHPB allows accurate energy calculation because it only assumes the heat and sound energy that was generated is negligible. However it can only take particles of up to 40mm and the operation is time consuming.

Briggs and Bearman (1996) examined the effects of different forms of crushing and the differences in the competencies of the materials as observed through the various stages of crushing. They made use of a Modified Hopkinson Pressure Bar (MHPB) to measure the damage present in the rocks. The MHPB is similar to the SHPB but the impact bar is propelled with a spring. They used the MHPB to enable the resolution of the force experienced by a rock as it is dynamically loaded in compression. They found that impact crushers produce material that contains less variation in strength than the feed because every particle was exposed to the breakage mechanism. It was

found that cone crushers did not break material as consistently as impact crushers. They also compared the performance of the MHPB to gyratory crushers and Barmac Rotopactor, but in this study these will all be grouped together under impact breakage.

2.1.2. ABRASION

Attrition is the term used for the comminution carried out by the action of the grinding media on the interstitial fine material. This reduction mechanism dominates in ball mill grinding. Therefore attrition takes place in any tumbling mill where fine material is present together with grinding media. The size of the grinding media and the fines, the amount of fines and the consistency of the pulp will have an influence on this mode of breakage. For successful attrition grinding to take place, the particle must be caught between adjacent balls or pebbles and the forces must be strong enough to break the particle. In autogenous grinding, abrasion is usually the dominant reduction mechanism (Digre, 1969).

Abrasion occurs when rocks are rubbed against each other and gradually wear down. Strictly speaking, pure abrasion is the breakage mechanism that takes place when the number of rocks in the charge of a batch grinding experiment is exactly the same before and after, but the total mass is smaller. When angular rocks from a coarse crushing plant are placed in a mill, the prominent points and edges are rapidly chipped off. The mass of the charge decreases as a result of the fines that are scraped off the surface of the rocks and discharges from the mill as slurry (Loveday and Naidoo, 1997). A reliable way to measure abrasion is to continuously remove the pulp that forms by the injection of water (Loveday, 2004). This approach enables AG/SAG modellers to estimate the amount of breakage that takes place in the AG/SAG environment that may be attributed to abrasion. Wear rate for fresh particles decrease with grinding time and will start showing similar behaviour to rounded particles after losing about 4% of their mass (Goldman and Barbery, 1988). As this rounding process proceeds, the size of the chips decreases until only pure abrasion occurs off the surface of the rounded pebbles. Therefore, the pebbles that arrive from bigger size classes into a specific size class are very different from fresh feed pebbles in that particular size class.

Loveday (2004) found that circuit variations using recycle crushing or changes in feed sizing will significantly change the average breakage rate parameters. For a perfectly rounded pebble, the total amount of material removed in the first chipping phase will be about 10-20% of the original weight of the particle (Digre, 1969). Rounding abrasion occurs at a slower but steadier rate than the original chipping phase. It happens when the static and dynamic forces acting on the grains in contact exceed the strength of the matrix or the bond between grains. Goldman and Barbery (1988) found that the breakage rate decreases with an increase in the level of fines in the load, showing a cushioning effect.

The rate of abrasion of rocks is influenced by the mill diameter, charge level, pulp level and the presence of balls (Loveday and Whiten, 2002). Wear rate is also influenced by load volume. The wear rate increases with load volume between 11% and 22%, but it was found that further increases in load volume from 33% to 50% resulted in slower wear rates (Goldman and Barbery, 1988).

As the sizes of rocks in AG/SAG mills decreases, a "critical size" is sometimes encountered (Napier-Munn, *et al.*, 1999). This is the size of rocks that the mill finds hard to break. Abrasion is a surface phenomenon and the breakage rate will reduce as the particle surface area reduces. At this critical size, the specific rate of breakage of rocks usually decreases to a minimum and this is usually in the 20-25mm size fraction (Napier-Munn, *et al.*, 1999). However, a critical size of 20-25 mm is too small for industrial mills and this size only applies to pilot scale mills. The probability of smaller particles to be broken or chipped by bigger ones increases. This may cause a steep increase in the rate up to the maximum (Napier-Munn, *et al.*, 1999). However the model that Loveday and Whiten (2002) developed indicated that the rocks in the critical size do not appear to be rate limiting. In fact it was found that these rocks wear away faster than larger rocks. The accumulation of pebbles in the critical size range was simply attributed to the number of rocks progressing from the larger size classes.

It is important to understand the factors that influence abrasion and wear, because it is a rate determining step (Loveday and Whiten, 2002). It is also the main contributor to the high power consumption of industrial mills. The specific rate of breakage of an

ore in mills can be determined by laboratory or pilot scale abrasion mills (Loveday and Whiten, 2002). Usually a single size fraction of an ore is used in a batch grinding experiment. The speed should be kept similar to the industrial mill that is being modelled. The breakage rate and breakage function of the process can then be determined.

2.1.2.1. Ore characterisation using the abrasion mill

Loveday and Naidoo (1997) conducted several tests in a 600mm diameter autogenous mill with a length of 500mm. They examined the factors that are most likely to influence the rate of abrasion such as rock mass, pulp hold-up, size distribution of rocks, mill speed, and lifter configuration. Experiments were conducted on pebbles that were already rounded in a mill. The fines were flushed out by a stream of water injected into the mill to minimise the effect of secondary milling. It was found that abrasion rate per unit mass increased significantly with rock mass. This is important to keep in mind while conducting abrasion test work because it must be attempted to keep the charge of the mill constant. A direct correlation of rock hardness to abrasion rate was also found (Loveday and Naidoo, 1997). They concluded that the size distribution of material produced by abrasion of rounded pebbles is independent of operating conditions. It was also found that the specific rate of abrasion could be correlated with the power intensity of the mill.

2.1.3. BED BREAKAGE

Devices that are used for bed breakage operate on the principle of generating high pressures to cause inter-particle breakage in a compressed bed of particles. The energy distribution in a packed bed is unequal. A coarse particle will be protected if it is surrounded by finer particles, but a smaller particle will easily be broken between coarser ones (Liu and Schönert, 1996). High pressure bed breakage may offer energy savings as well as other advantages for downstream process units, such as better liberation of the valuable minerals (Hosten and Özbay, 1998). One of the main advantages of particle bed comminution is the principle of transferring the energy

directly to the charge mass (Fuerstenau *et al.,* 1996). Therefore, breakage occurs as a result of these high stresses that are caused locally between the closely packed particles. The possibility of losing energy in the transfer process is also limited in this way. The better energy efficiency may also be attributed to the design where the particles are forced to pass between the rolls in comparison with SAG mills where there is a high stochastic hit-or-miss probability (Fuerstenau *et al.,* 1990). The compacting of the particles in the bed depends on factors such as ore hardness, feed size, wear characteristics of the ore and the moisture content (Tavares, 2005, Knecht and Patzelt, 2004, Fuerstenau and Abouzeid, 2007).

2.1.3.1. High pressure grinding rolls (HPGR)

This machine operates on the principle of generating high inter-particle stresses when a bed of solids is compressed as it moves down the gap between two pressurised rolls (Tavares, 2005). It is mainly used as a pre-grinding strategy to improve reduction ratios in milling circuits and produces considerably more fines than conventional crushers (Tavares, 2005). The High Pressure Grinding Rolls (HPGR) therefore already produces a fraction of the circuit product, but at the same time weakens the particles that remain unbroken or only partly broken. Particle bed breakage that occurs in the HPGR has the potential to enhance liberation of minerals because composite particles tend to break along grain boundaries (Hosten and Özbay, 1998). After the material is crushed between the two contra-rotating rolls, it will have been compressed to a density greater than 70% by volume (Napier-Munn *et al.* 1999). The variation of the size distribution within the discharge cake is insignificant. Therefore the breakage that takes place between the rolls is independent of lateral position (Tavares, 2005).

Lower energy consumption is probably the main advantage of HPGR technology. Van Drunick and Smit (2006) conducted pilot scale HPGR tests on several different ore types and all of their results confirmed the energy efficiency that was expected. Potential overall net energy savings of between 18-25% were recorded on a highly mineralized Gamsberg ore in comparison with a standard ball milling circuit (van Drunick and Smit, 2006). The best flotation results were obtained in association with

low grinding pressures for all the ore types that were tested. Bond Work index tests were also conducted on the HPGR product. These tests showed a decrease of 7% for hard ores and 3% for softer ores (van Drunick and Smit, 2006). Shi *et al.,* (2006) obtained similar results on lab scale with ore samples from Anglo Platinum. They reported energy savings between 8-29%. HPGR application in cement industries increased the capacity and reduced the energy consumption of five different HPGR circuits configurations that were investigated by Aydogan et al., 2006. A model for HPGR was developed at the JKMRC that makes use of the breakage function derived from impact and compressed bed tests (Benzer *et al.*, 2001).

The lengths of the rolls differ but longer rolls are often preferred because they limit the influence of the end effects. The end effects occur at the ends of the grinding rolls and are the result of lower pressure toward the ends of the rolls. This was also found by Schonert (1996) when he conducted particle breakage experiments with several different particle bed configurations (single layer, shallow bed and deep bed). The pressure near the walls of the pistons was much lower than in the centre, even in a shallow bed (Schonert, 1996). The end effects can also be eliminated by the correct recycling structure.

Tavares (2005) conducted ore crushing experiments on an HPGR and found that it does in fact produce a weakened product when the single-particle breakage characteristics of those particles were measured. The extent of weakening was found to be dependent on specific energy input and greater for coarser particles. A 2.5m diameter industrial scale unit was used to do test work on a copper/molybdenite ore with granitic host rock. He found that the extent of weakening was dependent on specific energy input and that it was greater for coarser particles, which subsequently resulted in decreasing energy savings with finer size reduction of the product. A comparison was made between the product size distributions from the HPGR, hammer mill and roll crusher. The HPGR produced a significantly greater proportion of fines than the other two ore breakage equipment investigated at that time. However, in that study no comparison was made between the product from an AG mill and an HPGR.

Chromite ore samples were ground in a rod mill and piston-die press by Hosten and Özbay (1998). The degree of chromite liberation and particle shape were analysed and the bed breakage sample from the piston-die press was found to be better liberated. It was also found that the particles from the rod mill had no shape differences as a function of particle size, but the bed breakage sample had particle profiles with less circularity at the finer end of the investigated size spectrum. The piston-die press produced more fines than the rod mill (Hosten and Özbay 1998).

HPGRs are already in operation in diamond and iron ore applications. Test work on gold and copper ores showed considerable operational and process benefits (Knecht and Patzelt, 2004).

Benefits of using HPGR technology that are recorded in literature include reduced energy consumption, lower wear costs, higher throughput and weakening of unbroken particles (Tavares, 2005). Test work on gold and copper ores showed an improved liberation (Knecht and Patzelt, 2004). This may be due to the micro cracks that are formed and the breakage that occurs around the grain boundaries instead of through the grain itself.

Some operational advantages of HPGRs are:

- Pressure is the main parameter that is used to control the operation of an HPGR. Therefore it is easier to find the optimum operating conditions.
- The residence time of the material between the gap is very small. This implies that after a crash stop the product can be restored to specification much quicker.
- The amount of off spec material that is produced during start-up and stopping is much less than other wet grinding plants.

Knecht and Patzelt (2004) undertook a study to investigate the benefits that HPGR applications may have for the platinum industry. They suspected that the liberation of the Platinum Group Element (PGE) particles would improve due to the preferred ore breakage along grain boundaries. They concluded that it would be more economical for platinum plants to make use of HPGR technology, but the lack of industrial

applications causes the platinum plants to revert to conventional proven technologies such as crushers and tumbling mills. However, the results from their test work indicated that the wear rates of the rolls from platinum samples are among the lowest of all the rock materials that were tested. Fuerstenau *et al.* (1990) made a comparative study of the energy consumption of single particles in ball mills as well as a rigidly mounted roll mill. They found that the size distributions of comminuted single particles from a roll mill tend to be finer than ball mill products on an equal energy consumption basis. Process efficiency, as measured by the rate of change of the reduction ratio with energy input, was found to be significantly higher in rigidly mounted rolls than in ball milling.

Fuerstenau *et al.* (1996) comminuted different minerals and ores in a piston-die press under conditions that simulate the environment that would be encountered in a packed bed. They investigated the influence of bed pressure, material hardness and feed size on energy absorption, energy utilisation and product size distributions. Investigations like these have also been carried out by other researchers since Schönert and co-workers like Hawkins and Manlapig (2006). This may be a valuable approach if a quick answer is needed when investigating the feasibility of a high pressure grinding roll plant, especially when only drill core or limited amounts of sample are available for tests.

2.2. LIBERATION AND MINERALOGY

Most ores that are industrially processed are heterogenous. This means that they are complex in composition and the valuable components are usually found in association with particular mineral components inside a matrix of other material that is usually the gangue. Platinum Group Minerals (PGMs) usually occur in association with base metal sulphides, often on the boundary between the sulphide and silicate. This association explains the high recoveries obtained by base metal sulphide flotation (Cabri, 1981). The purpose of comminution processes are to break these composite particles that consist of several mineral species into smaller pieces that are simpler in composition where individual particles are composites with mineral if interest predominant. This process, where the variety of minerals present in particles changes due to comminution, is called 'liberation'. Liberation also often refers to the degree

of exposure of a valuable mineral and corresponds to the potential of a particle to successfully undergo recovery through processes such as hydrometallurgical leaching and flotation.

The extent of mineral characterisation that can be performed depends on the availability of time, money, and mineralogical equipment. A brief overview of some instruments that are frequently used in applied mineralogy follows.

2.2.1. MINERAL CHARACTERISATION DEVICES

2.2.1.1. Optical microscope

Optical microscopes are used to examine slices of ore either as thin sections, polished-thin sections or ore mounts. This can be done under either transmitted or reflected light or both. Minerals can be identified, their textures, associations and particle shapes and sizes can be observed, and mineral proportions can be determined by point counting.

The optical microscope is most commonly used in the earlier stages of a mineralogical study in order to identify areas for more detailed study with other instruments (Petruk, 2000).

2.2.1.2. X-ray diffractometer

All minerals have unique X-ray diffraction (XRD) patterns. This is the result of their different crystal structures and the way in which the crystal lattice diffracts in X-rays. X-ray patterns can be used to identify minerals and, with the aid of Rietveld refinement, can be used to quantify mineral proportions. The sample is presented to the diffractometer as a finely ground powder.

2.2.1.3. SEM based mineral identification systems: Qemscan and MLA

The scanning electron microscope (SEM) became a useful piece of equipment after the development of the energy dispersive X-ray analyser (EDX) that measures the composition of spots. The Qemscan or Mineral Liberation Analyser (MLA) software then performs a mineral match by comparison to a reference library. The SEM with the EDX is used to analyse polished thick or polished thin sections or even unmounted samples. It is used to identify minerals, but also to show the sizes and relationships of mineral grains. Distributions of elements in minerals can also be obtained from X-ray images generated by the SEM.

The SEM operates on the principle of producing an electron beam under high vacuum. The irradiated material in the sample produces backscattered electrons, secondary electrons, and X-rays. The SEM is equipped with detectors to detect these signals (Petruk, 2000).

Qemscan technology is based on a SEM with EDX and image analysis facilities and it gives quantitative information about the particles in the field of view. The particles are mapped point by point. The Qemscan can work in point, line or area mode. It records the number and lengths of intercepts of all mineral species, as well as the number and type of transitions between phases, including background. The data that is generated can then be used to calculate modal abundances, particle and mineral surface areas, mineral associations, mineral grain size, particle size and particle liberation (Sutherland and Gottlieb, 1991).

This instrument also uses backscattered electrons to obtain textural info of ore particles. Mineral particles are mixed with graphite particles to prevent them from touching and to ensure a random dispersion. These particles are then hardened, sectioned and polished to a mirror finish. The slide is examined in a SEM. These serve as frames for the analysis of individual grains. An electron gun is used to scan the particles and then obtain X-ray counts. These X-ray counts are compared to the X-ray counts of a reference mineral file stored on a computer. This technique is

relatively slow and particles smaller than 5µm cannot easily be identified (Petruk, 2000).

The liberation data generated by the Qemscan is generally presented in the untransformed state. Therefore the results are generally made on area measurements for minimum bias. Modal, grain size and association data can then be collected from line scan measurements (Sutherland and Gottlieb, 1991).

The MLA makes use of the most advanced electron microscopes to provide consistent grey-levels in a back-scattered electron image for the different minerals in a sample (Naidoo, 2003). The different grey levels that are obtained are a result of the difference in their average atomic number. Cracks and other surface imperfections are taken into account and the X-rays generated from the electron beam impact are used to verify the identity of the minerals. A low noise, high-resolution image is a requirement for mineral identification and quantification. These high-resolution images allow the MLA to accurately discriminate the mineral phases within a particle (Fandrich et al. 2006)

The MLA produces the following results: mineral species present, mineral abundance in volume and weight percentages, elemental assay, particle or phase size and surface area, mineral associations, mineral liberation and false-colour images (Naidoo, 2003).

2.2.2. DEVELOPMENT OF LIBERATION RESEARCH

Most ores that contain valuable minerals occur naturally in heterogeneous form. The valuable mineral grains are encapsulated in the gangue matrix. It is therefore necessary to liberate and separate these valuable species from the gangue minerals. This is where comminution plays an important role. The degree of size reduction must be enough to liberate or expose the valuable minerals, but is a trade off with cost. Liberating gangue may introduce other problems (Meloy and Goth, 1985).

Over-grinding occurs when a particle that is already smaller than the required product size is re-broken (Pauw, O.G. 1988). This causes significant increases in energy

consumption and also results in excessive fines, which causes problems in downstream operations like flotation or filtering. A common remedy for this is to increase the re-circulating load of the milling circuit and the resulting reduction in residence time reduces the effect.

After the comminution stage, the product undergoes a variety of separation processes (froth flotation, heavy media separation etc) where the valuable particles are concentrated. The product particle size distribution as well as the degree of liberation that is achieved influences the efficiencies of the separation processes. It is therefore important to investigate size reduction while bearing the liberation in mind.

Several attempts have already been made to better understand, describe, or model liberation by Andrews and Mika (1975), Austin *et al.,* (1993), Hsih *et al.,* (1995), Fandrich *et al.,* (1997), Wei and Gay (1999), Gay (2004) and many more. Andrews and Mika (1975) investigated the quantitative description of liberation in conjunction with size reduction in a batch mill. The model could be applied to heterogeneous minerals which contain two mineral constituents. But the models have limited value because it is too complex and it is seldom that an industrially valuable ore only contains two different minerals.

Herbst *et al.*, (1988) developed a kinetic model for liberation by grinding. They extended population balance size reduction models in order to accommodate two minerals with any number of encapsulated valuable particles.

Austin *et al.* (1993) used a pilot scale SAG mill to grind ore and obtained the size distributions and calculated the apparent specific rates of breakage. They found that the apparent specific rates could not be used to predict the valuable sulphide distribution. The QEM-SEM image analysis technique was used and showed a better liberation as smaller sizes were considered. No consistent variation was found in liberation between the different operating conditions when similar particle sizes were compared.

An exposure model for valuable components was developed by Hsih *et al.*, (1995). They expressed it as a mathematical relationship that takes into account the valuable

mineral grain size, comminuted particle size and an inter-granular fracturing factor. However, other factors like hardness, cleavage, boundary phases, texture, and types of breakage were not incorporated. Fandrich *et al.,* (1997) developed a mineral liberation model for the particle bed breakage of a binary iron oxide ore. They conducted confined particle bed breakage tests at various specific energies and performed liberation measurements by QEM-SEM. Their liberation results and interfacial area measurements provided evidence of the existence of two forms of non-random breakage: preferential breakage and interfacial breakage. Their focus was on the existence of non-random breakage and made no comment on the conditions of the intensity of the breakage or energy where the best liberation was achieved.

Wei and Gay (1999) developed a new approach regarding liberation for comminution. They characterized the liberation distribution (distribution of valuable mineral in particles that underwent comminution) by a dispersion rate function that is related to the texture of the ore. This enables the dispersion model to predict the liberation of the mill product when the operating conditions or feed changes.

In 2004, Gay developed another new approach to model liberation for comminution. He made use of the probability theory. In this approach it is not necessary to have much information about the ore because the relationship between the feed and the product particles is estimated with the probability method. The probability in this instance is defined as the probability that a feed particle of a particular composition and size will form a particular product particle of a particular size and composition. This model can be applied to binary particles or even more complex particles.

2.3 EXPERIMENTS AND OBJECTIVES

In order to achieve the objectives mentioned in the introduction, the following approach is going to be followed:

- Different methods of breakage will be used to determine whether the mode of breakage has an influence on the condition of the particle after it has been

broken. The methods that will be used are impact breakage in the drop weight test, abrasion in a mill and bed breakage in an HPGR.

- In all the breakage experiments, different amounts of energy are going to be applied. This will be achieved by using different mill sizes in the abrasion experiments, using different drop weight masses and heights in the drop weight tests and different pressures in the HPGR. This means that a different energy input will be given per mass of ore for different samples. The size distributions of these samples will be examined in order to determine the degree of variance in the size distributions.
- Chemical assays and mineralogical analyses will be carried out on these samples to determine the compositions of the different fractions and mineralogical liberation of these samples.
- This is discussed in detail in Chapter 3, Experimental Procedure.

LITERATURE SURVEY – *In Summary:*

- Loveday and Naidoo (1996) and Loveday (2005) minimised the effect of secondary milling in abrasion testing by injecting a stream of water into the mill to flush out the fines and therefore provides useful size distribution data. This technique will also be used in this study for the same reason.
- Tavares (2005) made a comparative study between an HPGR, a roll crusher and a hammer mill. It was found that the HPGR produced much more fines than the roll crusher and the hammer mill. Hosten and Özbay (1998) found that the piston-die press produce more fines than a rod mill and that the piston-die press enhanced the liberation of chromites. However, no comparison between an HPGR and an AG mill was made. In this study the product from an AG mill will be compared with the product from an HPGR.
- Shönert (1996) found that the pressure near the walls of a piston is much lower than in the centre. Therefore, in this study only the material coming from the centre of the rolls will be used for analyses.
- Fandrich *et al.*, (1996) found the existence of non-random breakage in their liberation results and that bed breakage promotes this, but no indication was

given about the operating conditions that could be used in practice to achieve this. In this study, this will be investigated.

3. EXPERIMENTAL PROCEDURE

In this chapter the three different modes of breakage and the equipment that was used to perform experiments to investigate these modes of breakage are discussed. These experiments were performed in order to achieve the objectives described in the previous section. A detailed description of the procedure used in the experimental work is given.

Two distinctly different ore types were used for the majority of the experiments. The UG2 platinum ore from Lonmin and a gold ore from Target Gold mine were used for the impact and the abrasion test work. These ore types were selected because the UG2 is fragile and the Target gold ore is more competent. The objective was therefore to make it easier to notice the different breakage characteristics of the different ores. A Merensky reef sample was used to investigate the extent to which the PGMs are liberated under different inter-particle breakage conditions.

3.1. IMPACT

Standard drop weight tests were conducted on UG2 and Target gold ore samples. Drop weight tests were also performed on a big drop weight tester. The size classes and specific energy inputs of these tests are given in Table 3.1. These tests were done in order to determine the influence of various energy intensities on the product particle size distributions.

Table 3.1: Sizes and Specific Energies of drop weight tests

Size (mm)	Specific Energy (kWh/t)	
	STD drop weight	Big drop weight
-106+75		0.4, 0.25, 0.1
-63+53	0.4, 0.25, 0.1	0.4, 0.25, 0.1
-45+37.5	1, 0.25, 0.1	
-31.5+26.5	2.5, 1, 0.25	
-22.4+19	2.5, 1, 0.25	
-16+13.2	2.5, 1, 0.25	

For the standard drop weight test 80 to 100 kg of representative sample in the size range –106+13 mm was used. The entire sample was screened on 63mm sieve and the +63 mm material was crushed by a jaw crusher with a gap of 55 mm so as to generate additional particles for the tests. The original –63 mm fraction and the crushed material were subjected to sizing analysis using the screen sizes shown in Table 3.1. Random selection of the required number of particles for each set was made. The weight of the sample in each size class that was used for each of the three energy inputs was then determined and used to calculate the weight combinations, the drop weight mass and the drop weight height. The drop weight test procedure described in 3.1.1 was then followed.

For the big drop weight test, representative sample in the size range -106+53 mm was used. Random selection of the required number of particles for each set was made. The weight of the sample in each size class that was used for each of the three energy inputs was then determined and used to calculate the weight combinations and drop weight height.

3.1.1 DROP WEIGHT TEST PROCEDURE

The position of the height-limiting stop on the device was adjusted so that the drop weight head will be raised to the required test height. The rock specimen was placed on the anvil with a pair of tongs. The access door was closed and the drop weight head was raised up to the stop. The head was released. No head bounce must occur when the head is released. The remaining gap between the anvil and the face of the head was measured for the first ten specimens. The crushed particles were removed with a brush. This was repeated for the whole set.

After the tests the samples were screened, using a root two screen series. The Standard drop weight test procedure requires the samples to be screened down to 425μm. In this study all the samples were screened to 38μm instead of only screening to 425μm. This was done because valuable information is contained in the sub 425μm fraction and should be quantified. Considering that UG2 ore was one of the ore types used in this investigation and that the natural grain size of the chromites is

around 200μm (Chernet and Marmo, 2003), nothing of the phenomenon of breakage around the natural grain boundaries would have been observed if 425μm was the finest size fraction analysed.

3.2 ABRASION

The abrasion tests were conducted in two mills of different sizes. Different sized mills were used in order to supply different energy intensities to the rocks in the abrasion mill. Loveday (2004) used 75mm steel balls to increase the grinding rates. He used a hard, quartizitic rock. The tests in this study were done autogenously to promote abrasion and avoid the impact breakage that may be caused by steel balls. In addition to this, the UG2 ore that was used is very soft and the charge of the mill would decrease drastically if steel balls were added. The abrasion tests on the gold ore could have been conducted with steel balls, but the aim was to keep the conditions of the milling environment similar for the two ore types. To compensate for the hardness of the gold ore, the gold ore tests were done for a longer time.

A high water flow rate was used to flush out the fines to minimise secondary milling. Injection of water and removal of pulp from a batch grinding test offers a reliable way to monitor the average rate of abrasion and the discharge of fines (Loveday, 2004).

Two mills were used for the abrasion experiments. The pilot AG mill has a small aspect ratio but is big in size and the torque mill has a bigger aspect ratio, but is smaller in size. Pictures of the pilot and the torque mills can be seen in Figure 3.1 and the design variables of the mills are given in Table 3.2.

Figure 3.1: The pilot mill and the torque mill

The procedure that was followed for the abrasion test work is similar to the procedure followed by Loveday and Naidoo (1997) in that initial rounding runs were conducted from fresh feed rocks to condition the rocks for the abrasion tests. These conditioned rocks were then used to measure abrasion. After the abrasion test the mill was topped up using the conditioned rocks. The sizes of the rocks that were used for this study differs from what Loveday and Naidoo (1997) used in that some size classes were left open so that it would be easier to see when a rock moved into a smaller size class due to abrasion. They used a 600mm diameter mill and in this study a 600mm torque mill and a 1.68m pilot mill were used.

Table 3.2: Design variables of the mills

Design variable	*Pilot mill*	*Torque mill*
Diameter	1.68 m	0.597 m
Length	0.57 m	0.485 m
No. of lifters	11	12
Height of lifters	45 mm	25 mm
No. of grates	12	-
Total no of holes	888	144
Diameter of holes	19 mm	16 mm
Speed of mill	75 % of critical	variable

3.2.1 SEASONING PROCEDURE

A run was done for 11 minutes long and samples were taken every minute. The water flow rate for the pilot mill was 10//min. The first sample was taken for two minutes long because it takes a while for the water to make its way through the charge. The rest of the samples were taken for one minute long. After 11 minutes the mill was stopped and the content was removed. One of the objectives of the seasoning procedure was to prepare rounded rocks for the abrasion experiments.

3.2.2 SAMPLE HANDLING PROCEDURE

After the mill stopped, the charge was taken out, the contents was dried and screened and the different size fractions were weighed. The slurry samples that were taken were filtered and dried, split, screened and weighed. All the different mass fractions were recorded in order to obtain the particle size distributions. The number of rocks in each size class before and after each run was recorded to determine the amount of breakage that took place.

3.1.3 ABRASION PROCEDURE

The abrasion tests were similar to the seasoning tests, but these runs were only 2 minutes long. Therefore only one sample could be taken. This was done to avoid significant changes in the percent mill filling during the test. Only rounded rocks were used in these abrasion tests because excessive initial chipping would occur with angular rocks and this had to be avoided to isolate abrasion effects. The water flow rate for the pilot mill was 10//min. The feed size distributions that were used for the abrasion test work are shown in Table 3.3.

Three non consecutive discrete size classes as seen in Table 3.3 (Pilot mill UG2) were selected out of the standard root two series. This was done to avoid confusion in the accounting process when quantifying abrasion. The three discrete size classes were placed in the mill in the same mass ratio as the original bulk sample. A load of rocks was charged to the mill via the feed trunnion. The mill was filled up to a 30% volume

filling. The Seasoning (3.2.1) and Sample handling (3.2.2) procedures were followed and four repeats were performed. The rounded product pebbles from these runs were used in the Abrasion experiments.

Table 3.3: Feed size distributions

Size class	Pilot mill UG2	Pilot mill Gold ore	Torque mill UG2	Torque mill UG2	Torque mill UG2	Torque mill Gold ore	Torque mill Gold ore	Torque mill Gold ore
-150+106mm	137 kg	130 kg						
-106+75mm		282 kg						
-75+50mm	241 kg	129 kg					8 kg	
-50+38mm		194 kg	21 kg	79 kg		39 kg	37 kg	
-38+25mm	358 kg		47 kg		79 kg	21 kg	20 kg	60 kg
-25+18mm			11 kg					
Total	**736 kg**	**735 kg**	**79 kg**	**79 kg**	**79 kg**	**60 kg**	**60 kg**	**60 kg**

The same feed size distributions were used for the abrasion tests as for the seasoning tests as shown in Table 3.3 (Pilot mill UG2). The Abrasion procedure (3.2.3) and the Sample handling procedure (3.2.2) were followed. This experiment was repeated twice.

Two more abrasion tests were performed with rounded rocks, but with the feed size in only one size class. The first consisted of only big rocks (-150+75mm) and the second of only small rocks (-50+25mm). This was done to investigate the effect of having big rocks in a mill without the protection of smaller rocks and also to investigate the effect of small rocks when there are no big rocks present to break them.

The gold ore was already seasoned from previous experiments. The mill was filled up to a 40% volume filling in the size distribution that is shown in Table 3.3 (Pilot mill Gold ore). The Abrasion procedure (3.2.3) was followed for these rocks, but because of its competency it was tumbled for 21 minutes long. Samples were taken every 2 minutes. The first sample was taken for 3 minutes long and after that the samples were taken for 2 minutes long. This experiment was repeated twice.

The design variables of the Torque mill are given in Table 3.2. The UG2 sample that was used for the torque mill experiments were already rounded from the pilot mill

experiments. The Abrasion procedure (3.2.3) was followed but for 20 minutes long. Samples were taken every two minutes. All the samples could be taken for the same time (2 minutes) because the water and slurry moves easier through the smaller charge. The sample handling procedure (3.2.2) was followed. This was done with all the feed size distributions that are shown in Table 3.3 (Torque mill UG2). The mill was filled up to 30% of its volume.

The feed size distributions that were used for the Gold ore can be seen in Table 3.3 (Torque mill Gold ore). The Abrasion procedure (3.2.3) was followed but for 50 minutes long. A five minute long sample was taken every five minutes. The sample handling procedure (3.2.2) was followed. The mill was filled up to 30% of its volume.

3.2 BED BREAKAGE

The High Pressure Grinding Roll (HPGR) that was used for this study is a Polysius laboratory scale model. The studded rolls are 100mm wide and the diameter of the rolls is 250mm. The capacity of this model is 1-4 tons per hour depending on the operating conditions and ore. The motors of the HPGR are fitted with instrumentation to record the energy consumed draw in kWh. The product conveyor belt is fitted with a weightometer for measuring the total mass of the crushed material. The maximum hydraulic pressure setting that was used was 150 bar and that of Nitrogen pressure was 120 bar. A picture of the HPGR and one of its studded rolls can be seen in Figure 3.2.

Figure 3.2: The lab scale HPGR and a studded roll

The zero gap between the rolls is the space between the rolls when there is no material between the rolls. The minimum zero gap of this unit is 1mm to prevent the rolls from damaging each other and the maximum is 9 mm, but it is usually operated between 2-4mm. The working gap is the space between the rolls when ore is fed. The working gap is always bigger than the zero gap because the floating roll moves away from the fixed roll when it is operating. The pressure settings, feed particle size and ore type will influence the difference between the zero gap and the working gap. The approximate operating gap can be determined by measuring the thickness of the product cakes. The maximum feed top size that this unit can take is 20mm but 12mm is preferred.

A no load run was done before the experiments so that the no load power draw of the HPGR can be subtracted from the actual power draw under load. The ore is put into the feed hopper at the top of the HPGR using the feed conveyor belt. The speed of the feed conveyor belt can be varied. There is a level sensor in the hopper at the top of the HPGR and the speed of the feed conveyor belt can be adjusted accordingly in order to keep the level of ore in the feed hopper high. This ensures that the HPGR is operated under choke feed conditions. It is important to choke feed the HPGR to achieve high pressure inter-particle breakage. The discharge of the HPGR is onto the product conveyor belt, which takes the crushed ore to the product hopper that empties into a bulk storage bag. The discharge of the HPGR is usually in the form of cakes or large flakes because particles are broken under inter-particle pressure in this device.

However, the formation of flakes depends on the ore type. These flakes can easily be de-agglomerated given that the ore does not have high clay content. A summary of the tests performed using the HPGR is given in Table 3.4. These tests were performed in duplicates.

Table 3.4: Operating conditions of HPGR tests

Pressure (bar)		*Force*	*Ore type*		*Zero Gap*
Nitrogen	*Hydraulic*	*(N/mm^2)*			*(mm)*
20	30	1.5	Merensky		2.3
30	48	2.39	Merensky		2.3
40	60	2.99	Merensky		2.3
60	90	4.49	Merensky	UG2	2.3
90	120	5.99	Merensky		2.3
120	150	7.48	Merensky		2.3

EXPERIMENTAL PROCEDURE – *In summary:*

- Drop weight tests were performed to determine the influence of different energy intensities on the product particle size distribution. The drop weight tests were carried out on UG2 and Target gold ore.
- Abrasion experiments were performed in a 1.68x0.597m pilot mill and a 0.57x0.485m torque mill. This was done in order to see how the breakage changes when the size and aspect ratio of the mill changes. Another objective was to produce samples from the abrasion mode of breakage for further analyses.
- The effects of various operating conditions were investigated on the HPGR. This was also done in order to produce samples for further analyses and to compare bed breakage to the other modes of breakage.

4. RESULTS AND DISCUSSION

This chapter contains the results obtained from the test work conducted on the drop weight testers, the abrasion mills and the high pressure grinding rolls. The results of the Mineralogy that was performed on selected samples from these tests are given and each section provides the interpretation and discussion of these results.

4.1. IMPACT BREAKAGE

The impact breakage experiments were performed as the Standard JK drop weight test (size -16−13.2mm to -63+53mm) and the Mintek Big drop weight test (size -63+53mm to -150+106mm). The sizes of the different samples and the specific energies that were applied to break these samples are given in Table 3.1. The tests were performed on UG2 ore and Target gold ore. The product particle size distributions of the drop weight tests performed on the UG2 ore are given in Figure 4.1. For the overlapping size the apparatus that was used is indicated JK for the standard drop weight test and M for the big drop weight test.

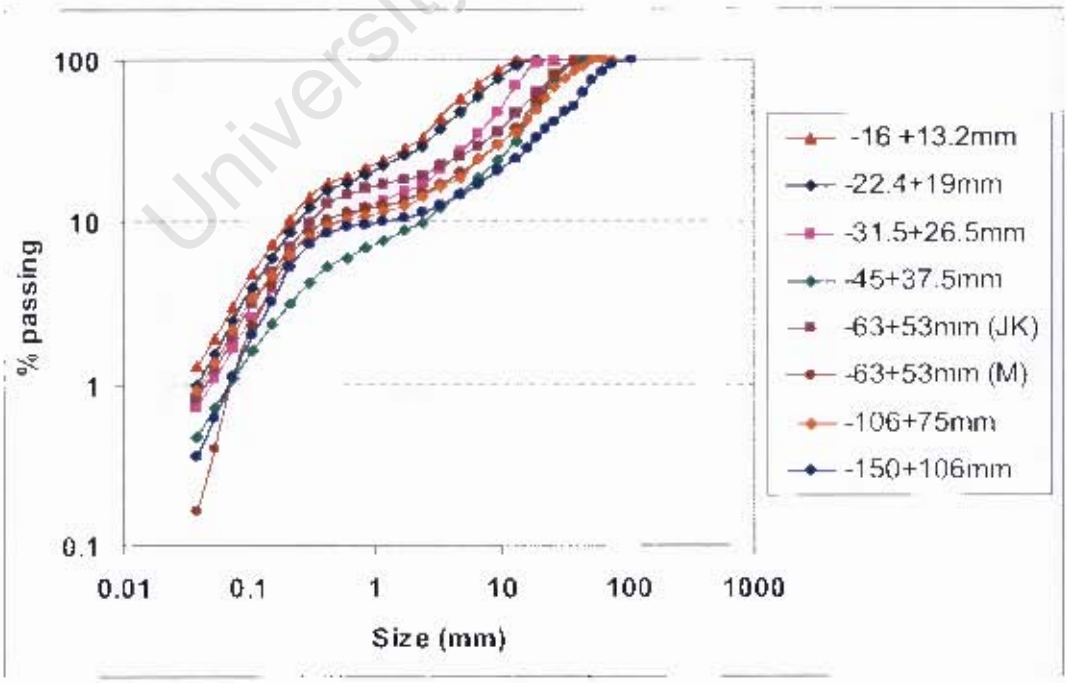

Figure 4.1: UG2 Drop weight size distributions (0.25 kWh/t)

The size distributions shown here are for the rocks broken at 0.25kWh/ton because it was the only energy input that could be applied to all the sizes. The rest of the size distribution data can be seen in Appendix A. The experimental t_{10} values were determined, the A and b values were calculated and the A x b curves can be seen in Figure 4.2.

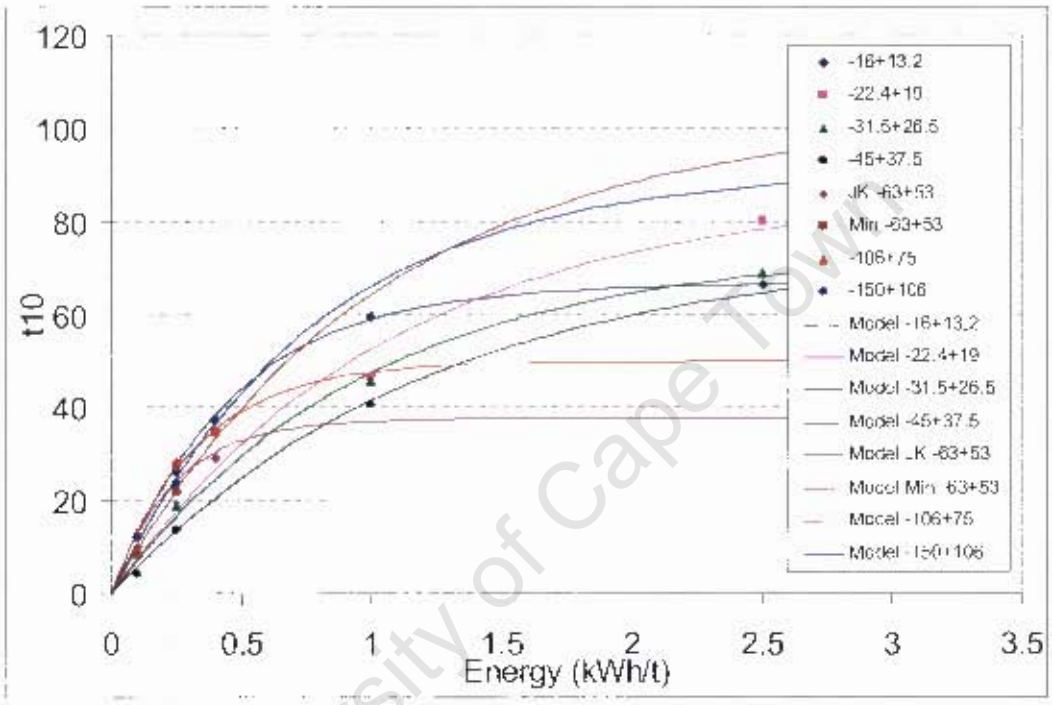

Figure 4.2: Experimental t10 values at various energy inputs for the UG2 samples

The product particle size distributions of the drop weight tests performed on Target gold ore can be seen in Figure 4.3. The particle size distributions shown here are for 0.25kWh/t because it was the only energy intensity that could be applied to all the rock sizes. The rest of the data is given in Appendix A. The experimental t10 values were determined, the A and b values were calculated and the A x b curves can be seen in Figure 4.4.

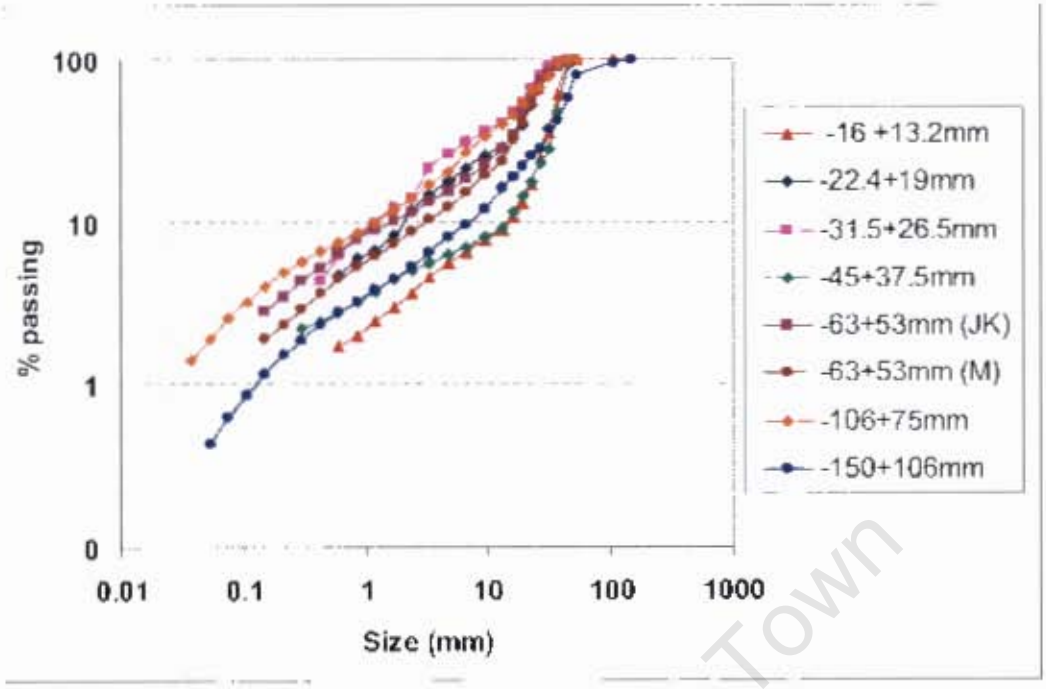

Figure 4.3: Target Gold dropweight size distributions (0.25 kWh/t)

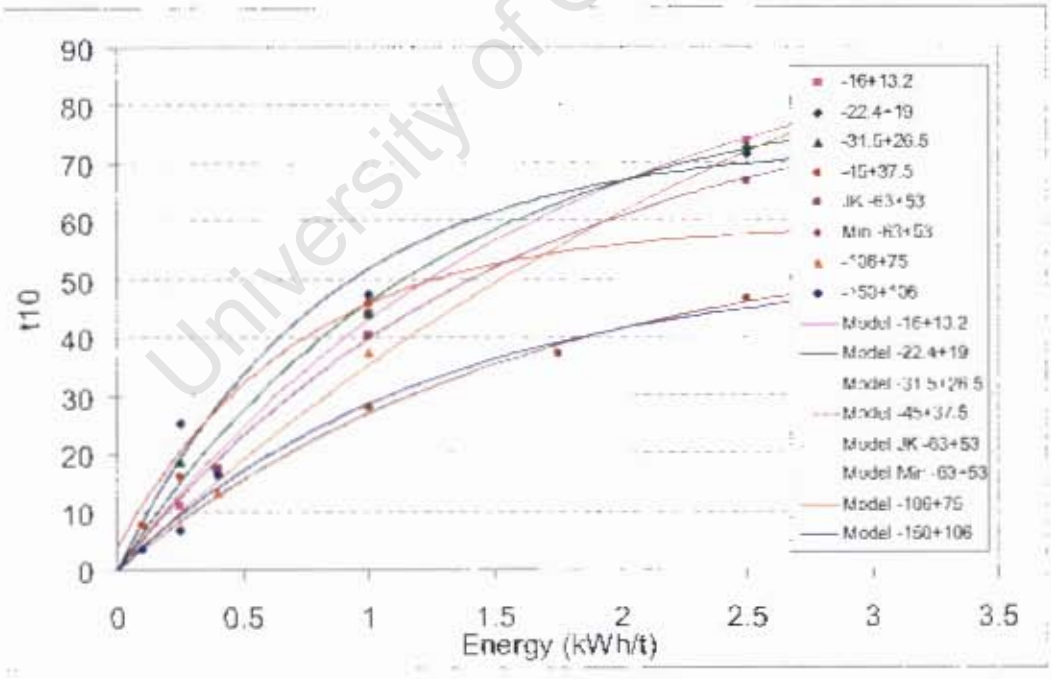

Figure 4.4: Experimental t10 values at various energy inputs for the Target samples

In Table 4.1, the calculated A and b values for UG2 and Target ore are given. The b value for the UG2 ore is generally higher than for Target ore and indicates that the UG2 ore is fragile in comparison to the Target ore.

Table 4.1: Calculated A and b values for UG2 and Target ore

UG2	-16+13.2mm	-22.4+19mm	-31.5+26.5mm	-45+37.5mm	JK -63+53mm	Min -63+53mm	-106+75mm	-150+106mm
A	66.63	86.91	74.22	74.22	37.59	102.91	50.02	91.33
b	2.16	0.93	1.02	0.82	4.16	0.98	3.07	1.29
A x b	144.06	80.66	75.85	60.95	156.52	100.80	153.81	117.59
Target	-16+13.2mm	-22.4+19mm	-31.5+26.5mm	-45+37.5mm	JK -63+53mm	Min -63+53mm	106+75mm	-150+106mm
A	95.88	73.26	83.76	59.30	84.45	58.46	136.03	52.00
b	0.60	1.23	0.80	1.41	0.64	0.62	0.30	0.80
A x b	57.11	89.86	66.92	83.70	53.86	36.18	40.85	41.60

There is a significant difference in the shapes of Figure 4.1 and Figure 4.3. This is because the chromites present in UG2 ore tend to break around natural grain boundaries, which is around 200µm (Chernet and Marmo, 2003). It causes the inflection point in the curves of the UG2 size distribution where the Target gold size distribution is smooth. This is better illustrated in Figure 4.5 and Figure 4.6.

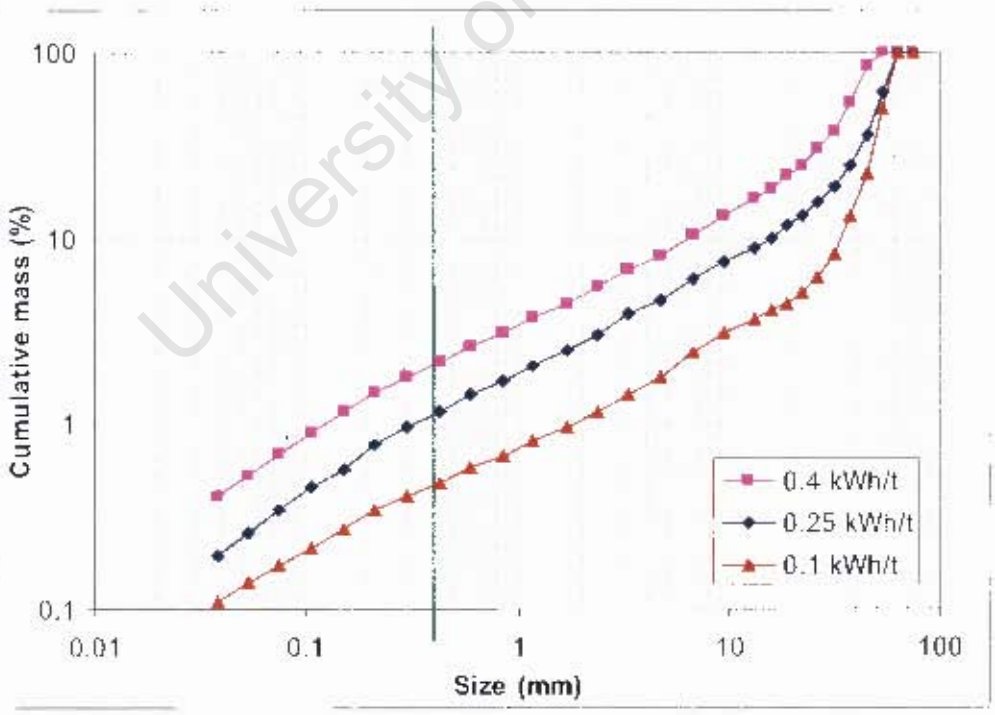

Figure 4.5: The full size distribution for the product of the -106+75mm Target ore broken with 0.4, 0.25 and 0.1 kWh/t

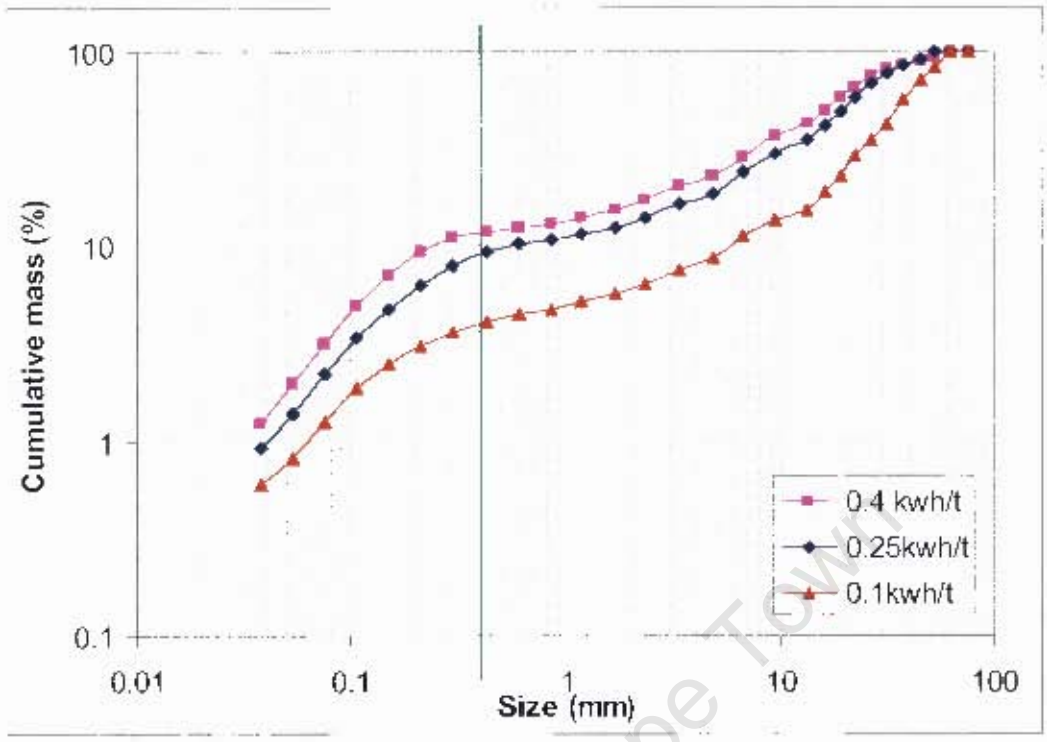

Figure 4.6: The full size distribution for the product of the -106+75mm UG2 ore broken with 0.4, 0.25 and 0.1 kWh/t

The green line in Figure 4.5 and Figure 4.6 shows where the sizing of the drop weight product would usually stop around 400µm. For the Target ore in Figure 4.5 it would not have made a difference, but the sub 400µm information for the UG2 ore in Figure 4.6 is important because the natural grain sizes of the chromites play a role. This is also the size range that is most important in terms of liberation and recovery because particles bigger than 400µm can not be recovered by flotation. The same trend was observed for all the size classes tested and the size distribution data for the other size classes can be seen in Appendix A.

4.2. ABRASION

The experiments conducted in the pilot and torque mills are described in this section. These tests were primarily performed to investigate abrasion as a mode of breakage and to determine what influence of different mill diameters has on the breakage.

4.2.1. PILOT MILL

The pilot mill has a diameter of 1.68m and length of 0.57m. The rest of its design variables are given in Table 3.2. The masses of the four initial rounding runs that were done on the UG2 ore can be seen in Table 4.2. The pilot mill was filled with a batch of 737 kg fresh ore for each batch. The mass of 737 kg, representing 30% volume filling, was made up of rocks in three discrete size classes as shown in Table 4.2. After 11 minutes the mill filling for batches 1, 2, 3 and 4 dropped from 30% to 17%, 18%, 16% and 19% respectively.

Table 4.2: Initial rounding runs to prepare rocks for abrasion tests

Size (mm)	BATCH 1		BATCH 2		BATCH 3		BATCH 4	
	t=0	t=11min	t=0	t=11min	t=0	t=11min	t=0	t=11min
-150+106	137	69	137	73	137	65	137	70
-106+75	0	29	0	29	0	30	0	28
-75+50	241	58	241	50	241	50	241	52
-50+38	0	53	0	65	0	67	0	59
-38+25	358	81	358	92	358	69	358	137
-25+18	0	54	0	56	0	48	0	55
-18+12	0	35	0	32	0	28	0	31
-12	0	45	0	41	0	36	0	38
Total	**737**	**423**	**737**	**441**	**737**	**393**	**737**	**470**
Mill filling	**30%**	**17%**	**30%**	**18%**	**30%**	**16%**	**30%**	**19%**

During these four runs 10 slurry samples were taken. The wet and dry mass data can be seen in Appendix B. The trend that is expected in this kind of experiment is the typical quick loss of mass as a result of the initial chipping (Austin *et al.*, 1987). Then the rate of mass loss slows down as abrasion takes over and chipping decreases where the wear rate is very slow and the mass loss is almost constant. It can be seen in Figure 4.7 that the mass loss is rapid at first and then it slows down to stabilise (Loveday, 2004). This run was only 11 minutes long because UG2 ore is fragile and

the average specific rate stabilised quickly. The Mass fraction remaining in the mill and average specific discharge rate of solids shown in Figure 4.7 is for batch 4, the data for the other runs are similar and can be seen in Appendix B.

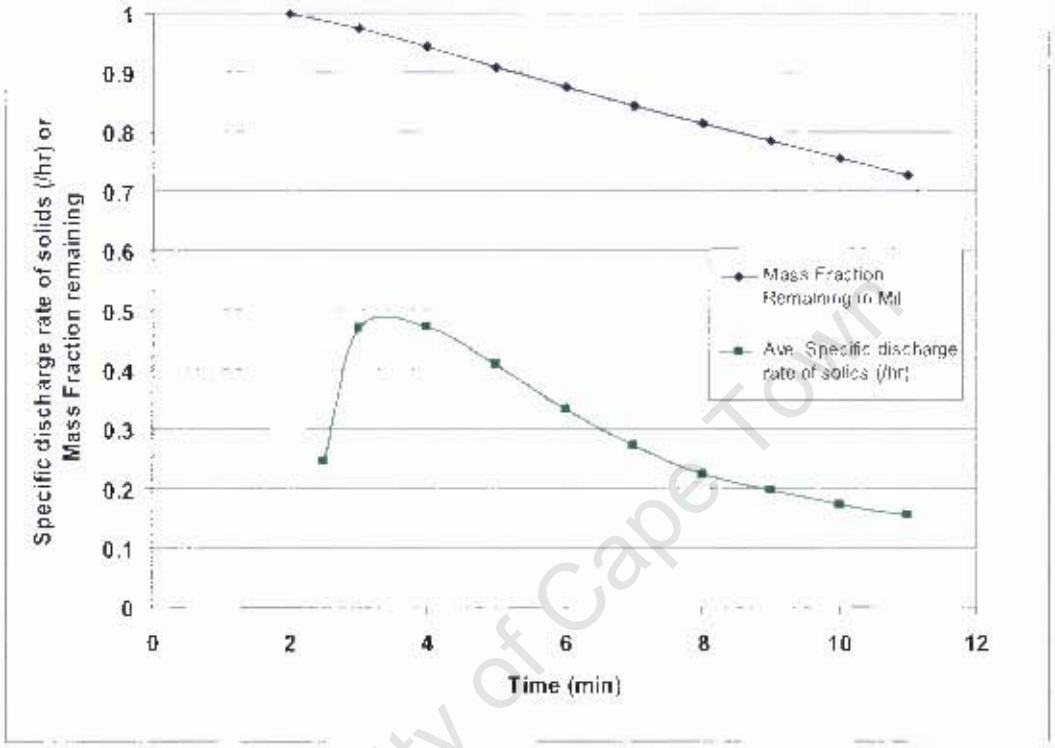

Figure 4.7: Mass fraction remaining in the Pilot mill and average specific discharge rate (Batch 4)

Each of the ten slurry samples was screened from the top size down to 38µm. An example of the resultant size distribution of all the slurry samples of one of these runs is given in Figure 4.8. The cumulative size distribution data for batch 1, 2, 3 and 4 can be seen in Appendix B. In Figure 4.8, it can be seen that the size distribution of the first slurry samples that were taken at 2 minutes are the coarsest and the size distributions then get finer and the 11th minute slurry samples are the finest. The conditions under which these tests were performed were identical. Repeatable results could therefore be expected. In all four batches the specific discharge rate peaked at 4 minutes after start-up (see Figure 4.8). This means that the fines that were generated by the initial chipping phase were held back by the charge and therefore the discharge rate peaked only at 5 minutes after start up.

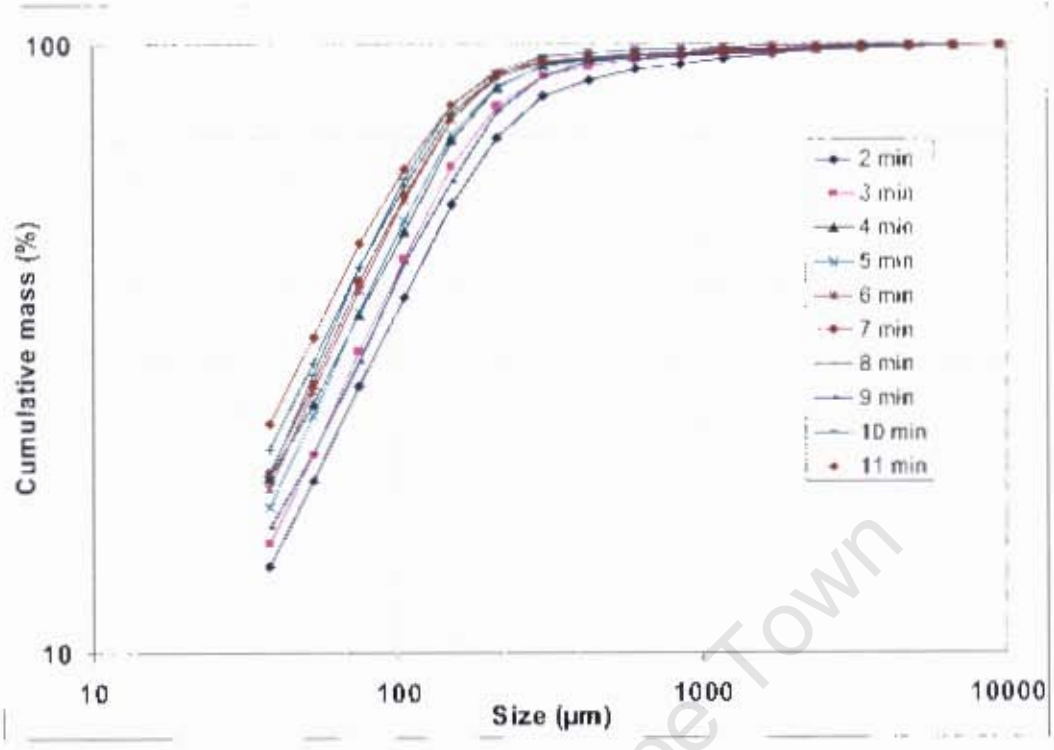

Figure 4.8: Size distribution for UG2 batch 4 in the Pilot mill

Figure 4.9 shows the size distribution over the whole size range for the four initial rounding batches. The masses and sizes of the rocks that were initially put into the mill are also shown. The steps in the size distributions that were caused by the discrete size classes that were put into the mill are smoothed out but still visible.

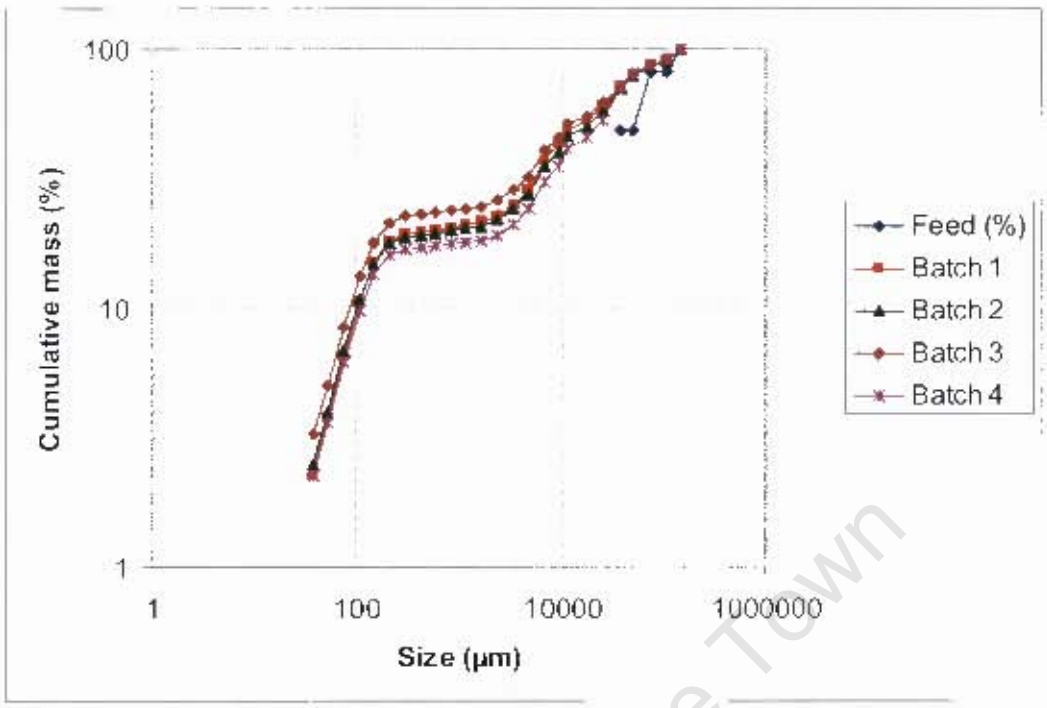

Figure 4.9: Initial rounding size distributions

From this data three sizes were selected namely 38µm, 106µm and 1180µm to assess the change in the rate of production of fines with time. In Figure 4.10 the trend for the production of fines in the 38µm fraction of the mill discharge increases from the 2nd minute to the 11th minute. The increase in the rate of –38µm fines production from the 2nd to the 4th minute is quick and then becomes more stable after that. The rate of fines production in the 106µm size fraction shows a much more rapid increase and only becomes more consistent after the 8th minute. The rate of production of fines in the 1180µm size class shows only an increase between the 2nd and the 4th minute. After that the rate of fines production is constant.

This means that in the first ten minutes of a grind out test with angular rocks in a pilot scale AG mill the rate of discharge of the fines will increase rapidly in the first two minutes and then become more constant. Figure 4.10 therefore shows that the rate of production of the fines in these three size fractions changes over time. Variations in the mineralogical compositions of these fractions may therefore occur.

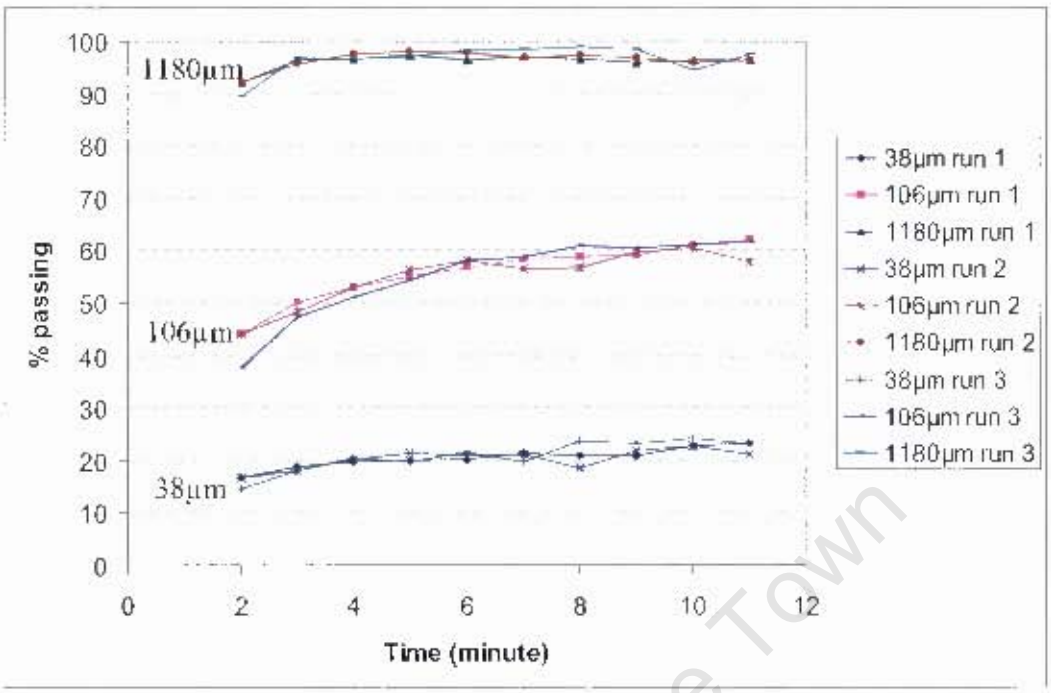

Figure 4.10: Mass percent passing 38µm, 106µm and 1180µm runs 1-3

One of the objectives of these runs was to prepare the rocks for the abrasion tests. These rounded UG2 rocks were used in an attempt to isolate abrasion. This time the number and mass of rocks were recorded in order to determine the amount of breakage that took place during the experiment. The mass and number of the rocks that were put into the mill as well as the mass and number of the rocks that remained after the 2 minute long run are given in Table 4.3.

The same initial mill filling (30%) was used as in the rounding experiments. The mill was only run for 2 minutes in an attempt to keep the contents of the mill constant. The charge was then removed, screened, weighed and the rocks counted. The mill was filled with the remainder of the rocks from the 2 minute run that was still in the size classes of interest and topped up with the conditioned rocks from the initial four runs to make up a similar charge for the repeat test.

Table 4.3: Abrasion test on the pilot mill

Time (t)	BATCH 1				BATCH 2			
	t=0		t=2min		t=0		t=2min	
Size (mm)	Mass	Number	t=2min	Number	Mass	Number	Mass	Number
106	137	33	117	27	137	31	91	19
75			15	6			39	12
50	241	583	198	473	241	581	196	482
38			32	185			29	109
25	358	5231	276	4315	358	4443	281	4522
18			33	1042			38	1165
12			10	976			10	921
Total	**736**	**5847**	**681**	**7024**	**736**	**5055**	**684**	**7230**
Mill filling	**30%**		**28%**		**30%**		**28%**	

In Table 4.3 the significant increase in the number of rocks after the run shows that many rocks were split and broken due to impact breakage. For batch 1 the initial charge comprised 33 rocks in the –150+106mm size class and after the 2 minute test 27 rocks remained. It was observed that 6 rocks moved down to the –106+75mm size class as a result of abrasion (the –106+75mm size class had no material in it initially). Afterwards these rocks were inspected and no chip marks were found, they were only more rounded. Similarly, from the 583 rocks in the –75+50mm size class 473 remained in this size class while 185 rocks where found in the –50+38mm size class which was initially empty. The number of rocks that remained in the same size class and that was found in the size class just below it do not add up to 583. This means that some rocks broke in such a way that the progeny rocks were still in the same size class, or a big enough piece of the original particle split off for it to be in the –50+38mm class. Table 4.3 shows a significant increase in the number of rocks in the smaller sizes while the numbers of bigger rocks did not change significantly. Similar results were obtained for batch 2.

A similar abrasion run was conducted with rocks in the two top size classes only, –150+106 and –106+75. The number and mass of rocks before and after grinding for 2 minutes are given in Table 4.4. It can be seen that numerous rocks were broken into size classes below 75mm.

Table 4.4: Big and small rock abrasion tests on the pilot mill

Time (t)	BATCH 3				BATCH 4			
	t=0		t=2min		t=0		t=2min	
Size (mm)	Mass	Number	Mass	Number	Mass	Number	Mass	Number
150	491	77	143	33				
106		94	244	94				
75			49	81				
50			11	152	673	1667	534	865
38			11	63		6041		5348
25			6	238			79	1334
18			6	776			23	4999
Total	**491**	**171**	**470**	**1437**	**673**	**7708**	**636**	**12546**
Mill filling	**20%**		**19%**		**27%**		**26%**	

This shows that the smaller rocks in the first two abrasion runs provided a sort of cushioning effect that protected the big rocks from breaking as the big rocks only broke the smaller rocks. In the third abrasion test the big rocks broke themselves. For the fourth batch, only small rocks were put into the mill and the results given in Table 4.4 indicate that breakage events took place and generated rocks in the sub 25mm size classes. The observations in this series of tests lead to the conclusion that the mode of breakage that was obtained in the pilot mill was a combination of impact breakage and abrasion.

A more competent ore, Target Gold ore was then used for further test work. This ore type was selected because it is much harder than UG2 and therefore more difficult to break, however it is lighter than the UG2. The Bond Ball Work Index for UG2 is 15.61 kWh/t and 17 kWh/t for Target Gold ore. This was also done in order to compare the breakage characteristics of a gold ore to the breakage characteristics of a platinum ore. These rocks were well rounded from previous experiments. The mill was filled to a slightly higher percent filling. Fewer breakage events took place in these experiments as shown in Table 4.5.

Table 4.5: Abrasion tests on Target Gold ore

Size	Run 1				Run 2			
	t=0	Number	t=21min	Number	t=0	Number	t=21min	Number
106	130	39	112	33	112	33	98	29
75	282	223	108	209	108	209	208	163
50	129	328	261	293	261	293	118	278
38	194	1424	134	998	134	998	93	624
25			28	394			23	340
18			3	141				112
12			2	198				
Total	735	2014	648	2266	615	1533	540	1546
Mill filling	39%		35%		33%		29%	

Only one batch of rocks of 735kg were availible for these tests. This was the same mass that was used for the UG2 tests. However, the Target ore has a much lower S.G. and it filled the mill up to 39% as seen in Table 4.5. After screening out the fines of batch 1 only 615kg was still available in the bigger size classes to do a second run. These runs were carried out for 21 minutes to make it easier to see the breakage that took place on this competent ore type.

4.2.2 TORQUE MILL (600mm)

The torque mill has a diameter of 0.597m and length of 0.485m. The other design variables are given in Table 3.2. In the torque mill, more breakage occurred as a result of abrasion than impact breakage. This could be observed in the similarity of the numbers of rocks before and after each test on both ore types. All the rock samples that were used in the torque mill experiments were rounded from the experiments described in section 3.1.1. Three size classes were put into the mill. The speed of this mill was set at 75% of critical. The mass and number of rocks in the charge were recorded before and after each run as shown in Table 4.6.

Table 4.6: UG2 Abrasion tests on the torque mill

	BATCH 1				BATCH 2				BATCH 3			
Size class	-50+38,-38+25,-25+18				-50+38,-38+25,-25+18				-50+38,-38+25,-25+18			
Time (t)	t=0		t=20		t=0		t=20		t=0		t=20	
Size	Mass	Number	Mass	Number	Mass	Number	Mass	Number	Mass	Number	Mass	Number
50	21	95	15	65	21	98	16.1	79	21	102	16	84
38	47	714	37	573	47	728	33.58	571	47	799	39	615
25	11	393	12	406	11	403	13.70	461	11	393	15	498
18	0	0	2	173	0	0	1.96	147	0	0	2	128
12	0	0	0	54	0	0	0.16	47	0	0	0	40
Total	**79**	**1202**	**66.14**	**1271**	**79**	**1229**	**65.50**	**1305**	**79**	**1294**	**72**	**1365**
Mill filling	**30%**		**25%**		**30%**		**25%**		**30%**		**27%**	

It can be seen from Table 4.7 that that the number of rocks in the smaller sizes increased. It can be deduced that using only the small rocks did not reduce the breakage that took place during a 20 minute long run. The reduction of the mill speed reduced the breakage slightly as seen in Table 4.7 for batch 9. The slurry size distribution data for all these tests can be seen in Appendix B.

Table 4.7: UG2 Abrasion tests on the torque mill

Size class	BATCH 4				BATCH 5				BATCH 9			
	-38+25				-38+25				-38+25 70% of critical			
Time (t)	t=0		t=20		t=0		t=20		t=0		t=20	
Size	Mass	Number	Mass	Number	Mass	Number	Mass	Number	Mass	Number	Mass	Number
38	79	1301	57	968	79	1335	55.415	944	79	1256	58	939
25			11	320			13.89	383			10	261
18			1	67			0.60	53			1	89
12			0	36			0.05	16			0	23
Total	**79**	**1301**	**69.52**	**1391**	**79**	**1335**	**69.96**	**1396**	**79**	**1256**	**69**	**1312**
Mill filling	**30%**		**26%**		**30%**		**27%**		**30%**		**26%**	

A similar set of experiments was done with bigger (-50+38mm) rocks. The results can be seen in Table 4.8. It is similar to the results shown in Table 4.7, with the reduction in mill speed again reducing the breakage. Therefore the lower mill speed cased slower abrasion rates. This is in agreement with the literature in that the specific rate of abrasion can be correlated with the power intensity of the mill (Loveday and Naidoo, 1997). The number of rocks retained in the top size is higher for the slower mill speed, but the mass loss is similar.

Table 4.8: UG2 Abrasion tests on the torque mill

Size class	BATCH 6				BATCH 7				BATCH 8			
	-50+38				-50+38				-50+38 speed 70% of critical			
Time (t)	t=0		t=35		t=0		t=35		t=0		t=35	
Size	Mass	Number	Mass	Number	Mass	Number	Mass	Number	Mass	Number	Mass	Number
50	80	386	47	245	80	402	45.84	245	79	426	51	266
38			16	151			14.83	140			12	124
25			1	23			0.65	16			1	15
18			0	21			0.72	43			1	37
12			0	30			0.1	49			0	16
Total	**80**	**386**	**63.54**	**470**	**80**	**402**	**62.14**	**493**	**79**	**426**	**64**	**458**
Mill filling	**30%**		**24%**		**30%**		**24%**		**30%**		**24%**	

More abrasion tests were then conducted using Target Gold ore. Only abrasion breakage took place as the number of rocks before and after the tests were exactly the same. This can be seen in Table 4.9. The size distribution data of the Target Gold ore runs can be seen in Appendix B.

Table 4.9: Target Gold Abrasion tests on the torque mill

Size class	BATCH 1				BATCH 2			
	-50+38,-38+25				-75+50,-50+38,-38+25			
Time (t)	t=0		t=50		t=0		t=50	
Size	Mass	Number	Mass	Number	Mass	Number	Mass	Number
75					8.57	15	8.32	15
50	39	258	37.08	255	37.08	253	34.19	239
38	21	245	19.88	248	19.88	248	19.55	258
25							0.11	4
18								
12								
Total	**60**	**503**	**57**	**503**	**66**	**516**	**62**	**516**
Mill filling	**30%**		**28%**		**33%**		**31%**	

4.3. BED BREAKAGE

HPGR test work was performed at 6 different operating pressures. The pressures and the specific press force (N/mm^2) as calculated from these pressures can be seen in Table 3.4. The tests were conducted on Merensky ore for the full range of operating pressures and on UG2 ore at one operating pressure. The size distributions, energy consumed and the throughput of these tests were recorded. The zero gap was not adjusted between these tests. The top size of both feed ores were <12mm.

The cumulative size distributions of the feed and the product for the UG2 ore can be seen in Figure 4.11 and for the Merensky ore in Figure 4.12. Tests were conducted at the operating pressure of 60 bar Nitrogen and 90 bar hydraulic. The specific press force (F) exerted by the rolls in (N/mm^2) and the specific energy (E) in (kWh/t) for these settings can be seen in the legends of Figure 4.11 and Figure 4.12 and are shown for the product size distributions. The raw size distribution data is given in Appendix C. The relationship between pressure and specific press force is also given in Appendix C and the method that was used to calculate specific press force from pressure is shown.

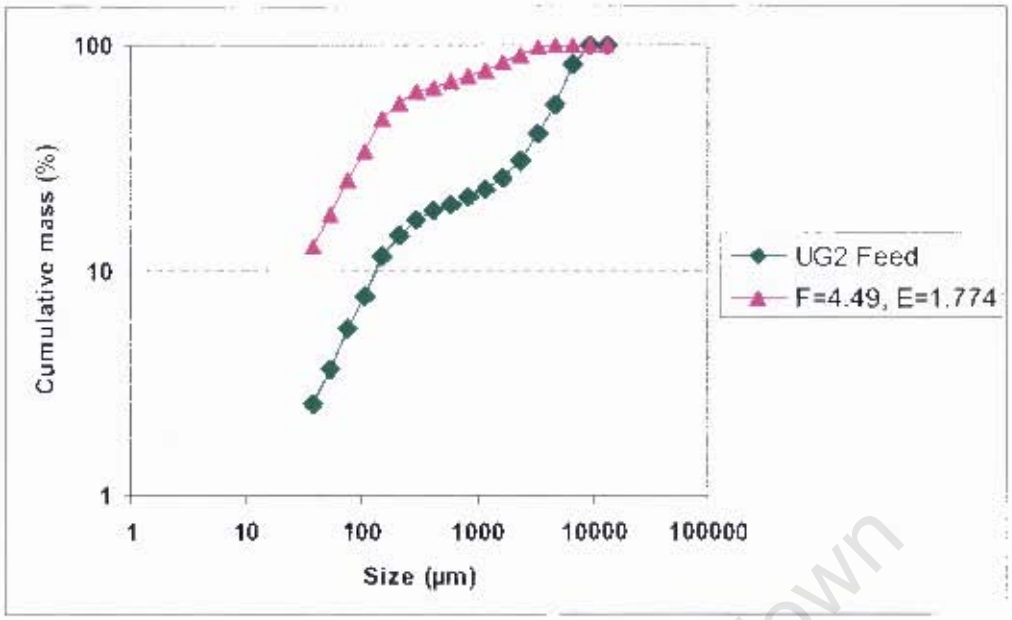

Figure 4.11: Cumulative size distributions for UG2 ore

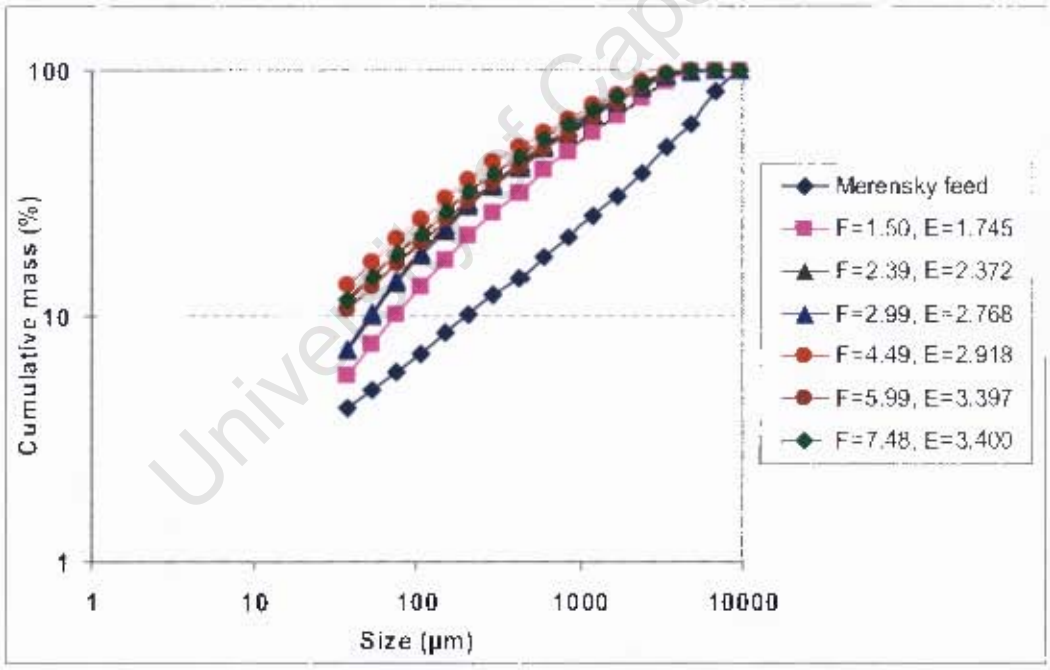

Figure 4.12: Cumulative size distributions for Merensky ore

Pictures of the feed and the product from the HPGR can be seen in Figure 4.13 for the UG2 ore. The flakes that form as a result of the compression between the rolls can be seen in Figure 4.13 (b).

(a) (b)

Figure 4.13: Pictures of the feed (a) and product (b) of the HPGR

For the Merensky ore, the specific energy that was used as a function of press force can be seen in Figure 4.14. The specific press force was increased from 1.5N/mm^2 to 7.5N/mm^2. The consumption of specific energy increases as the specific press force is increased. Therefore, the lower the specific press force, the lower the energy consumption.

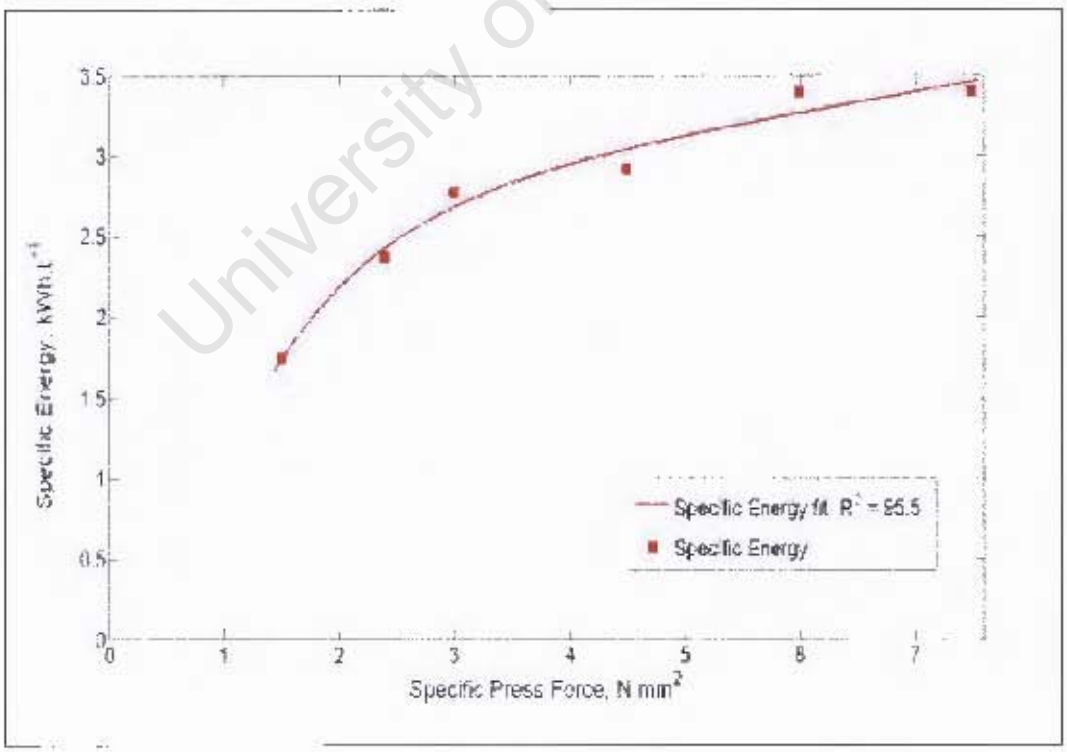

Figure 4.14: Specific energy as a function of specific press force

The percent passing 75µm, 300µm and 600µm for the Merensky ore are shown in Figure 4.15. A sharp increase in the percent passing the given mesh size up to 4N/mm^2 was observed for all sizes. When the specific press force is increased beyond 4N/mm^2 the grind no longer gets finer but the energy consumption still increases as seen in Figure 4.14. Therefore there is no benefit in operating beyond 4N/mm^2 for this ore type and operating beyond 4N/mm^2 will only result in unnecessary energy losses.

It can be observed that the trend lines for all three curves increase up to 4 N/mm^2 but do not increase significantly thereafter. It may therefore be concluded that an increase in specific press force provides a finer grind, but only up to a certain threshold that was found to be 4 N/mm^2 for this ore type.

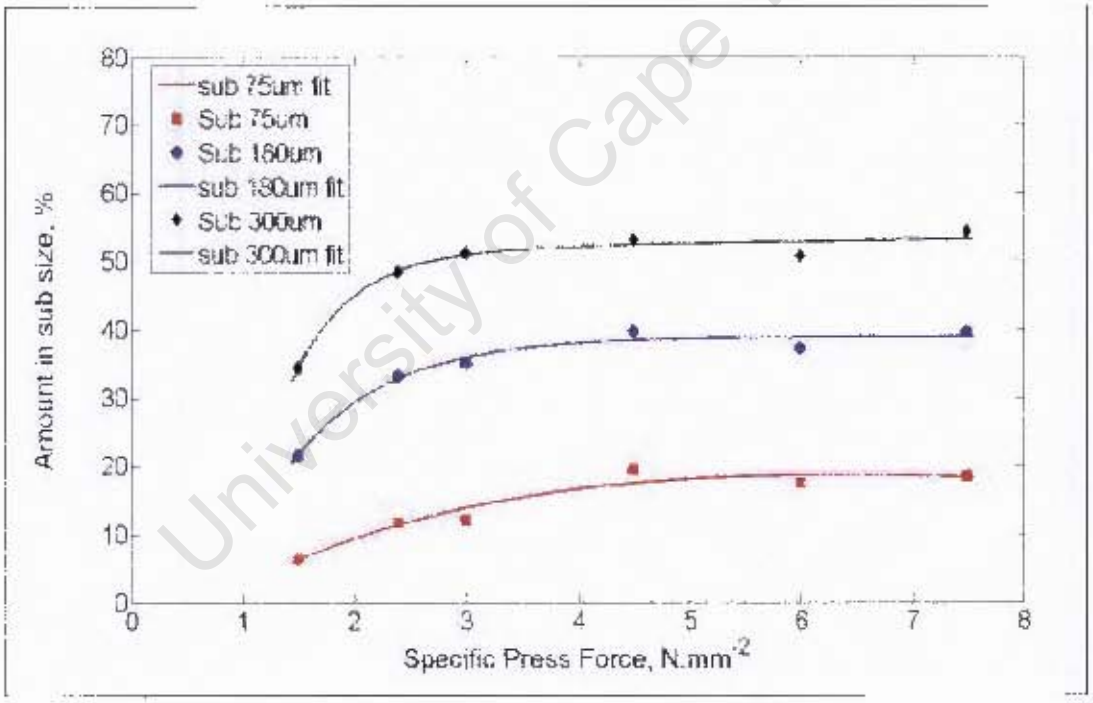

Figure 4.15: Percent passing given size as a function of specific press force

In Figure 4.16, the reduction ratio F50/P50 and F80/P80 is given as a function of specific press force. A more significant change in reduction ratio is visible for the F50/P50 curve than for the F80/P80 curve. However the F50/P50 reduction ratio also shows that the reduction ratio does not increase beyond 4N/mm^2. This confirms that the trend observed for the grind as a function of press force was not due to changes in

the feed size distribution. It can be observed that the F50/P50 curve is a better measure of the reduction ratio than the F80/P80 curve. Both these trend lines also show little increase after 4 N/mm^2.

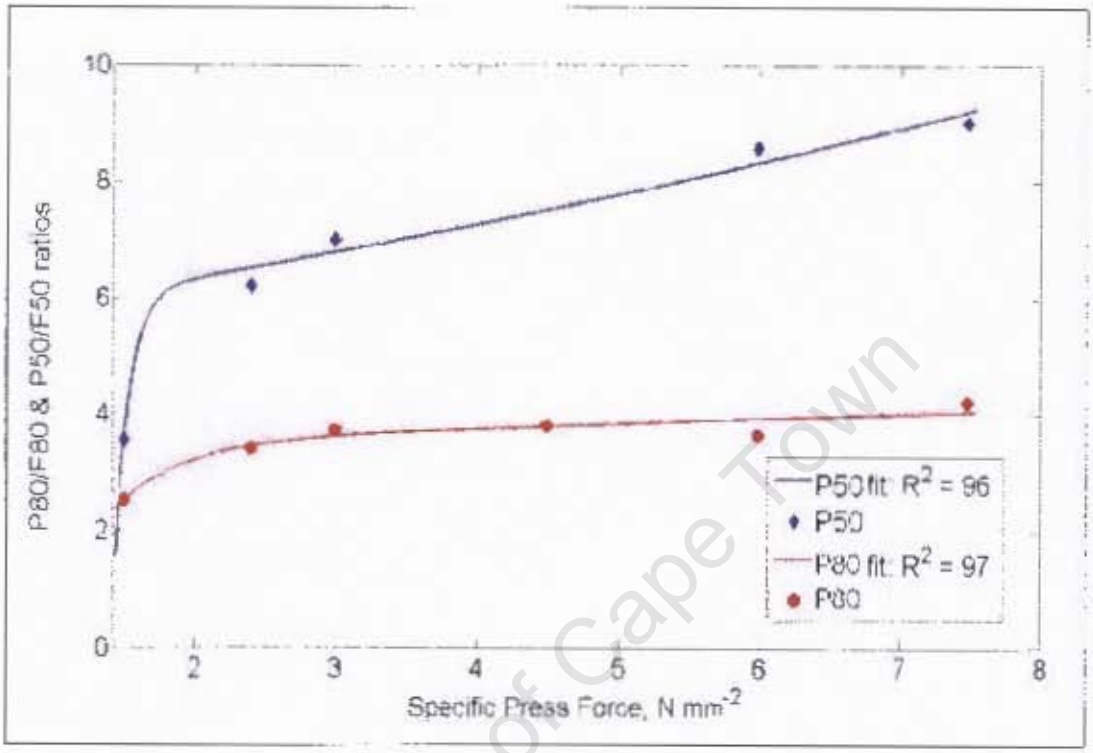

Figure 4.16: Reduction ratio as a function of specific press force

This implies that operation at very high pressures may result in higher energy consumption, while the same reduction ratios could be achieved at lower pressures. This phenomenon may be the result of the resistance of the material that becomes significant when the compression of the material reaches a certain threshold. It also may be the result of the edge effects that become significant at higher pressures when more material moves out to the sides of the rolls when the pressure increases.

4.4 MINERALOGY

Mineral liberation analyses (MLA) were conducted on certain samples to determine the liberation of PGM grains in key samples and to compare it with other samples that were broken under different conditions. Initially the chemical compositions of all the samples from breakage experiments that were carried out were determined. The objective of the chemical assays was to obtain useful information about samples that could be used to narrow down the number of samples for MLA.

For statistical reasons, no impact breakage or abrasion samples were analysed, because the fraction of fines obtained from these modes of breakage per test was insufficient for these analyses. A UG2 sample that was broken in the AG mill was used as a combination of impact and abrasion breakage. This mode of breakage produces enough sample mass to carry out a statistically significant analysis. A UG2 sample broken in the HPGR was also analysed. This was done in order to make a comparison between the compositions of the screened products of the two modes of breakage. Merensky samples that were crushed in a HPGR under various operating conditions were also analysed. A detailed discussion is given in this section.

The liberation classes of certain samples from the HPGR and the AG mill products were analysed with a Mineral Liberation Analyser (MLA). The MLA provides useful information about the number of PGM particles found in each liberation class as well as an indication of the volume of these particles. There are six liberation classes and a description of each liberation class is given in Table 4.10. An example of the modes of occurrence in these six classes is given in Figure 4.17.

Table 4.10: Description of Liberation classes

L	Liberated PGMs
SL	PGMs associated with liberated BMS (Base Metal Sulfides)
AG	PGMs attached to Silicate or Oxide gangue particles
SAG	PGMs associated with BMS attached to Silicate or Oxide gangue particles
SG	PGMs associated with BMS locked in Silicate or Oxide gangue particles
G	PGMs locked within Silicate or Oxide gangue particles

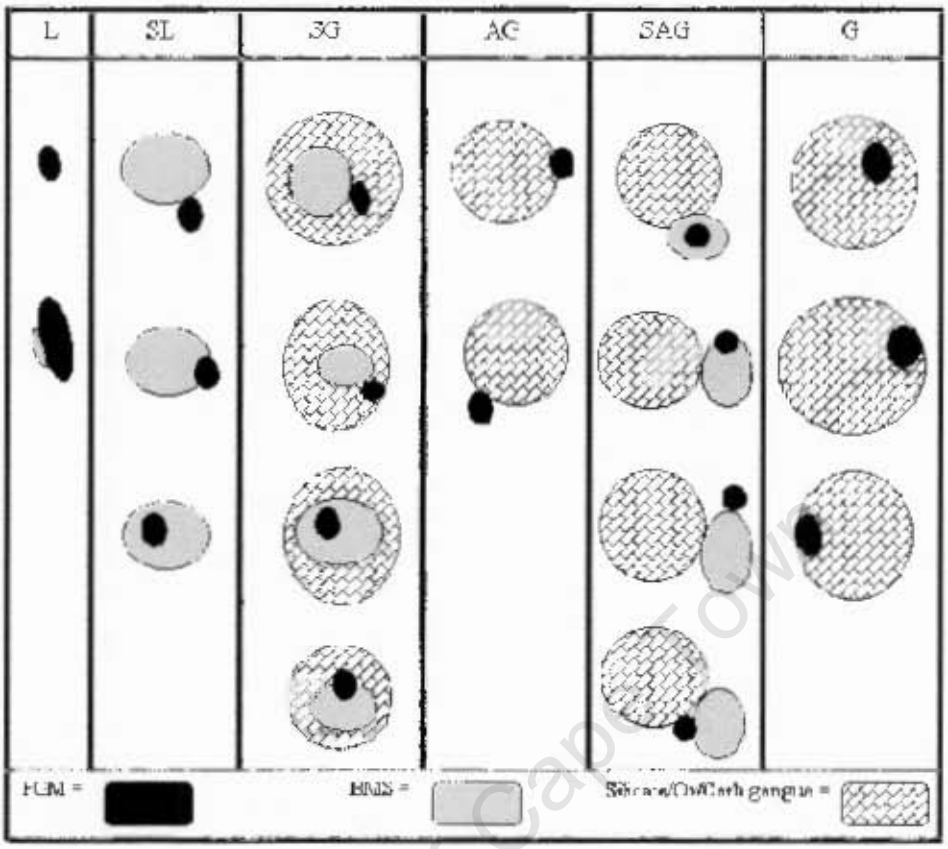

Figure 4.17: Example diagrams of PGM modes of occurrence

The main minerals present in the UG2 and Merensky ore that were used for this project that occur in association with PGMs are given in Table 4.11 and Table 4.12. The Group classification indicates the floatability of the mineral where the sulphides are the fastest floating and semi-metals the slowest.

Table 4.11: Main minerals in UG2 that occur in association with PGMs

Mineral name	Formula	% of PGMs	Group
Cooperite	**PtS**	34	Sulphides
Tetraferroplatinum	**PtFe**	17.5	Alloys
	PtPdS	16	Sulphides
	PtRhCuS	8	Sulphides
Potarite	**PdHg**	4.5	Semi-metals
Zvyagintsevite	**PtPb**	4.5	Alloys
	PtRhAsS	2.5	Sulphides
	PdPb	2.5	Alloys
Michenerite	**PdBiTe**	1.5	Semi-metals
	Other	9	

Table 4.12: Main minerals in Merensky that occur in association with PGMs

Mineral name	Formula	% of PGMs	Group
Tetraferroplatinum	**PtFe**	37.8	Alloys
Cooperite	**PtS**	15.8	Sulphides
Moncheite	**PtTe**	13.8	Semi-metals
Kotulskite	**PdTe**	6.5	Semi-metals
Maslovite	**PtBiTe**	3.8	Semi-metals
	PtAs	2.5	Semi-metals
	Other	20	

4.4.1 COMPARISON OF LIBERATION ACHIEVED ON A UG2 SAMPLE WITH THE HPGR AND AG MILL

Table 4.13 shows the assays that were performed on the UG2 samples. The rest of the data that was generated by the ICP1 analysis can be seen in Appendix D and include the percent Mg, Al, Ca and Fe in these samples.

Table 4.13: UG2 impact & abrasion and bed breakage

Size	Bed breakage		Impact & Abrasion	
	Si (%)	Cr (%)	Si (%)	Cr (%)
300 µm	11.80	14.75	9.75	17.00
212 µm	7.20	20.50	6.96	20.40
150 µm	7.52	20.20	7.03	21
106 µm	9.30	18.35	9.28	18.5
75 µm	12.00	14.60	10.8	16.3
53 µm	13.20	13.20	12.3	14.5
38 µm	13.20	12.80	12.25	14.35

In Table 4.13 it can be observed that the majority of the chromites are in the -212+106µm size range. This is because the natural grain size of the chromites is closest to those two classes. Nevertheless, the –38µm fraction was chosen for the MLA in order to compare the liberation that is achieved with an AG mill to HPGR because that is the fraction that is already of recoverable size.

The volume % of grains is given in Figure 4.18 to compare the liberation classes of the HPGR product sample to those of the AG mill product sample.

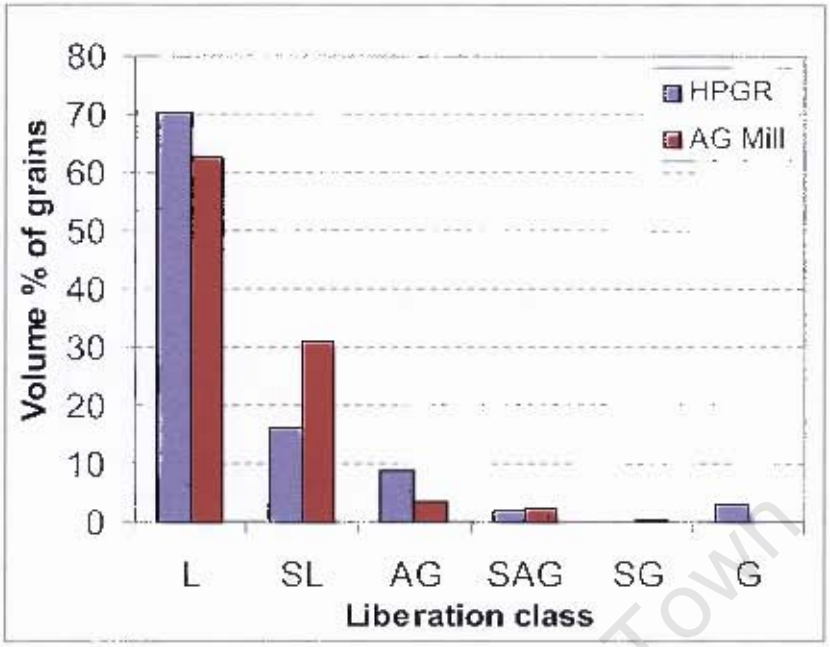

Figure 4.18: Volume % of grains for each liberation size class for the HPGR and AG mill samples of UG2 ore (sub 38µm)

From the % volume the HPGR product samples show better liberation of the PGM than the AG mill product sample in the L class. However the AG mill product had a higher volume of liberated particles in the SL class. The presence of nuggets in the sample may skew the results. It is therefore recommended that both the number of PGM grains observed and the volume % be considered in the analysis for each liberation class. A comparison of the liberation classes in terms of the cumulative number of PGM grains from the HPGR product sample to that of the AG mill product sample is given in Figure 4.19. The liberation classes are presented as a proxy for the grade and the cumulative number of grains as a proxy for recovery to get a pseudo grade recovery curve (Becker *et al.*, 2007).

It can be seen that similar results to what was observed for the volume % were obtained with the number of grains. From the illustration in Figure 4.17 it can be seen that the PGM grains are exposed only in the L and SL liberation classes. Therefore if the number of grains in the L and SL classes in Figure 4.19 is considered, the total for the HPGR product is 75 grains while that for the AG mill product sample is 85 grains. It can be concluded that for this ore the AG mill gave better liberation in the sub

38µm size fraction. However, the size distribution of the sub 38µm material was never determined. If an extrapolation is made on both the HPGR and the AG mill size distributions, the sub 38µm AG mill sample is finer than the HPGR sample. Therefore it may be the case that the sub 38µm AG mill sample is liberated much better, but not necessarily recoverable as a large fraction of the AG mill sample may be sub 10µm and difficult to recover via flotation.

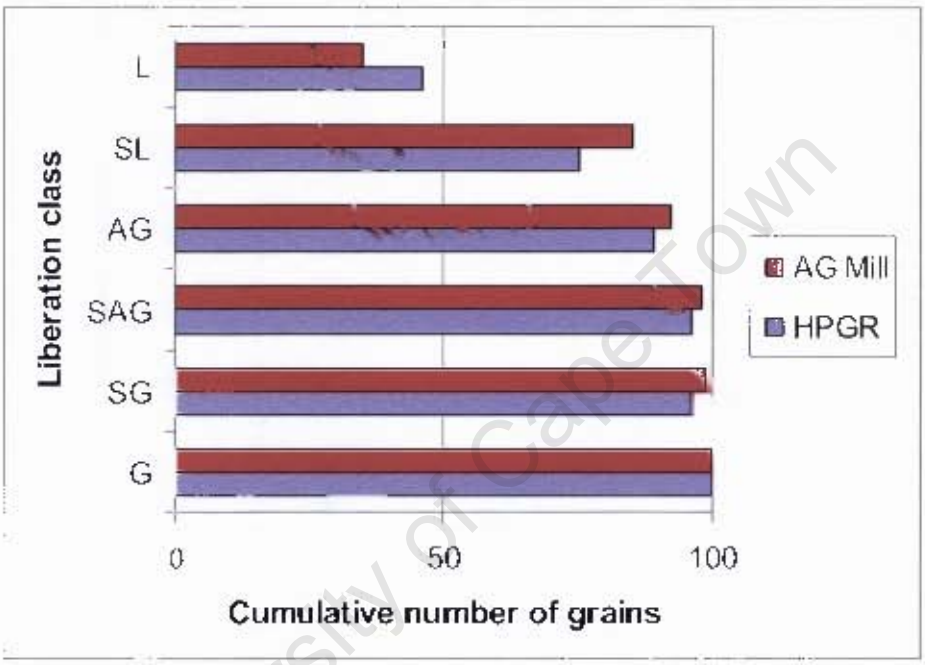

Figure 4.19: Pseudo grade recovery curve for the HPGR and AG mill sample for UG2

The volume % and the number of grains per hundred found in each liberation class for the HPGR and AG mill product sample for UG2 is given in Appendix E.

4.4.2 COMPARISON OF THE EFFECT OF OPERATING PRESSURE ON LIBERATION ACHIEVED WITH AN HPGR

Fire assay for PGM analyses were conducted on all the Merensky reef samples that were broken in the HPGR. This was done to determine the effect of the different specific press forces that were applied on the composition of the screened product

samples. Table 4.14 shows the PGM and Au data as cumulative percent of total PGM and Au for each of these operating pressures and the cumulative size distribution data. The coefficient of variance between the 48 bar sample and the 150 bar sample is also shown.

Table 4.14: Merensky fire assay for PGM data for 30 to 150 bar

PGM + Au (% of total PGM + Au)							48 and 150
Size (µm)	30 PGM	48 PGM	60 PGM	90 PGM	120 PGM	150 PGM	Co of var (%)
10000	100.0	100.0	100.0	100.0	100.0	100.0	0
1000	84.0	90.4	89.2	89.8	74.7	87.8	2.89
425	65.8	78.0	78.0	72.2	64.4	74.2	5.07
212	48.6	64.7	64.8	57.0	54.4	62.2	3.98
150	33.6	47.3	48.7	38.8	40.4	50.5	6.55
75	19.6	**35.0**	36.3	25.8	20.6	**38.3**	8.97
38	0.0	**20.2**	21.2	14.6	10.6	**22.0**	8.63
mass (%)							48 and 150
Size (µm)	30 bar	48 bar	60 bar	90 bar	120 bar	150 bar	Co of var (%)
10000	100	100	100	100	100	100	0
1000	61.56	69.75	73.66	66.82	71.95	68.52	1.79
425	42.47	48.43	50.52	46.95	49.16	55.35	13.40
212	28.22	31.38	32.22	33.94	32.69	32.10	2.26
150	22.30	24.50	24.67	25.38	24.74	24.53	0.11
75	13.26	14.20	13.14	15.14	14.73	14.19	0.10
38	4.61	3.50	2.69	7.35	7.74	5.73	51.24

In Table 4.14 the coefficient of variance is small except for the smallest mass % value. However, the g/t PGM values were similar. These runs were repeated and the product samples were also analysed. The results were similar and therefore repeatable and can be seen in Appendix E. Three feed samples were taken as belt cuts. They were also screened and analysed and the data can be seen in Appendix E. The liberation of four Merensky samples was determined. They were the -38µm and –75+38µm fractions crushed at a higher specific press force of 7.5N/mm^2 (150 bar) and at a lower specific press force of 2.5 N/mm^2 (48 bar).

In Figure 4.20 it is observed that a higher percentage of the volume is liberated in the sample broken under higher specific press force in the L and the SL liberation classes.

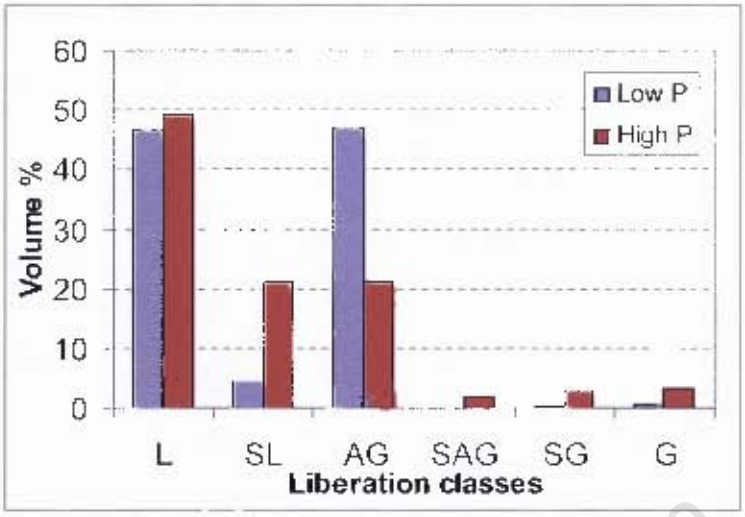

Figure 4.20: Volume % of grains for each liberation class for the HPGR Lower and Higher Specific Press Forces of Merensky ore in the sub 38µm size class

However the number of grains that occurs in the lower P sample is higher than the number of grains in the higher P sample of the L class. The opposite is true for the SL class. This can also be observed in Figure 4.21 where the cumulative number of grains for each liberation class is shown.

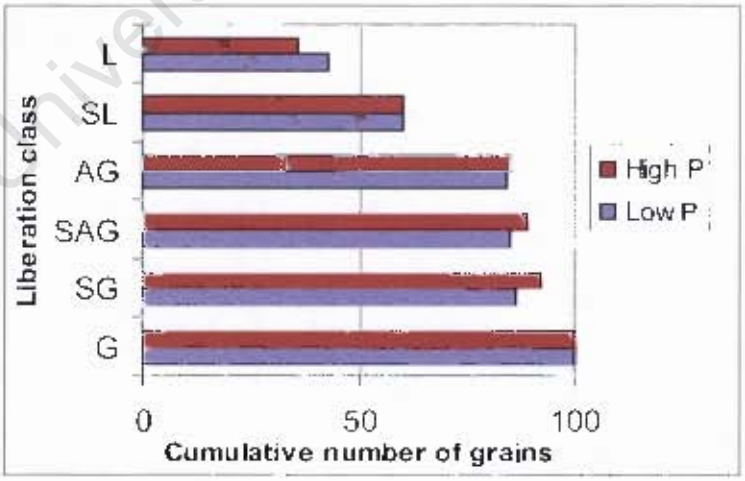

Figure 4.21: Pseudo grade recovery curve for the HPGR Lower and Higher Specific Press Force samples for Merensky ore in the sub 38µm size class

The total number of PGM grains occurring in both the L and SL classes together is equal. It may therefore be concluded that the effect of operating pressure on the liberation of this size class is not significant.

The volume % and the number of grains per hundred found in each liberation class for the HPGR product sample for the sub 38µm size fraction of the Merensky sample is given in Appendix E. Therefore if both volume and number of grains are considered, the higher pressure gave better liberation of the sub 38µm fraction. However, the extent to which these samples will not be recoverable is not known and the higher pressure may produce better liberation but those particles may not be recoverable.

For the -75+38µm size class, it was observed that the Volume % of the samples broken at Lower Pressure and Higher Pressure is similar in the L class but the Lower Pressure sample's Volume % is higher in the SL class. This can also be seen in Figure 4.22.

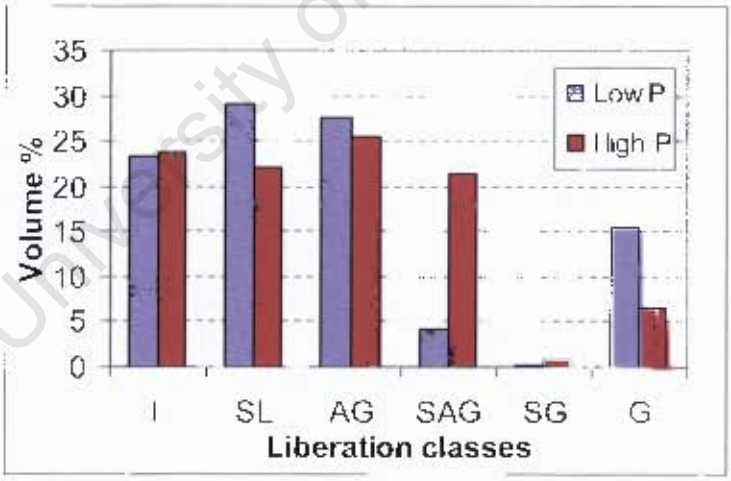

Figure 4.22: Volume % of grains for each liberation size class for the HPGR Lower and Higher Specific Press Force of Merensky ore in the size class –75+38µm

In Figure 4.23 it was observed that the sample broken under higher pressure has a higher number of particles in the L class than the lower pressure sample, but the opposite is true for the SL class.

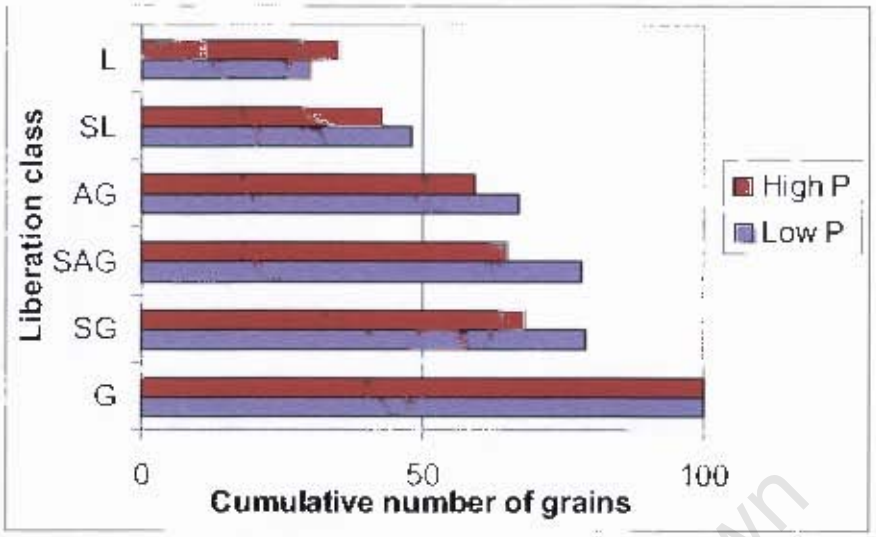

Figure 4.23: Pseudo grade recovery curve for the HPGR Lower and Higher specific Press Force samples for Merensky ore in the size class – 75+38µm

Figure 4.23 therefore shows that the lower specific press force sample is better liberated as it has a higher cumulative number of grains in the SL class. The volume % and the number of grains per hundred found in each liberation class for the HPGR product sample for the -75µm +38µm size fraction of the Merensky sample is given in Appendix E.

Therefore the –38µm fraction of the higher specific press force sample was better liberated, and the 75+38µm fraction of the lower specific press force sample was better liberated. But the unrecoverable fraction of the sub 38µm sample is unknown for the higher pressure sample. In addition to this, the energy consumption of the HPGR is significantly lower at a lower specific press force and it is therefore advisable to operate at the lowest possible pressure that will give the required grind. This is in agreement with the findings of van Drunick and Smit, 2006 that the best flotation results were obtained in association with low grinding pressures for all the ore types that were tested. The mineralogy therefore supports their findings.

4.5 COMPARISON OF SIZE DISTRIBUTIONS FROM DIFFERENT MODES OF BREAKAGE

4.5.1 UG2 ORE

The product particle size distributions of UG2 ore that were produced by various modes of breakage are given in Figure 4.24. The "Chipping and Abrasion" mode was achieved by grinding angular rocks (of three discrete sizes between –150 and +38mm with a size class empty in between) in the pilot mill with a large diameter for 11 minutes. The "Mostly Abrasion" mode was achieved by grinding a similar batch of rounded rocks in the pilot mill with the large diameter for 2 minutes and the "Abrasion" mode is from grinding rounded rocks (-50+19mm) in the smaller torque mill for 20 minutes. The "Impact" mode is from the drop weight tester the product of the -106+75mm rocks is shown at an input energy of 0.4kWh/t and both "Bed breakage" modes are from the HPGR, but the "N" is for a normal feed size distribution of -12mm and the "T" is for a truncated feed size distribution of -12+4mm.

Test work on the various modes were conducted over a range of input energies, so direct comparison of the amount of breakage is not meaningful. The comparison conducted here is of the form of the product distribution, into what size range the product reports for the different types of breakage.

If we consider the "Abrasion" mode, the increase in cumulative mass percent between 0.038 and 0.2 mm can be observed. Between 0.2 mm and 10 mm hardly any increase in the cumulative mass percent can be observed. After 10 mm, a sharp increase up to 100% of mass at 50 mm can then be seen. This means that the rounded rocks that were initially placed in the mill did not undergo much impact breakage or chipping. Only fines abraded off the surface of the rounded pebbles. The "Mostly Abrasion" curve has a similar shape, but the increase from the fines up to the original particle sizes is not as sharp as the "Abrasion" curve. Therefore chipping took place to some extent and caused the slight increase in the cumulative mass percent between 9 and 20

mm. This can be explained by the large diameter (1.68m) of the pilot mill that was used for this test in comparison with the smaller diameter (0.6m) of the torque mill that was used to achieve the "Abrasion" mode of breakage.

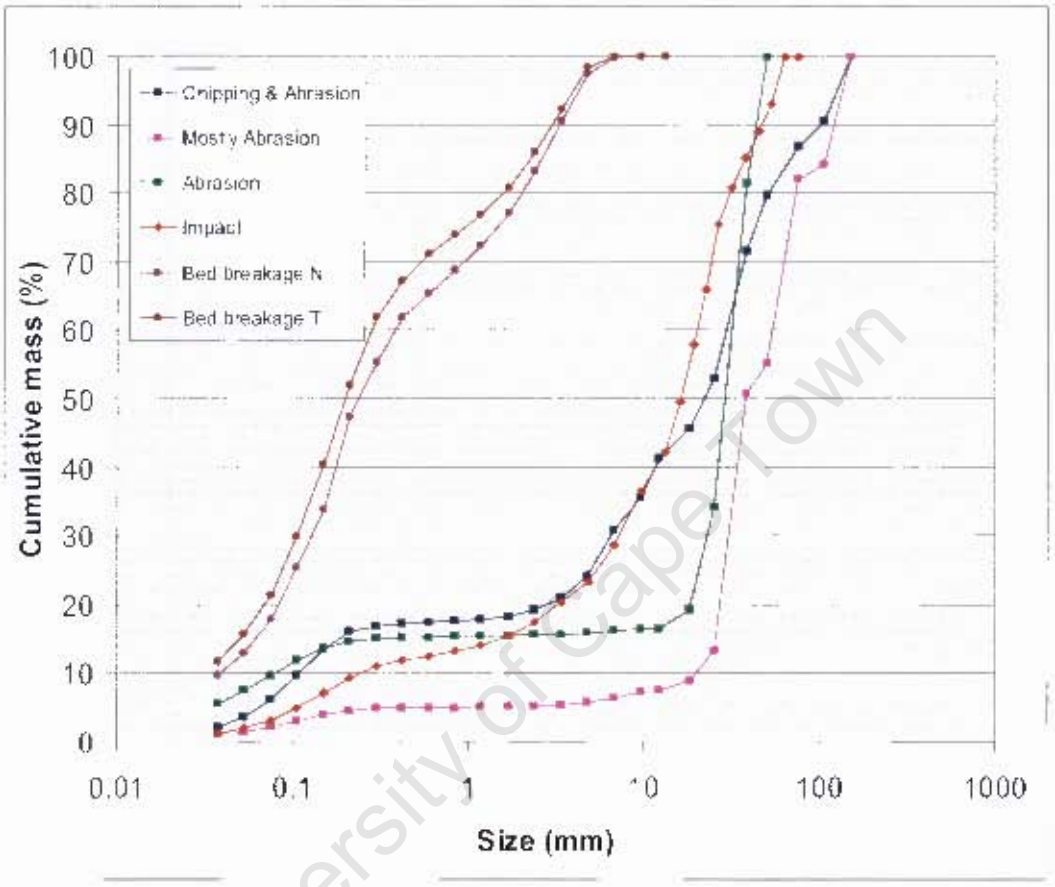

Figure 4.24: Product Particle size distributions of UG2 ore produced by various modes of breakage

The red line in Figure 4.24 represents the product particle size distribution of the product of the drop weight test. In this mode of breakage no progeny particles remained in the same size class as the original rock. The increase in cumulative mass is more consistent throughout the size range. The shape of the "Chipping and Abrasion" mode looks like a combination of the "Abrasion" and the "Impact" modes. This is because angular rocks were used for this test and extensive chipping and impact breakages takes place before abrasion takes over as the primary mode. All of these four curves show the bend around 0.2 mm and that is approximately the size of the natural chromite grain. The two left most curves that can be seen in Figure 4.24

are the product size distributions from the HPGR. These curves show that with bed breakage there is no formation of a critical size that is difficult to break as in the abrasion and impact modes that are attributed to mills. The truncated feed produced more fines than the feed with a natural size distribution and consumed about 0.8kWh/t more energy.

In Figure 4.25 the same product particle size distributions can be seen but with normalised size fractions. The original particle size is 1 and the product particle sizes are fractions of this top size. The bed breakage of the HPGR produces a far higher reduction ratio than the other modes of breakage.

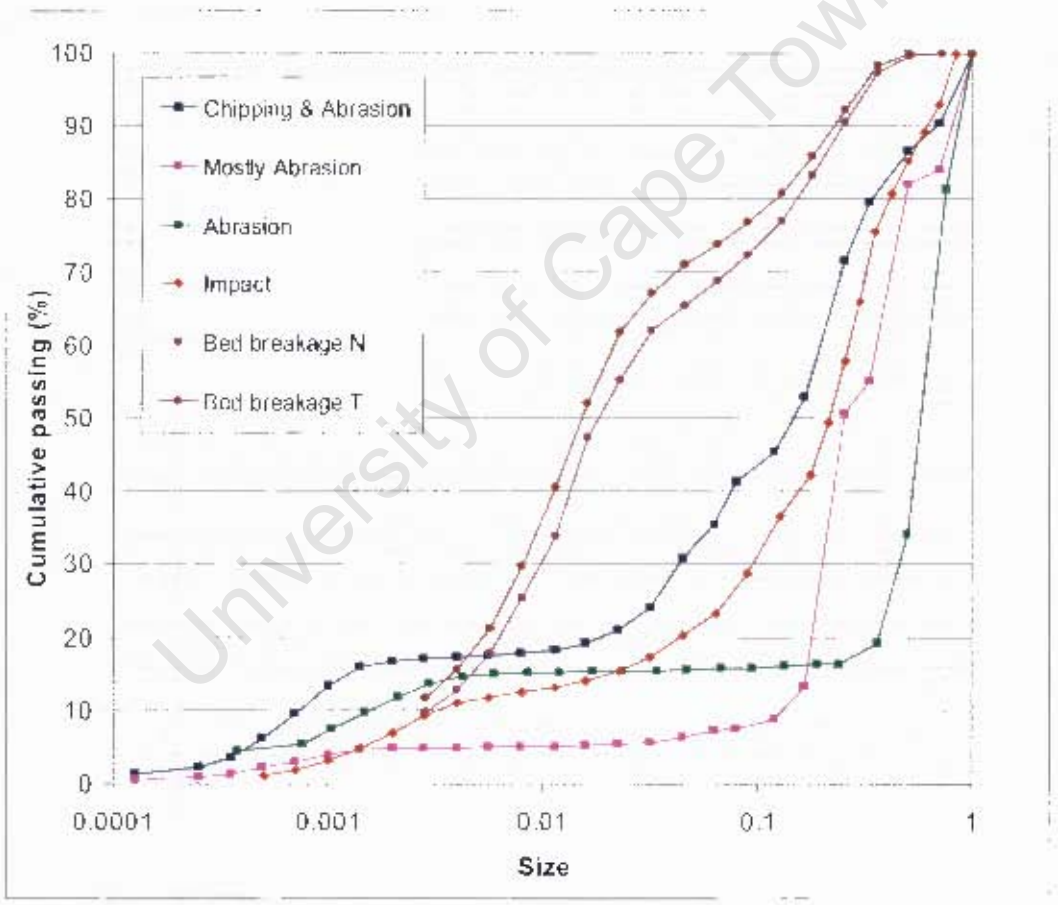

Figure 4.25: Product Particle size distributions of UG2 ore produced by various modes of breakage (normalised sizes)

In Figure 4.26 the mass percent retained in each size fraction can be seen. The particle sizes are given as a fraction of the top size where the majority of the product particles from each mode of breakage can be observed. The sharp peaks at the coarse end are for the abrasion mill with a mixed feed of three particle sizes, so have no physical significance other that reflecting the original feed size. The majority of the product particles from the "Abrasion" mode remained very close to the original size as the curve peaks around 0.9 and fines were produced and can be observed around 0.002. The curve of the "Mostly Abrasion" mode shows that the majority of the rounded rocks stayed in the three original size classes and fines formed around 0.001.

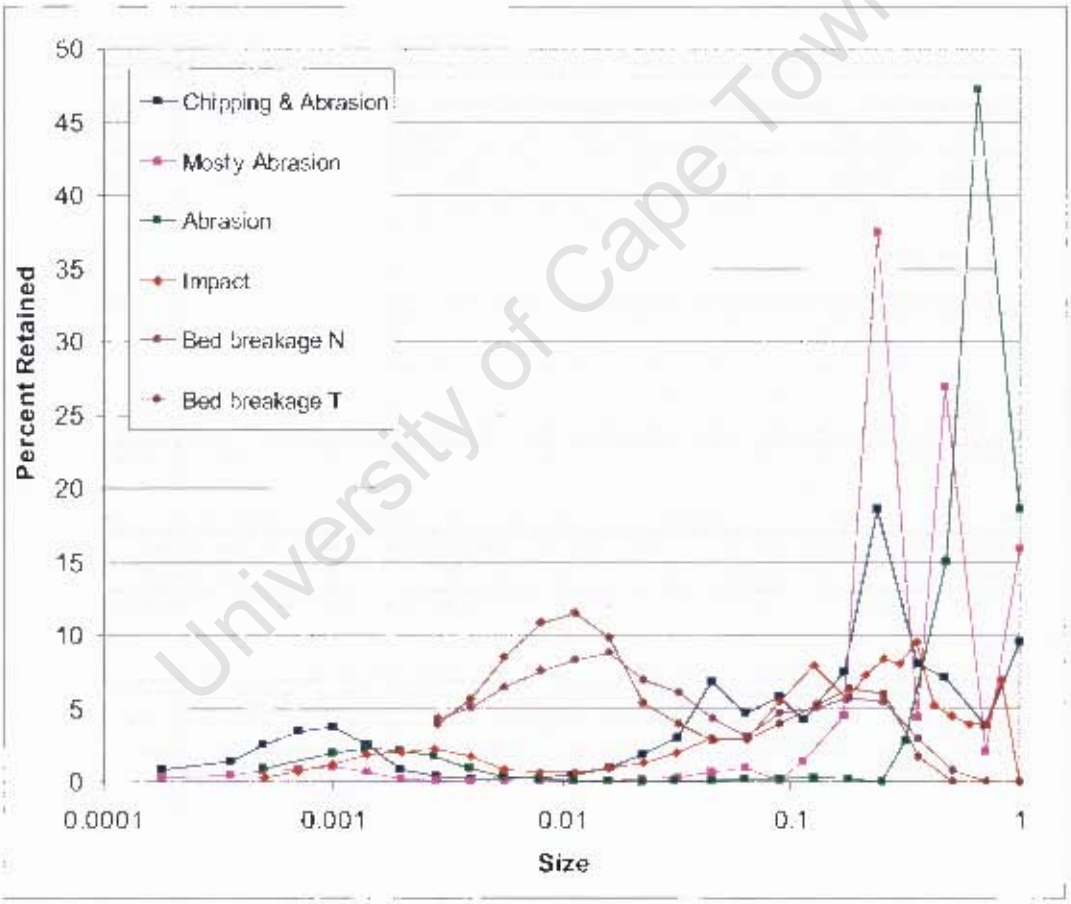

Figure 4.26: Mass percent retained per size

The "Chipping and Abrasion" mode peak has lost a considerable number of the top-size rocks, with true product below the peak at 0.25. There is significant material in the intermediate size range down to about 0.025 – representing chipped fragments,

and then a peak at 0.001 of fines production. Therefore, the angular rocks chipped significantly and also formed some fines due to abrasion. The "Impact" curve is more evenly spread and it is noticeable that no mass remained in the original size. This mode caused the formation of some fines around 0.003. Both "Bed breakage" curves show that fines were produced extensively and that no mass remained in the original particle size. As the HPGR feed size was so much finer than the other feed particles (about one tenth the size), this normalised size reduction can be a bit misleading. In absolute size, it peaks at the same size range as the fines production from the other modes of breakage.

4.5.2 TARGET GOLD ORE

The product particle size distributions of Target Gold ore that were produced by various modes of breakage are given in Figure 4.27. The "Mostly Abrasion" mode was achieved by grinding rounded rocks (of a normal size distribution between –106 and +38mm) in the pilot mill with a large diameter for 21 minutes. The "Abrasion" mode was achieved by grinding rounded rocks (-50+19mm) in the smaller torque mill for 50 minutes. The "Impact" mode is from the drop weight tester. The product size distribution of the -106+75mm rocks is shown for an input energy of 0.4kWh/t and the "Bed breakage" mode is from the HPGR, a normal feed size distribution of -12mm was the feed size.

If we consider the "Abrasion" mode, a very slight increase in cumulative mass percent between 0.038 and 0.1 mm can be observed. Between 0.1 mm and 25 mm no increase in the cumulative mass percent can be observed. After 25 mm a sharp increase up to 100% of mass at 50 mm can then be observed. This means that the rounded rocks that were initially placed in the mill did not undergo any impact breakage or chipping. Only fines abraded off the surface of the rounded pebbles, producing about 4% mass loss. The "Mostly Abrasion" curve has a similar shape, producing about 10% fines. The increase from the fines up to the original particle sizes is not as sharp as the "Abrasion" curve therefore chipping did take place to some extent and caused the slight increase in the cumulative mass percent between 20 and 30 mm. This can be explained by the larger diameter (1.68m) of the pilot mill that was used for this test in

comparison with the smaller diameter (0.6m) of the torque mill that was used to achieve the "Abrasion" mode of breakage.

The red line in Figure 4.27 represents the product particle size distribution of the product of the drop weight test. In this mode of breakage no progeny particles remained in the same size class as the original rock. The increase in cumulative mass is more consistent throughout the size range. The left most curve that can be seen in Figure 4.27 is the product size distribution from the HPGR. This curve shows that with bed breakage there is again no formation of a critical size that is difficult to break as in the milling modes. The bed breakage produces a consistent increase in cumulative mass percent across the size range.

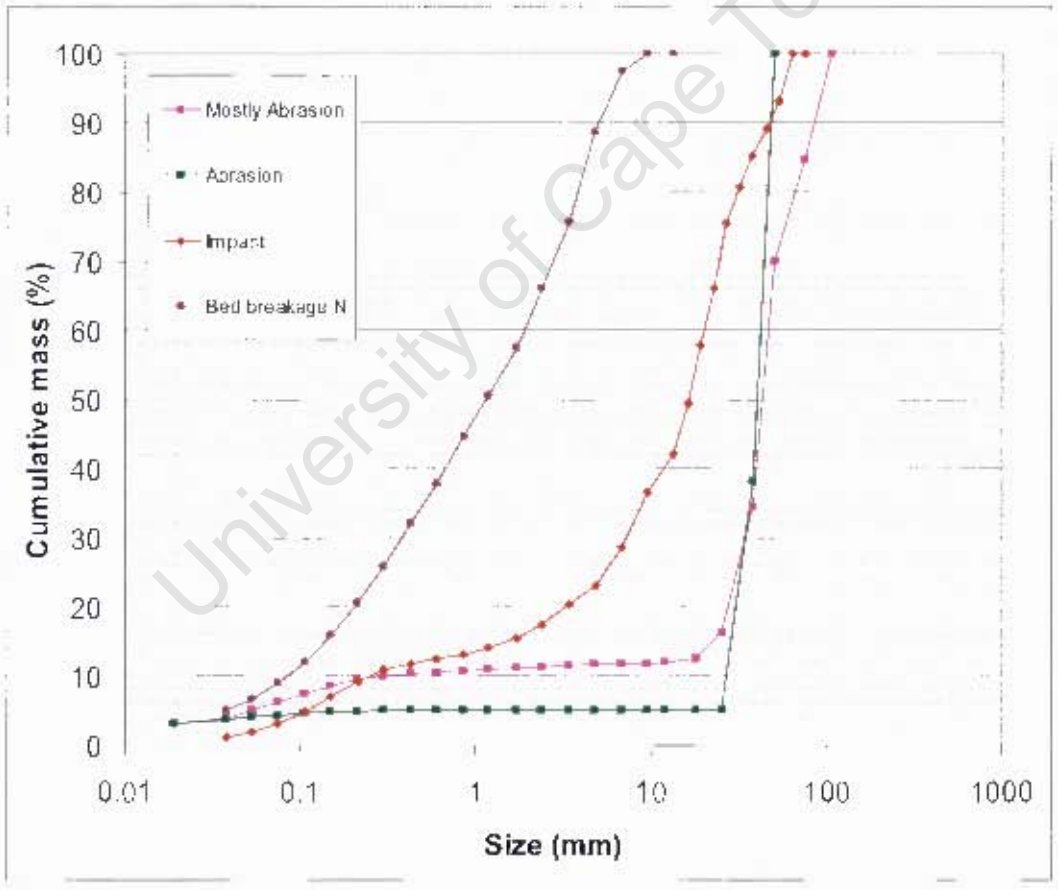

Figure 4.27: Product Particle size distributions of Target Gold ore produced by various modes of breakage

In Figure 4.28 the same product particle size distributions can be seen but with normalised size fractions.

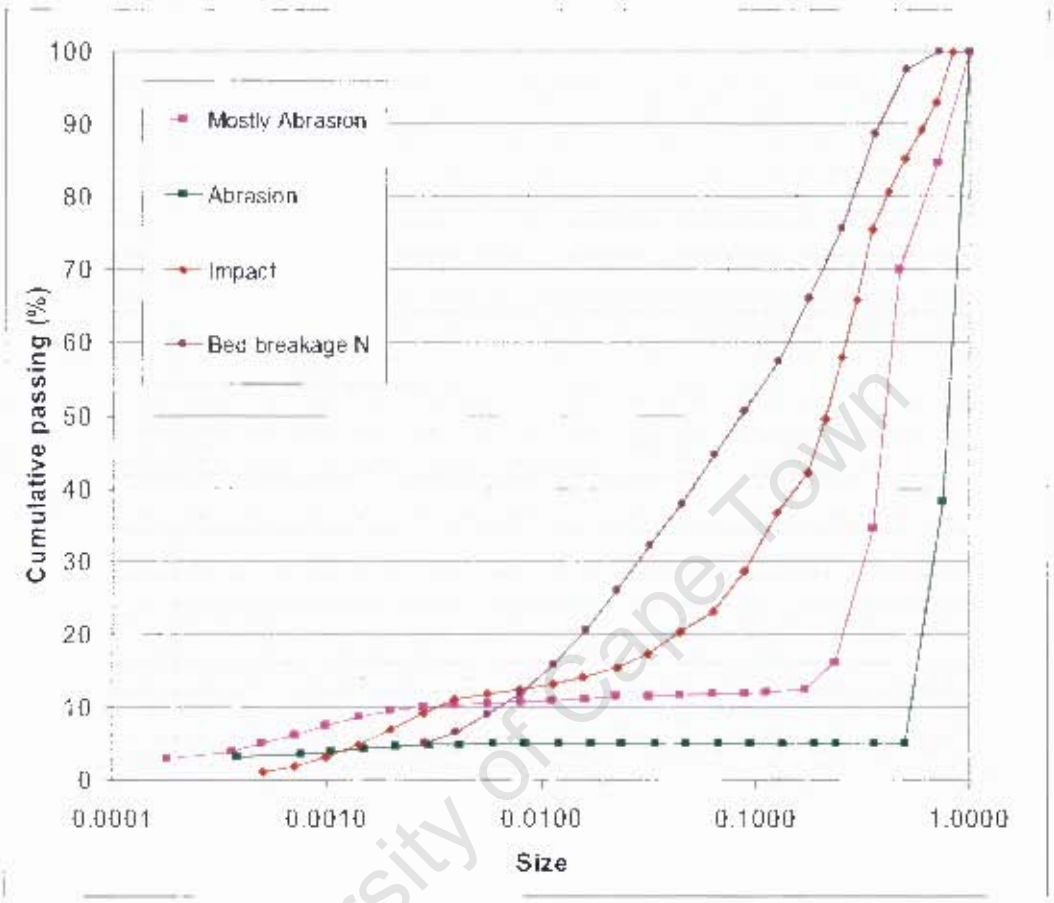

Figure 4.28: Product Particle size distributions of Target Gold ore produced by various modes of breakage (normalised sizes)

In Figure 4.29 the mass percent retained in each size fraction can be seen. The particle sizes are given as a fraction of the top size where the majority of the product particles from each mode of breakage can be observed. All the product particles from the "Abrasion" mode remained in the original size as the curve peaks at 1 and the second highest point on the curve is the other size that was originally placed in the mill and the sum of these two points is 95% of the mass. Therefore very little fines were produced and they are around the 0.001 size. The curve of the "Mostly Abrasion" mode shows that the majority of the rounded rocks remained in the three original size classes, about 4% by mass of chipped fragments in the 0.2 size class, and

fines formed around 0.001. The "Impact" curve is more evenly spread, peaking at around 1/10th of the original size, and it is noticeable that no mass remained in the original size. This mode caused the consistent formation of fines across the size range. The "Bed breakage" curve shows that fines were produced extensively and that no mass remained in the original particle size.

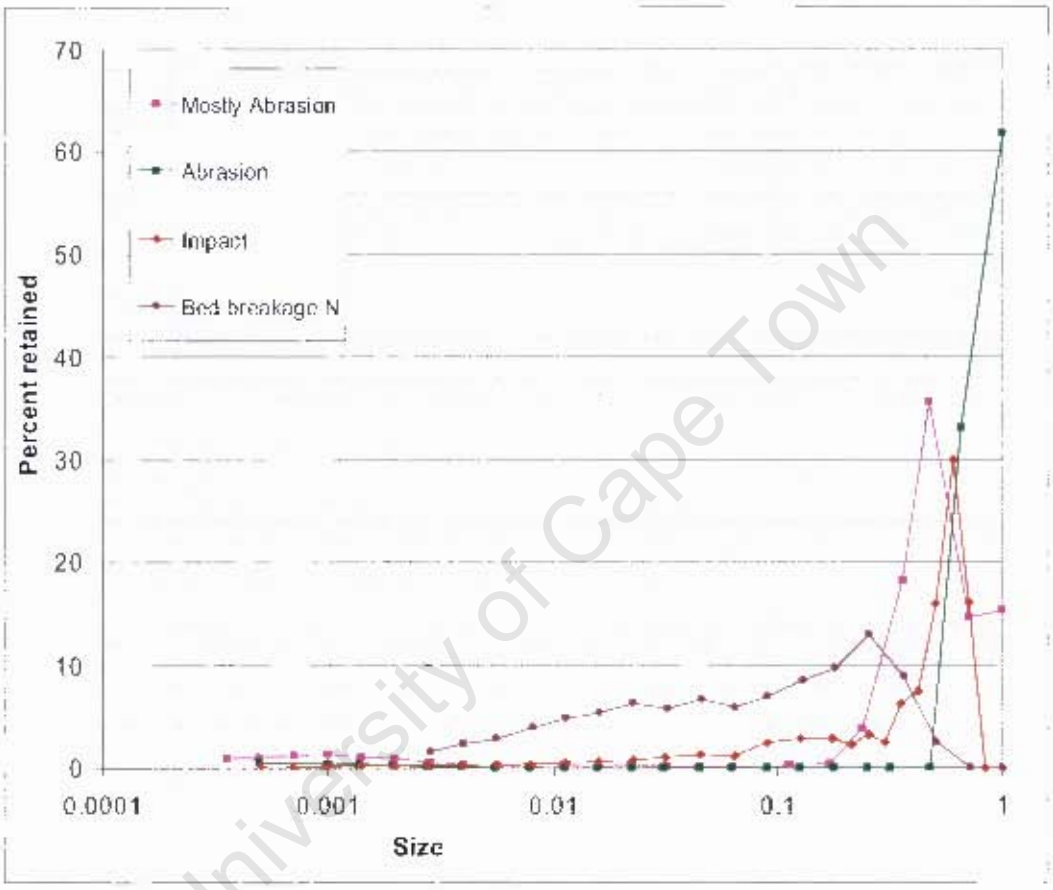

Figure 4.29: Mass percent retained per size

In Figure 4.30 the product particle size distributions of UG2 and Target Gold ore is given for Impact breakage and Bed breakage. Both the "Impact" and the "Bed breakage" tests for these two ore types had the same initial feed size as seen in Figure 4.30. The curves shown in Figure 4.30 are the same ones that were previously shown to compare the different modes of breakage. This is just to compare the results obtained by the two different ore types. The impact tests were at the same energy and the HPGR test at the same pressures, so the degree of breakage is directly comparable between the ores for these tests.

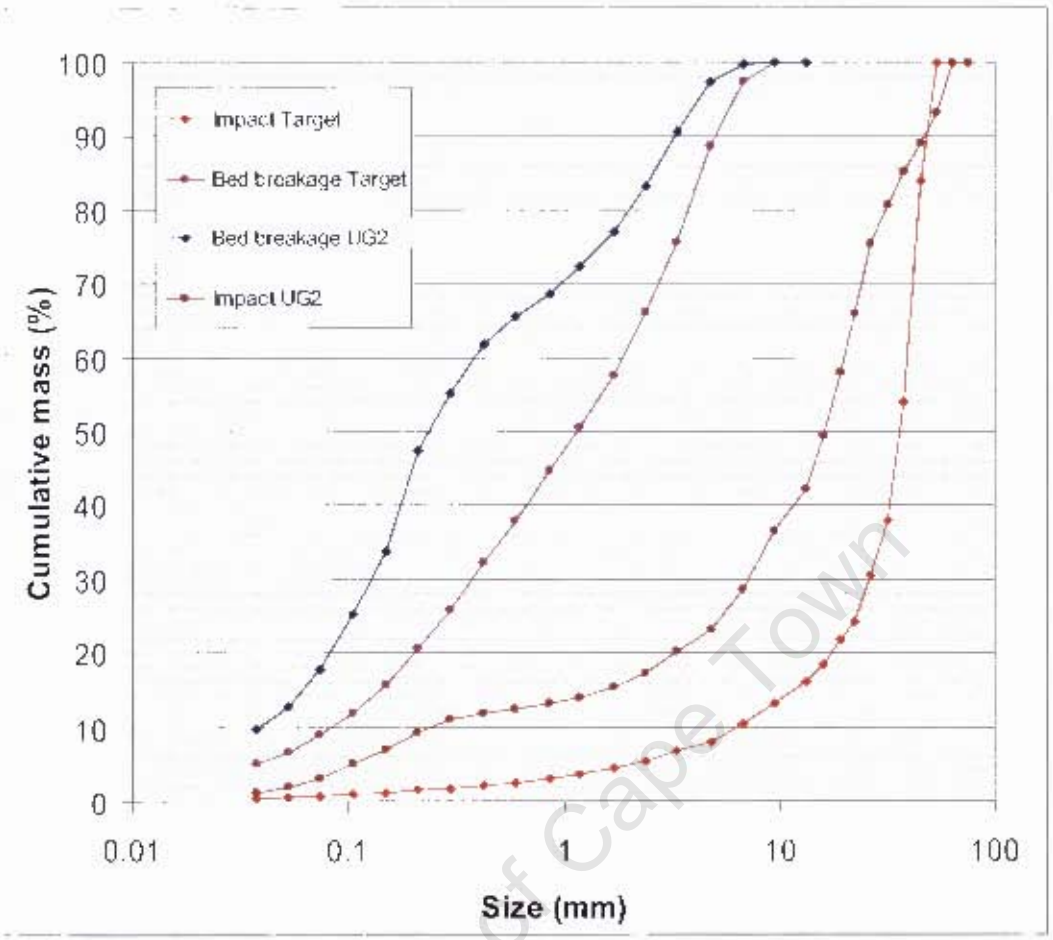

Figure 4.30: Product Particle size distributions of UG2 and Target Gold ore for Impact and Bed breakage

The UG2 is more fragile than the Target Gold ore and can be seen in both the Impact and the Bed breakage size distributions. The Bed breakage produced much more fines with the UG2 ore than the Target ore. Additionally there is a distinct bimodal distribution in the UG2 which is absent from the Target ore – reflecting the difference in the ore structures. The Impact breakage produced more small particles in the size range 0.2 to 30mm but almost the same amount of fines.

Figure 4.31 shows the product particle size distributions of UG2 and Target Gold ore that were produced by abrasion in the pilot mill and the torque mills. These curves are also the same distributions that were used to compare the different modes of breakage that are shown here to compare the influence of the same mode of breakage on the different ore types. The "Abrasion" curves show again how fragile the UG2

(dark blue curve) ore is in comparison with the Target Gold (green curve) ore. Very little fines were produced by the Target ore in comparison with the UG2 ore especially if it is considered that the Target ore test was done for 50 minutes long and the UG2 only for 20 minutes long. The "Mostly Abrasion" size distribution for the Target ore lies above the UG2 size distribution. This is only because the UG2 test was done for only 2 minutes where the Target ore test was done for 21 minutes. However between 10 and 30mm on the "Mostly Abrasion" curve for UG2 already shows some chipping occurring while the Target ore did not chip as much, despite the run length being 10 times longer.

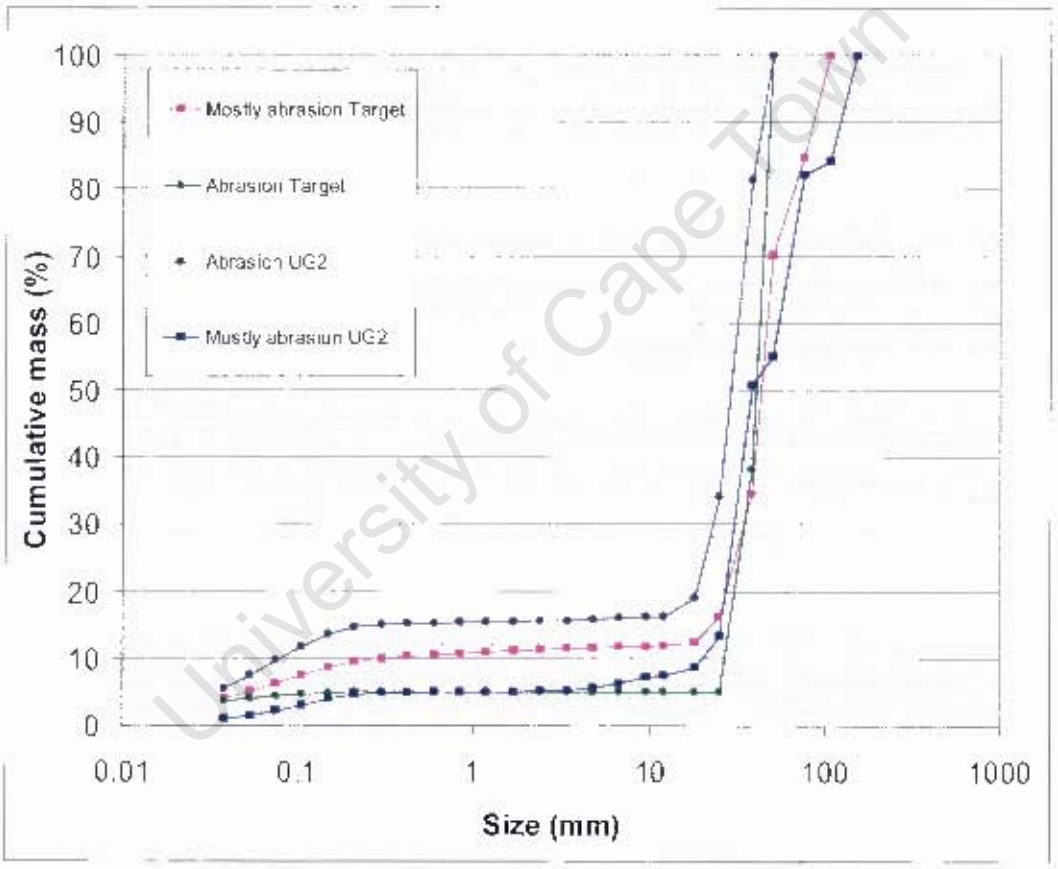

Figure 4.31: Product Particle size distributions of UG2 and Target Gold ore for Abrasion

The difference in the curves of the same mode of breakage for the two different ore types is remarkable for all these modes of breakage. UG2 ore is much more fragile than the Target Gold ore and there are also two distinct mineral phases in the UG2 (chromitite and the hanging wall or footwall) that may have an influence on the

breakage size distribution. When the ore contains a large amount of waste rock (hanging wall and footwall) the breakage size distribution may change from the distinct bimodal shape of the UG2 product and become similar to the normal Rosin-Rammler distribution. The difference at the finer end of the size range may largely be attributed to the breakage of the UG2 around grain boundaries.

RESULTS AND DISCUSSION – *In summary:*

- The drop weight A and b values show that the Target ore is much more competent than the UG2 ore.
- It was observed that when angular rocks are placed in a mill the rate of mass loss out of the mill is quick because of the initial chipping and it then slows down when abrasion becomes the primary mode of breakage and the mass loss becomes constant.
- The mill discharge becomes finer with time as abrasion dominates.
- In the first two minutes the rate of discharge of fines will increase rapidly and then stabilize.
- When big and small rocks are present in the charge, the small rocks may provide a cushioning effect and prevent the bigger rocks from breaking.
- A reduction in mill speed and mill diameter result in fewer impact breakages.
- The shapes of the UG2 size distributions show that the UG2 breaks around the natural grain boundaries of the chromites to some extent for the impact, abrasion and bed breakage.
- For the HPGR, the relation of specific press force to pressure is linear.
- Energy consumption of the HPGR increases with specific press force
- Reduction ratio does not increase beyond a certain specific press force. It was found to be 4N/mm^2 for the Merensky ore.
- The AG mill gave better liberation of the sub 38µm size class.
- For the HPGR the higher pressure gave better liberation in the sub 38µm size class than lower pressure.
- For the HPGR crushing, the lower pressure gave better liberation in the -75+38µm size class as compared with the higher pressure.

- There will be no build up of a critical size of material with bed breakage in the HPGR as is the case with abrasion and impact that are attributed to milling.
- A truncated HPGR feed produces a finer product and consumes more energy.
- UG2 ore is much more fragile than Target Gold ore and produces much more fines, especially below 0.2 mm which is approximately the natural chromite grain size.

5. CONCLUSIONS AND RECOMMENDATIONS

The results that were obtained through the experimental work and analyses conducted are summarized in this chapter. Future test work that could be useful is discussed and some suggestions for this work are made.

5.1 SUMMARY OF SCOPE OF WORK

A study was undertaken to investigate the influence of different modes of breakage and energy inputs on the appearance of the progeny pieces of a broken particle. Impact, abrasion and bed breakage were investigated as three distinctly different modes of breakage. The particle size distributions of the products from the breakage experiments were studied. Mineral liberation analyses were carried out on certain samples in order to determine the liberation of the valuable particles in these samples.

5.2 GENERAL OBSERVATIONS

- The Target ore is much more competent than the UG2 ore. The Target ore abrasion experiments were conducted for longer periods than the UG2 experiments in order to get significant amounts of sample. Fewer impact breakages took place in the torque mill with the Target ore and in two cases only abrasion took place and exactly the same number of rocks were present before and after the 50 minute long run.
- The sub 400µm fraction contains valuable information for some ore types.
- It was observed that when angular rocks are placed in a mill, the rate of mass loss out of the mill is quick because of the initial chipping and it then slows down when abrasion becomes the primary mode of breakage and the mass loss becomes constant.
- It takes some time for the slurry to move through the charge in the pilot mill. The transport is much faster in the smaller Torque mill.
- When big and small rocks are present in the charge, the small rocks may provide a cushioning effect and prevent the bigger rocks from breaking.

- A reduction in mill speed results in fewer impact breakages.
- The thickness of the discharge cake of the HPGR decreases with increasing specific press force.
- The Merensky ore produced bigger and more competent flakes than the UG2 ore.

5.3 CONCLUSIONS

Two distinct modes of breakage were observed in the mills: chipping and abrasion.

The chipping produces a coarser product and is followed by abrasion which produces a finer product but at a slower rate. It was also observed that the discharging slurry samples become finer as abrasion starts taking place to a greater extent instead of chipping. These two modes of breakage may be investigated separately so that these may feed into mill models as separate sets of tests.

The abrasion rate decreases as a function of mill speed.

The rate of abrasion for the experiments conducted at a lower mill speed was significantly slower than the abrasion rates at high mill speed.

Energy consumption of the HPGR increases with specific press force, but the reduction ratio doesn't increase beyond a certain specific press force. The threshold point was found to be 4N/mm^2 for the Merensky ore.

When the specific press force is increased, the energy consumption increases accordingly. But once a certain threshold is reached, the reduction ratio no longer increases with increasing specific press force. Therefore optimum operating conditions must be found in order to avoid energy inefficiencies.

The sub 38µm sample produced by abrasion was better liberated than the sub 38µm sample from bed breakage.

The MLA results showed that for the sub 38µm abrasion sample a bigger volume percent and more particles per hundred were properly liberated in comparison with the sub 38µm bed breakage sample. The size distributions of the sub 38µm fractions are unknown and therefore the recoverability of the bed breakage sample may not be worse, but this was not investigated in the current study.

For the HPGR it was found that operating at a higher pressure gave better liberation in the sub 38µm size class than operating at lower pressure. However, operating the HPGR at a lower pressure gave better liberation than higher pressure for the particles in the -75+38µm size class.

The size distributions of the sub 38µm fractions are unknown and therefore the recoverability of the lower pressure sample may be higher. A particle that is unrecoverable because it is too fine is lost, but a particle that is not liberated may be liberated in down stream processes. The fact that the lower pressure gave better liberation in the -75+38µm fraction shows that operating at a lower pressure is advantageous, especially when feeding into a flotation circuit, where recovery in this size range is optimal. This is in agreement with literature that the best flotation results were obtained at low grinding pressures for all ore types.

The state of liberation for the samples broken by different modes of breakage and intensities of breakage is different.

It was observed from the MLA results that abrasion produced a better liberated product and that lower energy intensities were more advantageous for bed breakage both in terms of liberation and in terms of energy efficiency.

There is a relationship between the energy intensity of the breakage event and the size distribution of the product.

When two rocks are broken with different energy intensities the difference in the progeny particles are visible. This is also true for the whole size distribution. Lower input energies with the impact breakage experiments produced fewer, bigger pieces and a coarser size distribution. The abrasion experiment confirmed this. When a slower mill speed (less energy) was used fewer chipping events were observed and abrasion was the dominant mode of breakage which caused a finer size distribution. The energy intensities that were used with the bed breakage experiments also confirmed that there is a relationship between the energy intensity and the size distribution of the product. However, this was only true until a threshold was reached and the higher energies had no further influence on the reduction ratios of the products. Therefore, there is a definite relationship between the energy intensity of the breakage event and the size distribution of the product. This relationship will be different for the various modes of breakage.

There is a relationship between the mode of breakage and the size distribution of the product.

The method that was used to break the rocks influenced the particle size distribution of the final product. Size distribution data from the various modes of breakage showed that in the HPGR there is no formation of a critical size that is difficult to break as in the abrasion and impact modes that are attributed to mills.

This phenomenon can easily be observed in the bigger particles from the different modes of breakage, but this was also found to be true on the micro scale. The fines that were produced during abrasion were different from the fines produced by bed breakage. The sub 38µm fines from the abrasion tests were much finer than the sub 38µm fines from the bed breakage tests. The influences of the various modes of breakage were also observed in the extent to which the platinum group minerals were liberated in these samples.

The feed size distribution of the HPGR influences the energy consumption and final grind.

The HPGR product where the feed was truncated at 4mm produced a finer product size distribution and consumed approximately 0.8kWh/t more energy.

UG2 ore is more fragile than Target Gold ore.

The UG2 ore produces finer particle size distributions than the Target Gold ore even when the Target Gold abrasion tests were done for a much longer time and therefore consumed more energy. The difference at the finer end of the size range may largely be attributed to the breakage of the UG2 around grain boundaries.

5.4 RECOMMENDED FUTURE WORK

The size distribution of the sub 38μm fraction could be determined in order to see how much of the various samples are recoverable. However, the best way to determine the extent to which these particles can be recovered is to perform flotation test work on the different samples. The difference between a closed circuit HPGR product and the product from an HPGR followed by a ball mill may be compared with a product from a conventional SAG/ball mill circuit and followed by flotation test work.

CONCLUSIONS AND RECOMMENDATIONS – *In Summary:*

- The difference between impact and abrasion as a mode of breakage in an AG mill and bed breakage in an HPGR was investigated and it was found that abrasion liberated the valuable particles better. However, the extent to which these will be recoverable is unknown and indicates an area for further study.
- The influence of different operating conditions of the HPGR was investigated and the lower operating pressure was found to be more advantageous. This is in terms of energy consumption and liberation of the valuable particles.

- There is a relationship between the energy intensity of the breakage event and the size distribution of the product.
- There is a relationship between the mode of breakage and the size distribution of the product.
- The feed size distribution of the HPGR influences the energy consumption and final grind.
- UG2 ore is more fragile than the Target Gold ore.

REFERENCES

Andrews, J.R.G. and Mika, T.S. (1975). Comminution of a heterogeneous material: development of a model for liberation phenomena. *Proceedings: XI International Mineral Processing Congress.* 61-88.

Austin, L.G., Sutherland, D.N. and Gottlieb, P. (1993). An analysis of SAG mill grinding and liberation tests. *Minerals Engineering.* 6 (5), 491-507.

Aydogan. N. A., Ergün, L. and Benzer, H. (2006). High pressure grinding rolls (HPGR) applications in the cement industry. *Minerals Engineering.* 19, 130-139.

Banini, G.A. (2002). An integrated description of rock breakage in comminution machines. PhD Thesis, University of Queensland, Australia.

Bbosa, L., Powell, M.S. and Cloete, T.J. (2006). An investigation of impact breakage of rocks using the Split Hopkinson Pressure Bar. *Journal of the South African institute of mining and metallurgy.* 106, 291-296.

Benzer, H., Ergun, L., Lynch, A.J., Oner, M., Gunlu, A., Celik, I.B. and Aydogan, N. (2001). Modelling Cement Grinding Circuits. *Minerals Engineering.* 14 (11), 1469-1482.

Becker, M., Mainza, A.N., Powell, M.S. Bradshaw, D.J. and Knopjes, B. (2007). Quantifying the influence of classification with the 3-product cyclone on liberation and recovery of PGMs in UG2 ore. *Automated Mineralogy.* Brisbane, Australia.

Briggs, C.A. and Bearman, R.A. (1996). An Investigation of Rock Breakage and Damage in Comminution Equipment. *Minerals Engineering.* 9 (5), 489-497.

Bond, F.C. (1962). Laws of rock breakage. *Symposium on Size Reduction.* Frankfurt, Germany.

Bond, F.C. (1963). Some recent advances in grinding theory and practice. *British Chemical Engineering.* 8 (9), 631-634.

Bourgeois, F.S. and Banini, G.A. (2002). A portable load cell for in-situ ore impact breakage testing. *International Journal of Minerals Processing.* 65, 31-54.

Bwalya, M.M., Moys, M.H. and Hinde, A.L. (2001). The use of the discrete element method and fracture mechanics to improve grinding rate prediction. *Minerals Engineering.* 14 (6), 565-573.

Cabri, L.J. (1981). *Platinum-Group Elements: Mineralogy, Geology, Recovery.* Montreal: The Canadian Institute of Mining and Metallurgy. 28-237.

Chernet, T. and Marmo, J. (2003). Direct comparison on mechanical and digital size analyses of Kemi Chromite, Finland. *Minerals Engineering.* 16, 1245-1249.

Digre, M. (1969). *Acta polytechnica scandinavica: Chemistry including metallurgy series no. 88.* Trodheim: Norges Tekniske Vitenskapsakadimi. 2-25.

Dukino, R.D., Loo, C.E. and Swain, M.V. (1997). Characterization of strength of Australian iron ores by tumble-drum and drop tests. *Trans. Institution of Mining and Metallurgy.* 106 (C), 80-88.

Fandrich R.G., Bearman, R.A., Boland, J. and Lim, W. (1997). Mineral liberation by particle bed breakage. *Minerals Engineering.* 10 (2), 175-187.

Fandrich, R., Gu, Y., Burrows, D. and Moeller, K . (2006). *Modern SEM-based mineral liberation analysis.* Available: http://www.sciencedirect.com. Last accessed 14 August 2007.

Fuerstenau, D.W., Kapur, P.C., Schoenert, K. and Marktscheffel, M. (1990). Comparison of energy consumtion in the breakage of single particles in a rigidly mounted roll mill with ball mill grinding. *International Journal of Mineral Processing.* 28, 109-125.

Fuerstenau, D.W., Gutsche, O. and Kapur, P.C. (1996). Confined particle bed comminution under compressive loads. *International Journal of Mineral Processing.* 44-45, 521-537.

Fuerstenau, D.W. and Abouzeid, A.Z.M. (2007). *Role of feed moisture in high-pressure roll mill comminution.* Available: http://www.sciencedirect.com. Last accessed 14 August 2007.

Gay, S.L. (1999). Numerical verification of a non-preferential-breakage liberation model. *International Journal of Minerals Processing.* 57 (2), 125-134.

Gay, S.L. (2004). A liberation model for comminution based on probability theory. *Minerals Engineering.* 17, 525-534.

Goldman, M. and Barbery, G. (1988). Wear and chipping of coarse particles in autogenous grinding: Experimental investigation and modelling. *Minerals Engineering.* 1 (1), 67-76.

Hawkins, R. and Manlapig, E.V. (2006). Determining an appearance function for compressed bed breakage. *Proceedings: XXIII International Mineral Processing Congress*, 3 - 8 Sep. 2006. Istanbul, Turkey. ISBN 975-7946-27-3, Volume 1, 184-189.

Herbst, J.A., Rajamani, K., Lin, C.L. and Miller, J.D. (1988). Development of a multicomponent-multisize liberation model. *Minerals Engineering.* 1 (2), 97-111.

Hosten, C. and Özbay, C. (1998). A comparison of particle bed breakage and rod mill grinding with regard to mineral liberation and particle shape effects. *Minerals Engineering.* 11 (9), 871-874.

Hsih, C.S., Wen, S.B. and Kaun C.C. (1995). An exposure model for valuable components in commintuted particles. *International Journal of Mineral Processing.* 43, 145-165.

King, R.P. and Bourgeois. F. (1993). Measurement of fracture energy during single-particle fracture. *Minerals Engineering.* 6 (4), 353-367.

King, R.P. and Schneider, C.L. (1998). Mineral liberation and the batch comminution equation. *Minerals Engineering.* 11 (12), 1143-1160.

Kiss. L. and Schönert, K. (1980). Liberation of two-component material by single particle compression and impact crushing. *Aufbereitungs-Technick.* 5, 223-230.

Knecht, J. and Patzelt, N. (2004). High pressure grinding rolls – applications for the platinum industry. *International Platinum Conference 'Platinum Adding Value'.* The South African Institute of Mining and Metallurgy.

Klymowsky, R., Patzelt, N., Knecht, J. and Burchardt, E. (2006). An overview of HPGR technology. *International Autogenous and Semiautogenous Grinding Technology.* IV, 11-26.

Liu, J. and Schönert, K. (1996). Modelling of interparticle breakage. *International Journal of Minerals Processing.* 44-45, 101-115.

Loveday, B.K. and Naidoo, D. (1997). Rock abrasion in autogenous milling. *Minerals Engineering.* 10 (6), 603-612,

Loveday, B.K. (2004). The use of FAG and SAG batch tests for measurement of abrasion rates of full-size rocks. *Minerals Engineering.* 17, 1093-1098.

Loveday, B.K. and Whiten, W.J. (2002). Application of a rock abrasion model to pilot-plant and plant data for fully and semi-autogenous grinding. *Trans. Institution of Mining and Metallurgy.* 111 (C), 39-43.

Naidoo, V. (2003). *Mineral liberation analyser for Mintek.* Available: www.min-eng.com/appliedmineralogy. Last accessed 13 August 2007.

Meloy, T.P. and Goth, K. (1985). Liberation in a homogeneous two-phase ore. *International Journal of Mineral Processing.* 14, 45-55.

Mular, A.L. and Jurgensen. (1982). *Design and installation of comminution circuits.* New York: Society of Mining Engineers AIME. 426-426.

Napier-Munn, T.J., Morrell, S., Morrison, R.D. and Kojovic, T. (1999). *Mineral comminution circuits: their operation and optimisation.* Queensland: Julius Kruttschnitt Mineral Research Centre. 10-227.

Pauw, O.G. (1988). The Minimization of overbreakage during Repetitive impact breakage of single ore particles. *Powder Technology.* 56, 251-257.

Petruk, W (2000). *Applied mineralogy in the mining industry.* Amsterdam: Elsevier. 2-35.

Schönert, K. (1996). The influence of particle bed configurations and confinements on particle breakage. *International Journal of Minerals Processing.* 44-45, 1-16.

Shi, F., Lambert, S and Daniel, M. (2006). A study of the effects of HPGR treating platinum ores. *International Autogenous and Semi-Autogenous grinding technology.* Vancouver, Canada.

Sutherland, D.N. and Gottlieb, P. (1991). Application of automated quantitative mineralogy in mineral processing. *Minerals Engineering.* 4 (7-11), 753-762.

Tavares, L.M. (1999). Energy absorbed in breakage of single particles in drop weight testing. *Minerals Engineering.* 12 (1), 43-50.

Tavares, L.M. (2005). Particle weakening in high-pressure roll grinding. *Minerals Engineering.*18, 651-657.

Tavares, L.M. and King, R.P. (1998). Single-particle fracture under impact loading. *International Journal of Minerals Processing.* 54, 1-28.

Tavares, L.M. and King, R.P. (2002). Modelling of particle fracture by repeated impacts using continuum damage mechanics. *Powder Technology*. 123, 138-146.

van Drunick, W. and Smit, I. (2006). Energy efficient comminution – HPGR experience at Anglo research. *International Autogenous and Semiautogenous grinding technology*. Vancouver, Canada.

Wei, X, and Gay, S. (1999). Liberation modelling using a dispersion equation. *Minerals Engineering*. 12, 219-227.

Yang, L.M. and Shim, V.P.W. (2005). An analysis of stress uniformity in split Hopkinson bar test specimens. *International Journal of Impact Engineering*. 31, 129-150.

APPENDIX A DROPWEIGHT DATA

Table A.1: Size distributions UG2 (Small sizes)

Size (mm)	-16 +13.2mm	-22.4 +19 mm	-31.5 +26.5mm	-45 +37.5mm	-63 +53mm (JK)	-63 +53mm (M)
53000	100	100	100	100	100	100
37500	100	100	100	100	95.359	97.558
26500	100	100	100	76.510	80.154	80.200
19000	100	100	94.379	52.914	62.004	55.127
13200	100	93.097	69.710	31.067	46.841	37.358
9500	85.714	76.319	48.096	23.854	35.389	29.926
6700	71.574	59.228	34.268	18.885	29.466	23.738
4750	58.746	48.078	26.726	15.099	25.399	20.183
3350	44.023	36.910	21.044	12.202	22.004	17.008
2360	33.333	28.976	17.127	9.928	19.377	14.986
1700	28.086	25.533	15.301	8.886	18.185	13.630
1180	24.101	22.160	13.509	7.774	16.969	12.711
850	21.672	19.836	12.226	6.976	16.009	12.006
600	19.291	17.424	10.671	6.030	14.552	11.316
425	17.396	15.589	9.287	5.272	12.931	10.437
300	14.286	12.321	7.264	4.241	9.933	8.525
212	10.398	8.686	5.295	3.200	6.995	6.058
150	7.289	6.047	3.856	2.361	4.899	4.077
106	4.762	3.915	2.580	1.623	3.133	2.274
75	3.013	2.447	1.677	1.087	1.924	1.124
53	1.944	1.555	1.093	0.723	1.226	0.401
38	1.312	0.996	0.720	0.475	0.807	0.166
-38	0.000	0.000	0.000	0.000	0.000	0.000

Table A.2: Size distributions Target gold (Small sizes)

Size (µm)	-16+13.2mm	-22.4+19mm	-31.5+26.5mm	-45+37.5mm	-63+53mm (JK)	-63+53mm (M)
63000	100	100	100	100	100	100
53000	100	100	100	100	100	97.048
37500	100	100	100	100	96.283	90.850
26500	100	100	100	100	89.560	79.457
19000	100	100	100	91.828	81.965	64.463
13200	100	100	91.175	47.698	72.663	52.834
9500	100	95.666	57.718	27.878	58.502	41.204
6700	59.194	77.019	35.982	23.044	45.758	31.712
4750	34.409	49.556	25.497	17.644	34.157	23.648
3350	23.602	37.104	20.781	14.503	28.070	19.339
2360	16.613	27.865	16.103	11.596	22.410	15.230
1700	12.097	22.178	12.843	9.212	18.390	12.391
1180	10.215	18.309	10.516	8.098	15.465	10.325
850	8.441	15.264	8.810	7.062	13.219	8.719
600	7.097	13.277	7.513	6.288	11.574	7.391
425	5.968	11.268	6.277	5.574	10.133	6.246
300	5.000	9.767	5.436	5.026	8.960	5.331
212	4.140	8.055	4.435	4.508	7.870	4.498
150	3.333	6.258	3.480	3.742	6.492	3.654
106	2.581	4.820	2.691	3.211	5.167	2.904
75	1.989	3.700	2.085	2.793	4.326	2.338
53	1.559	2.812	1.607	2.467	3.455	1.919
38	1.237	2.051	1.205	2.206	2.828	1.606
-38	1.022	1.607	0.955	1.980	2.250	1.511

Table A.3: Size distributions UG2 and Target gold (big sizes)

	UG2 ore		Target gold ore	
Size (µm)	**-106 +75mm**	**-150 +106mm**	**-106+75mm**	**-150+212mm**
106000	100	100	100	100
75000	100	92.496	100	100
63000	100	84.509	100	100
53000	100	74.576	100	94.505
45000	91.243	63.159	100	79.196
37500	83.836	51.874	94.487	57.297
31500	76.298	47.521	77.808	41.882
26500	67.705	41.027	68.032	36.703
22400	57.545	37.614	63.210	28.312
19000	48.937	33.027	53.351	25.435
16000	42.031	28.282	44.684	22.158
13200	35.530	24.550	39.631	18.724
9500	29.629	20.650	33.515	16.489
6700	24.260	17.019	27.092	12.223
4750	18.787	14.585	20.489	9.763
3350	16.515	12.696	17.343	8.092
2360	14.159	11.472	14.067	6.459
1700	12.613	10.655	11.746	5.357
1180	11.563	10.088	10.000	4.493
850	10.804	9.682	8.637	3.812
600	10.210	9.256	7.598	3.254
425	9.303	8.494	6.629	2.794
300	8.003	7.305	5.791	2.345
212	6.255	5.309	4.948	1.898
150	4.728	3.230	4.058	1.548
106	3.418	2.041	3.207	1.164
75	2.202	1.127	2.582	0.859
53	1.380	0.614	1.935	0.633
38	0.918	0.365	1.417	0.437
-38	0.638	0.000	0.990	0.287

APPENDIX B ABRASION DATA

Table B.1: Wet and dry mass out of pilot mill over time for seasoning of UG2

Batch 1			Batch 2			Batch 3			Batch 4		
Time (min)	Wet mass (kg)	Dry mass (kg)	Time (min)	Wet mass (kg)	Dry mass (kg)	Time (min)	Wet mass (kg)	Dry mass (kg)	Time (min)	Wet mass (kg)	Dry mass (kg)
2	12.33	7.92	2	12	7.5	2	7.48	3.95	2	10.58	0.49
3	31.99	23.7	3	23.5	16.29	3	26.31	16.29	3	27.28	17.32
4	40.11	28.31	4	36.36	25.51	4	35.44	23.67	4	34.36	23.23
5	40.65	30.47	5	38.67	26.04	5	39.39	25.8	5	36.82	25.06
6	40.93	28.18	6	39.58	26.14	6	37.93	24.76	6	38.72	24.54
7	40.3	27.32	7	41.69	27.01	7	39.11	24.06	7	42.58	23.33
8	39.47	25.55	8	38.83	24.07	8	36.3	22.77	8	33.8	21.95
9	31.66	24.05	9	39.04	23.03	9	36.43	22.61	9	34.62	21.77
10	37.99	24.58	10	38.65	23.37	10	35.85	22.11	10	34.98	21.35
11	34.22	21.75	11	36.86	22.51	11	30.1	19.6	11	35.4	21.12
average (kg/min)	34.97	24.18	average (kg/min)	34.52	22.15	average (kg/min)	32.43	20.56	average (kg/min)	32.91	20.02

Table B.2: Cumulative size distribution UG2 seasoning data batch 1 pilot mill

Size (µm)	2 min	3 min	4 min	5 min	6 min	7 min	8 min	9 min	10 min	11 min
13200	100	100	100	100	100	100	100	100	100	100
9500	100	100	100	100	100	100	100	100	100	100
6700	100	99.02	99.05	99.58	99.53	99.60	99.57	98.61	99.71	100
4750	98.36	98.66	98.79	99.36	98.68	99.18	98.84	98.16	99.04	99.03
3350	97.38	98.36	98.43	98.82	98.26	98.59	98.55	97.62	98.62	98.30
2360	95.76	98.00	97.98	98.59	97.85	98.27	98.00	97.14	97.91	97.79
1700	93.44	97.07	97.20	98.01	97.08	97.69	97.18	96.50	97.08	97.07
1180	92.26	96.38	96.61	97.50	96.59	97.29	96.61	95.98	96.42	96.58
850	90.83	95.54	95.84	96.80	95.97	96.70	95.78	95.26	95.52	95.79
600	89.47	94.68	95.10	96.08	95.30	95.98	95.14	94.54	94.76	95.09
425	87.43	93.24	93.95	95.00	94.30	94.94	94.16	93.49	93.75	94.09
300	82.70	89.71	91.20	92.61	92.10	92.83	92.21	91.47	91.87	92.23
212	74.62	82.64	85.24	86.83	87.46	88.40	88.20	87.52	88.15	88.73
150	58.61	66.39	69.40	72.07	73.72	75.17	75.66	75.29	76.65	77.72
106	44.14	50.27	53.05	55.26	56.88	58.41	58.94	59.15	61.27	62.25
75	31.02	35.58	37.17	38.36	39.60	40.92	40.28	41.33	43.48	43.90
53	21.89	24.83	26.01	26.91	27.33	28.60	28.12	28.43	30.37	31.09
38	16.67	18.77	19.62	20.07	20.16	21.28	20.88	20.97	22.85	23.28
-38	12.60	14.08	14.84	14.88	14.76	15.74	15.41	15.48	18.33	17.00

Table B.3: Cumulative size distribution UG2 seasoning data batch 2 pilot mill

Size (µm)	2 min	3 min	4 min	5 min	6 min	7 min	8 min	9 min	10 min	11 min
13200	100	100	100	100	100	100	100	100	100	100
9500	100	100	100	100	100	100	100	100	100	100
6700	100	99.52	100	100	100	99.35	100	99.25	98.78	99.62
4750	98.36	99.11	99.73	99.82	99.43	98.75	99.62	98.77	98.18	99.37
3350	97.38	98.53	99.36	99.66	99.31	98.53	99.09	98.42	97.53	98.81
2360	95.76	98.00	98.98	99.34	98.87	98.12	98.61	97.96	97.17	98.11
1700	93.44	96.67	98.26	98.65	98.29	97.41	97.89	97.30	96.49	97.16
1180	92.26	95.78	97.74	98.08	97.78	96.88	97.37	96.87	96.00	96.48
850	90.83	94.74	97.04	97.36	97.10	96.20	96.74	96.20	95.24	95.62
600	89.47	93.62	96.19	96.60	96.41	95.47	96.06	95.50	94.54	94.83
425	87.43	91.60	94.64	95.20	95.20	94.21	94.82	94.32	93.32	93.61
300	82.70	88.61	92.29	93.29	93.55	92.45	91.98	92.82	91.84	92.07
212	74.62	79.15	84.22	86.45	87.75	86.20	86.46	86.79	87.00	87.08
150	58.61	65.15	70.70	73.97	76.18	74.24	75.00	76.47	76.92	76.85
106	44.14	48.26	53.00	56.32	58.11	56.66	56.75	59.74	60.45	57.96
75	31.02	34.79	38.23	40.74	41.66	40.79	39.76	43.25	44.01	40.87
53	21.89	24.07	27.00	28.44	28.50	28.37	26.20	29.75	30.62	28.32
38	16.67	18.08	20.29	21.31	20.93	21.15	18.49	21.81	22.70	21.18
-38	12.60	14.08	15.75	16.09	15.40	16.00	13.13	15.96	16.81	16.35

Table B.4: Cumulative size distribution UG2 seasoning data batch 3 pilot mill

Size (µm)	2 min	3 min	4 min	5 min	6 min	7 min	8 min	9 min	10 min	11 min
13200	100	100	100	100	100	100	100	100	100	100
9500	100	100	100	100	100	100	100	100	100	99.73
6700	99.74	99.51	100	99.67	99.5	100	100	100	98.61	99.73
4750	99.05	99.51	99.58	99.42	99.32	99.62	100	99.94	97.65	99.30
3350	98.08	99.36	99.16	99.13	99.13	99.38	99.89	99.69	97.00	99.03
2360	95.97	99.02	98.64	98.74	98.93	99.20	99.71	99.44	96.29	98.65
1700	92.66	98.10	97.77	97.95	98.66	98.93	99.42	99.09	95.47	98.16
1180	89.78	96.97	96.79	97.22	98.42	98.61	98.98	98.60	94.54	97.54
850	87.49	95.85	95.88	96.35	98.23	98.17	98.57	98.13	93.73	96.84
600	85.39	94.55	94.84	95.70	97.54	97.72	97.88	97.53	93.00	95.95
425	82.35	92.62	93.53	94.56	96.43	96.78	96.84	96.47	92.07	94.75
300	76.78	88.66	90.76	92.13	94.24	94.83	94.92	94.55	90.42	92.87
212	67.10	80.54	84.46	86.39	89.16	90.18	90.72	90.32	86.92	88.99
150	51.91	64.65	69.10	72.66	76.21	77.63	78.82	78.15	77.07	78.44
106	37.79	47.48	51.14	54.36	58.22	58.91	61.00	60.54	61.16	61.84
75	26.85	33.62	36.69	37.89	41.27	41.05	43.70	43.31	44.95	44.64
53	19.37	24.14	26.75	27.10	29.33	28.18	31.75	31.19	32.50	31.85
38	14.62	17.97	20.48	19.70	21.71	19.82	23.67	23.33	24.13	23.20
-38	11.45	13.87	16.27	14.71	16.35	14.54	18.03	17.78	18.46	17.21

Table B.5: Cumulative size distribution UG2 seasoning data batch 4 pilot mill

Size (µm)	2 min	3 min	4 min	5 min	6 min	7 min	8 min	9 min	10 min	11 min
13200	100	100	100	100	100	100	100	100	100	100
9500	100	100	100	100	100	100	100	100	100	100
6700	99.54	99.83	99.60	99.74	100	99.59	100	99.48	99.41	99.29
4750	99.24	99.38	99.41	99.46	99.90	99.38	99.49	99.04	99.27	98.90
3350	98.89	98.94	99.24	99.08	99.76	99.21	99.24	98.50	99.08	98.60
2360	98.15	97.83	98.83	98.61	99.54	98.85	98.82	97.77	98.79	98.18
1700	96.18	96.99	97.95	97.82	99.20	98.25	98.00	97.32	98.61	97.86
1180	94.57	96.28	97.35	97.20	98.89	97.74	97.39	96.65	98.52	97.36
850	92.71	95.08	96.75	96.34	98.55	97.01	96.48	96.03	98.41	96.79
600	91.13	94.05	96.00	95.65	97.99	96.37	95.87	94.94	97.97	96.19
425	87.43	91.99	94.66	94.33	96.80	95.19	94.82	93.52	96.91	95.14
300	82.41	88.80	92.57	92.41	95.14	93.59	93.41	88.97	95.53	93.87
212	70.54	79.29	85.27	85.63	89.19	88.17	88.67	77.71	90.98	89.86
150	54.58	63.27	69.67	71.02	75.42	75.54	77.11	59.43	79.59	79.85
106	38.48	44.65	49.28	51.40	55.62	56.33	58.63	43.77	60.26	62.65
75	27.56	31.41	36.06	36.54	39.54	40.86	43.18	30.06	43.21	47.17
53	19.16	21.16	25.71	24.63	27.00	27.77	30.02	21.31	28.59	33.17
38	13.88	15.12	19.42	17.45	18.65	19.76	21.62	16.11	19.47	23.78
-38	10.84	11.62	15.87	13.75	14.19	15.39	16.67	13.06	14.62	18.64

Table B.6: Wet and dry mass out of pilot mill over time for abrasion of UG2

	Batch 1		Batch 1	
Time	Wet mass	Dry mass	Wet mass	Dry mass
2 min	36.62	25.00	36.57	22.05

Table B.7: Cumulative size distribution UG2 rounded data pilot mill

Size (µm)	Feed (%)	Batch 1	Batch 2
150000	100.00	100.00	100.00
106000	81.39	84.10	87.64
75000	81.39	82.07	82.34
50000	48.63	55.16	55.71
38000	48.63	50.82	51.77
25000	0.00	13.32	13.59
18000	0.00	8.83	8.43
11200	0.00	7.47	7.07
9500	0.00	7.34	7.07
6700	0.00	6.36	5.82
4750	0.00	5.66	5.12
3380	0.00	5.36	4.90
2360	0.00	5.19	4.74
1700	0.00	5.10	4.64
1180	0.00	5.05	4.61
850	0.00	5.01	4.57
600	0.00	4.98	4.55
425	0.00	4.94	4.51
300	0.00	4.84	4.44
212	0.00	4.64	4.22
150	0.00	3.99	3.65
106	0.00	3.01	2.80
75	0.00	2.17	1.88
53	0.00	1.39	1.20
38	0.00	0.94	0.77
-38	0.00	0.63	0.50

Table B.8: Wet and dry mass out of pilot mill over time for abrasion of Target ore

Batch 1			Batch 2		
Time (min)	Wet mass (kg)	Dry mass (kg)	Time (min)	Wet mass (kg)	Dry mass (kg)
3	28.95	3.206	3	22.93	3.104
5	28.58	6.928	5	26.92	5.725
7	30.54	5.583	7	28.12	4.985
9	27.52	5.248	9	28.12	4.565
11	29.76	4.854	11	28.63	4.002
13	30.46	5.677	13	27.67	4.254
15	30.2	5.477	15	29.05	4.65
17	27.08	6.322	17	28.18	5.023
19	30.8	5.379	19	28.35	5.212
21	31.18	5.345	21	29.36	5.032

Table B.9: Cumulative size distribution Target abrasion data pilot mill

Size (µm)	3 min	5 min	7 min	9 min	11 min	13 min	15 min	17 min	19 min	21 min
18000	100	100	100	100	100	100	100	100	100	100
13200	100	100	100	100	100	100	100	100	100	100
9500	100	100	100	100	100	100	100	100	100	100
6700	99.55	100	99.13	99.52	100	100	100	100	100	100
4750	98.45	99.60	98.73	96.55	99.80	100	99.88	99.23	99.88	99.23
3350	97.51	99.20	97.87	95.18	99.53	99.27	98.31	98.77	98.31	98.77
2360	96.12	98.43	97.17	92.71	98.83	98.50	97.30	97.73	97.30	97.73
1700	94.22	97.60	96.23	89.25	98.17	97.40	95.92	96.53	95.92	96.53
1180	92.91	96.87	95.20	86.79	97.33	96.27	95.08	95.23	95.08	95.23
850	91.14	95.87	94.23	83.04	96.27	95.00	93.84	93.83	93.84	93.83
600	89.57	94.93	92.80	81.86	95.37	93.97	92.67	92.60	92.67	92.60
425	87.27	93.30	90.60	79.97	93.50	92.43	90.69	90.60	90.69	90.60
300	84.56	90.50	86.53	77.58	90.23	89.87	88.31	87.30	88.31	87.30
212	79.28	87.10	81.90	72.17	86.23	86.53	83.34	83.13	83.34	83.13
150	72.03	80.43	73.03	63.97	78.43	80.13	75.92	74.67	75.92	74.67
106	62.31	73.03	63.20	52.68	69.73	72.97	66.14	65.33	66.14	65.33
75	53.12	62.97	49.57	42.39	57.27	62.87	57.06	52.10	57.06	52.10
53	43.24	52.67	37.33	31.67	50.00	57.03	47.43	38.77	47.43	38.77
38	34.44	44.30	26.70	22.49	39.80	48.70	38.65	28.10	38.65	28.10
-38	27.33	36.30	19.63	15.75	29.77	40.83	30.60	19.37	30.60	19.37

Table B.10: Wet and dry mass out of torque mill over time for abrasion of UG2

Batch 1			Batch 2			Batch 3		
-50+38,-38+25,-25+18			-50+38,-38+25,-25+18			-50+38,-38+25,-25+18		
Time (min)	Wet mass (kg)	Dry mass (kg)	Time (min)	Wet mass (kg)	Dry mass (kg)	Time (min)	Wet mass (kg)	Dry mass (kg)
2	18.15	0.51	2	21.36	0.46	2	17.8	0.33
4	22.58	1.13	4	22.33	1.22	4	21.9	0.71
6	22.5	1.58	6	22.07	1.56	6	22.35	0.81
8	22.45	1.54	8	17.56	1.56	8	21.78	0.85
10	22.7	1.70	10	22.96	1.93	10	21.97	0.74
12	21.18	0.74	12	15.18	0.56	12	21.95	0.38
14	22.3	1.45	14	22.18	1.65	14	22.02	0.84
16	22.56	1.61	16	22.84	1.45	16	22.16	0.83
18	22.17	1.37	18	22.53	1.23	18	20.53	0.71
20	22.18	1.07	20	22.85	1.41	20	22.23	0.81

Table B.11: Wet and dry mass out of torque mill over time for abrasion of UG2

Batch 4			Batch 5			Batch 9		
-38+25			-38+25			-38+25 speed 70% of critical		
Time (min)	Wet mass (kg)	Dry mass (kg)	Time (min)	Wet mass (kg)	Dry mass (kg)	Time (min)	Wet mass (kg)	Dry mass (kg)
2	13.47	0.38	2	18.13	0.39	2	19.31	0.40
4	17.8	0.52	4	22.73	0.58	4	24	0.60
6	17.01	0.75	6	22.44	0.77	6	23.92	0.79
8	18.16	0.86	8	22.82	0.88	8	23.9	0.90
10	17.76	0.93	10	22.96	0.88	10	24.08	0.91
12	17.75	0.72	12	22.72	0.68	12	24.17	0.70
14	17.66	0.65	14	22.7	0.62	14	24.37	0.64
16	16.91	0.75	16	22.82	0.79	16	24.18	0.81
18	17.73	0.74	18	21.89	0.96	18	24.33	0.99
20	17.53	0.58	20	23.44	0.98	20	24.55	1.01

Table B.12: Wet and dry mass out of torque mill over time for abrasion of UG2

Batch 6			Batch 7			Batch 8		
-50+38			-50+38			-50+38 speed 70% of critical		
Time (min)	Wet mass (kg)	Dry mass (kg)	Time (min)	Wet mass (kg)	Dry mass (kg)	Time (min)	Wet mass (kg)	Dry mass (kg)
2	18.3	0.84	2	19.73	0.94	2	18.41	0.74
4	21.64	1.25	4	16.3	1.39	4	24.22	1.25
6	21.56	1.65	6	20.54	1.84	6	23.72	1.35
8	21.68	1.90	8	19.85	1.77	8	23.1	1.45
10	21.49	1.91	10	19.13	1.99	10	24.12	1.26
12	21.46	1.48	12	18.8	1.64	12	23.73	1.52
14	21.64	1.34	14	18.65	1.48	14	22.94	1.53
16	21.68	1.71	16	20.47	1.90	16	22.9	1.58
18	21.2	2.08	18	21.34	2.30	18	22.73	1.99
20	21.44	2.12	20	21.85	2.35	20	23.39	1.75

Table B.13: Cumulative size distribution data batch 1 UG2 Torque mill

Size	2min	4min	6min	8min	10min	12min	14min	16min	18min	20min
13200	100	100	100	100	100	100	100	100	100	100
9500	100	100	100	100	100	100	100	100	100	100
6700	100	100	99.5	98.5	98.7	98.9	98.2	98.4	98.8	96.8
4750	99.4	98.6	98.7	97.8	97.6	96.6	95.5	96.5	96.6	95.2
3380	99.1	97.9	98.0	96.8	96.2	95.6	94.2	94.9	95.3	93.9
2360	98.6	97.2	97.4	95.9	95.4	94.6	93.1	93.9	94.1	93.2
1700	98.0	96.8	96.9	95.3	94.5	94.0	92.5	93.0	93.2	92.6
1180	97.7	96.5	96.6	95.0	94.2	93.7	92.1	92.6	92.9	92.3
850	97.5	96.3	96.4	94.8	94.0	93.5	91.7	92.4	92.6	92.1
600	97.0	95.8	95.9	94.2	93.4	93.0	91.2	91.8	92.1	91.7
425	96.3	95.2	95.4	93.6	92.8	92.5	90.3	91.3	91.6	91.2
300	95.2	94.1	94.4	92.7	91.8	91.6	88.2	90.4	90.7	90.4
212	92.7	91.7	92.1	90.3	89.3	89.4	83.1	88.0	88.6	88.5
150	87.1	86.1	86.7	84.9	83.9	84.3	72.4	82.6	83.7	84.0
106	76.4	74.8	75.9	74.0	73.2	74.2	57.7	71.3	73.6	74.6
75	63.8	61.3	62.8	60.1	60.1	61.8	43.5	56.9	60.7	62.5
53	50.3	47.0	48.1	45.7	45.7	47.7	32.9	42.7	46.3	48.7
38	38.0	33.3	33.5	33.3	33.0	34.9	27.9	31.4	33.2	35.4
-38	31.4	27.1	27.1	27.2	27.0	28.9	25.3	25.8	26.6	28.8

Table B.14: Cumulative size distribution data batch 2 UG2 Torque mill

Size	2min	4min	6min	8min	10min	12min	14min	16min	18min	20min
13200	100	100	100	100	100	100	100	100	100	100
9500	100	100	100	100	100	100	100	100	100	100
6700	100	99.1	99.5	100	99.4	100	99.4	99.1	99.4	99.2
4750	99.3	98.7	99.2	99.1	98.3	98.6	98.3	97.6	98.2	98.2
3380	99.0	98.3	98.4	98.8	97.9	98.1	97.1	97.0	97.2	97.5
2360	98.5	97.9	98.0	98.4	97.6	97.6	96.5	96.4	96.3	96.5
1700	98.2	97.6	97.6	98.0	97.3	97.1	96.0	95.8	95.7	95.9
1180	98.1	97.4	97.4	97.8	97.2	96.8	95.7	95.6	95.4	95.6
850	98.0	97.2	97.2	97.6	97.1	96.6	95.4	95.4	95.2	95.4
600	97.6	96.9	97.0	97.2	96.8	96.3	95.0	95.0	94.7	94.9
425	97.2	96.5	96.6	96.8	96.4	95.8	94.5	94.5	94.2	94.4
300	96.6	95.8	95.9	96.0	95.7	95.1	93.7	93.8	93.4	93.6
212	94.9	93.8	94.1	94.3	93.8	93.3	91.8	92.0	91.5	91.9
150	90.9	89.0	89.7	90.1	89.2	88.9	87.1	87.6	87.0	87.8
106	82.0	77.7	78.8	80.9	78.7	78.9	76.6	77.1	77.0	78.7
75	70.0	61.8	63.9	68.5	63.6	64.8	62.0	61.7	62.5	66.4
53	55.8	45.8	50.0	53.9	49.2	49.4	47.1	47.1	48.7	52.1
38	41.0	31.3	38.3	39.9	36.9	35.8	34.3	34.6	38.0	37.8
-38	33.3	24.4	33.0	32.7	31.0	29.6	28.8	29.3	32.9	31.3

Table B.15: Cumulative size distribution data batch 3 UG2 Torque mill

Size	2min	4min	6min	8min	10min	12min	14min	16min	18min	20min
13200	100	100	100	100	100	100	100	100	100	100
9500	100	100	100	100	100	99.4	100	100	100	100
6700	100	100	100	100	100	98.6	100	99.1	99.1	100
4750	100	99.9	99.4	98.6	98.7	98.2	98.3	98.6	97.9	98.5
3380	99.5	99.3	99.0	98.0	98.4	97.7	97.7	98.0	97.2	97.6
2360	99.2	98.9	98.7	97.8	97.9	97.5	97.2	97.3	96.4	97.2
1700	98.9	98.6	98.5	97.5	97.6	97.4	96.8	96.9	95.9	96.9
1180	98.7	98.5	98.3	97.3	97.4	97.2	96.6	96.5	95.6	96.7
850	98.5	98.4	98.0	97.1	97.1	96.9	96.4	96.1	95.3	96.4
600	98.3	98.0	97.8	96.8	96.9	96.7	96.0	95.8	94.7	96.1
425	98.0	97.8	97.5	96.6	96.6	96.4	95.6	95.4	93.5	95.7
300	97.5	97.3	97.0	96.0	96.3	95.7	95.0	94.6	90.0	95.1
212	96.2	96.1	95.7	94.7	95.1	94.5	93.5	93.1	83.7	93.8
150	92.3	92.4	91.8	90.8	91.5	94.1	89.6	88.9	71.0	90.1
106	85.5	85.6	84.8	83.9	84.8	87.3	82.6	81.9	56.4	83.7
75	71.9	72.0	71.1	70.8	71.7	73.8	69.3	68.6	43.3	70.9
53	56.4	56.3	55.5	55.3	57.0	58.5	54.2	53.5	33.8	56.7
38	43.2	42.5	43.0	43.4	43.6	45.5	41.3	41.2	24.0	44.6
-38	33.3	33.1	33.4	34.1	33.7	35.8	32.0	32.5	12.9	35.0

Table B.16: Cumulative size distribution data batch 4 UG2 Torque mill

Size	2min	4min	6min	8min	10min	12min	14min	16min	18min	20min
13200	100	100	100	100	100	100	100	100	100	100
9500	100	100	100	100	100	100	100	100	100	100
6700	100	100	100	100	100	100	98.8	100	100	99.3
4750	99.1	99.3	98.6	99.3	99.4	99.2	97.6	99.2	98.9	99.0
3380	98.7	98.6	98.2	98.8	98.8	98.4	97.1	98.3	98.1	98.4
2360	98.1	97.8	97.6	98.1	98.4	97.7	96.8	97.9	97.5	97.8
1700	97.6	97.2	97.2	97.7	97.9	97.2	96.4	97.5	97.1	97.4
1180	97.4	96.9	97.0	97.5	97.7	97.0	96.2	97.2	96.9	97.3
850	97.2	96.7	96.9	97.3	97.6	96.7	96.1	97.1	96.7	97.2
600	96.9	96.2	96.5	97.0	97.3	96.5	95.9	96.8	96.5	97.0
425	96.6	95.8	96.1	96.7	97.0	96.2	95.6	96.6	96.2	96.7
300	96.0	95.0	95.5	96.2	96.4	95.7	95.2	96.1	95.7	96.2
212	94.5	93.1	94.0	94.7	95.1	94.4	94.0	94.9	94.4	95.1
150	90.6	88.7	90.3	91.1	91.6	91.0	90.8	91.8	91.2	92.0
106	81.9	78.9	82.0	82.5	83.2	82.8	83.0	83.9	83.3	84.3
75	70.3	65.9	70.5	70.8	71.3	71.2	71.9	72.5	72.0	73.1
53	56.4	51.6	56.6	56.2	56.8	56.8	57.8	57.7	57.8	58.8
38	42.5	38.7	42.0	41.3	41.4	41.8	42.3	42.7	46.9	43.8
-38	34.4	32.1	33.9	33.6	32.5	34.1	34.1	34.8	41.9	36.4

Table B.17: Cumulative size distribution data batch 5 UG2 Torque mill

Size	2min	4min	6min	8min	10min	12min	14min	16min	18min	20min
13200	100	100	100	100	100	100	100	100	100	100
9500	100	100	100	100	100	100	100	100	100	100
6700	100	100	100	100	99.2	100	100	100	100	99.1
4750	99.8	99.3	98.6	98.9	98.2	99.2	99.0	99.2	98.7	98.2
3380	99.7	99.0	98.0	98.5	97.8	98.8	98.5	98.7	98.1	97.5
2360	99.5	98.7	97.6	98.0	97.4	98.1	98.1	98.4	97.6	97.0
1700	99.3	98.5	97.3	97.5	97.0	97.7	97.8	97.9	97.1	96.6
1180	99.2	98.3	97.0	97.3	96.8	97.4	97.6	97.6	96.9	96.4
850	99.1	98.1	96.9	97.2	96.7	97.3	97.5	97.5	96.7	96.3
600	98.9	97.8	96.6	96.8	96.4	97.0	97.2	97.1	96.4	95.9
425	98.5	97.5	96.2	96.5	96.1	96.6	96.9	96.8	96.0	95.6
300	98.0	96.9	95.5	95.9	95.5	96.0	96.3	96.2	95.4	95.1
212	96.7	92.2	94.2	94.6	94.1	94.8	94.9	94.9	94.0	93.9
150	93.6	88.5	90.4	90.8	90.7	91.2	91.5	91.4	90.4	90.7
106	86.1	80.9	81.6	81.3	82.5	82.9	82.2	83.4	82.3	82.8
75	75.3	70.0	68.5	67.5	70.8	70.2	68.1	71.9	70.5	70.3
53	61.3	56.0	53.9	52.2	56.3	54.9	53.0	57.4	56.0	55.7
38	46.8	40.6	41.0	38.7	41.6	40.9	40.0	43.0	42.9	42.0
-38	38.2	32.4	34.0	33.1	33.9	34.2	33.8	35.2	35.9	35.1

Table B.18: Cumulative size distribution data batch 6 UG2 Torque mill

Size	2min	4min	6min	8min	10min	12min	14min	16min	18min	20min
13200	100	100	100	100	100	100	100	100	100	100
9500	100	100	100	100	100	100	100	100	100	100
6700	100	99.1	99.1	98.9	99.4	100	98.6	98.9	98.3	99.4
4750	98.2	97.4	97.6	97.0	97.0	98.1	96.6	97.0	96.3	97.8
3380	96.4	95.9	96.4	95.5	95.7	96.9	95.5	95.9	95.0	96.3
2360	94.9	94.4	95.3	94.4	94.4	95.8	94.3	95.2	93.9	95.2
1700	93.7	93.2	94.3	93.4	93.3	95.0	93.4	94.5	93.1	94.1
1180	93.1	92.6	93.8	93.0	92.8	94.6	93.0	94.2	92.6	93.6
850	92.4	92.1	93.3	92.5	92.3	94.2	92.6	93.8	92.2	93.1
600	91.7	91.4	92.7	91.9	91.7	93.6	92.0	93.2	91.7	92.6
425	90.7	90.4	91.7	90.9	90.7	92.7	91.1	92.3	90.9	91.6
300	88.9	88.5	90.0	89.0	88.9	91.1	89.3	90.7	89.5	89.9
212	85.3	84.6	86.2	84.9	84.9	87.4	85.5	87.1	86.4	85.8
150	77.6	75.4	77.4	74.8	75.8	78.6	77.0	79.0	79.2	76.3
106	67.9	63.5	65.9	62.2	64.2	66.8	60.4	67.9	69.2	61.5
75	54.2	46.1	49.9	44.9	48.4	49.1	45.3	51.9	54.3	42.7
53	42.3	33.3	35.5	30.2	34.4	33.8	34.7	37.5	40.5	28.6
38	34.0	23.9	24.8	18.9	24.6	24.1	27.9	27.6	30.5	19.7
-38	28.6	19.8	19.5	14.1	18.6	18.0	26.5	21.1	25.7	14.6

Table B.19: Cumulative size distribution data batch 7 UG2 Torque mill

Size (µm)	2min	4min	6min	8min	10min	12min	14min	16min	18min	20min
13200	100	100	100	100	100	100	100	100	100	100
9500	100	100	100	100	100	100	100	100	100	100
6700	99.1	97.9	98.3	100	100	100	99.3	98.3	98.1	98.5
4750	97.2	95.9	96.3	98.0	97.4	97.8	96.9	96.3	96.6	96.1
3380	95.7	94.5	94.3	96.9	96.0	96.2	95.4	94.7	95.5	94.9
2360	94.0	93.3	92.8	95.8	95.0	95.2	94.0	93.7	94.5	94.1
1700	92.4	92.1	91.6	95.0	94.3	94.2	92.8	92.9	93.7	93.3
1180	91.6	91.5	91.0	94.5	93.7	93.8	92.3	92.2	93.3	93.0
850	90.7	90.8	90.4	94.0	93.1	93.3	91.7	91.5	92.8	92.5
600	89.8	90.4	89.8	93.5	92.6	92.9	91.0	91.0	92.3	91.9
425	88.8	89.5	89.0	92.6	91.7	92.0	90.3	90.1	91.5	91.2
300	86.9	88.0	87.1	91.3	90.0	90.6	88.7	88.4	90.2	89.7
212	82.9	84.3	82.6	87.6	86.2	86.6	84.7	84.4	86.7	86.2
150	75.5	76.2	73.8	79.7	77.5	78.0	76.7	75.6	78.8	78.7
106	63.2	63.0	58.3	66.5	63.1	63.8	62.8	61.0	64.7	65.2
75	48.9	47.3	42.3	51.3	47.1	47.3	47.3	44.6	47.2	48.6
53	36.1	34.9	31.1	38.1	34.3	34.5	34.6	32.6	34.6	34.7
38	27.0	25.9	22.6	28.0	24.4	25.2	25.6	23.5	25.5	24.0
-38	21.1	20.0	18.0	20.9	18.8	19.0	20.0	18.2	19.6	18.1

Table B.20: Cumulative size distribution data batch 8 UG2 Torque mill

Size (µm)	2min	4min	6min	8min	10min	12min	14min	16min	18min	20min
13200	100	100	100	100	100	100	100	100	100	100
9500	100	100	100	100	100	100	100	100	100	100
6700	100	98.2	98.4	98.6	99.5	98.7	98.6	98.8	98.6	99.0
4750	98.0	96.7	96.6	96.6	97.4	95.8	97.0	96.7	95.9	97.1
3380	97.3	95.1	94.8	94.2	96.3	94.2	95.7	95.1	94.7	96.1
2360	96.4	94.1	93.6	92.6	95.0	92.9	94.8	94.1	93.6	95.2
1700	95.8	93.2	92.7	91.6	94.2	92.0	93.9	93.4	92.9	94.5
1180	95.2	92.6	92.1	90.9	93.4	91.3	93.4	92.8	92.4	94.0
850	94.7	92.0	91.4	90.3	92.7	90.8	92.8	92.4	91.9	93.6
600	94.2	91.3	90.8	89.7	92.1	90.0	92.1	91.9	91.4	93.0
425	93.3	90.4	90.0	88.8	91.0	89.1	91.2	91.2	90.6	92.3
300	91.8	88.7	88.3	87.1	89.2	87.4	89.6	89.7	89.3	91.0
212	88.4	85.1	84.6	83.3	85.3	83.9	86.2	86.3	86.0	87.8
150	82.0	78.3	77.0	75.8	78.1	77.4	79.5	79.2	79.4	81.3
106	69.6	65.6	63.6	62.5	65.4	65.9	66.1	65.7	67.4	68.7
75	54.4	51.2	48.3	47.4	50.5	52.4	50.6	51.1	53.1	53.3
53	41.2	39.0	34.5	33.9	37.3	39.9	37.6	39.7	39.9	39.3
38	31.2	29.5	24.1	23.4	27.5	30.2	27.8	32.2	29.5	28.5
-38	24.5	22.9	16.7	16.2	20.6	23.3	21.6	27.9	22.2	21.4

Table B.21: Cumulative size distribution data batch 9 UG2 Torque mill

Size	2min	4min	6min	8min	10min	12min	14min	16min	18min	20min
13200	100	100	100	100	100	100	100	100	100	100
9500	100	100	100	100	100	100	100	100	100	100
6700	100	100	100	99.4	99.1	100	98.9	98.5	100	100
4750	99.7	99.5	99.6	98.8	98.3	98.9	97.9	97.9	98.7	98.0
3380	99.4	99.1	99.0	98.3	97.9	98.5	97.3	97.2	98.2	97.1
2360	98.8	99.0	98.6	98.0	97.5	98.1	96.8	96.8	97.6	96.4
1700	98.5	98.6	98.4	97.8	97.3	97.8	96.5	96.4	97.2	96.0
1180	98.3	98.3	98.1	97.6	97.1	97.5	96.3	96.0	97.0	95.8
850	98.2	98.1	98.0	97.5	97.0	97.3	96.1	95.8	96.7	95.6
600	98.0	97.8	97.8	97.3	96.8	97.1	95.9	95.6	96.5	95.4
425	97.7	97.5	97.5	97.1	96.5	96.8	95.6	95.3	96.2	95.1
300	97.2	96.9	97.0	96.7	96.1	96.4	95.2	94.8	95.7	94.4
212	96.1	95.7	95.7	95.8	95.1	95.1	94.0	93.5	94.5	93.1
150	92.5	92.0	92.8	93.0	92.2	92.2	91.2	90.6	91.2	89.4
106	84.5	83.6	85.6	86.2	85.2	85.5	84.4	83.4	83.7	81.1
75	73.2	72.7	73.5	76.3	74.1	74.5	73.1	71.6	73.0	70.3
53	57.3	56.0	59.9	61.1	58.9	61.2	58.8	56.7	57.7	54.5
38	45.2	44.0	46.2	49.1	46.6	49.3	46.3	43.1	46.5	41.8
-38	35.2	33.6	37.0	38.6	36.5	40.8	37.4	33.3	37.1	31.9

Table B.22: Wet and dry mass out of torque mill over time for abrasion of Target ore

Batch 1			Batch 2		
-50+38,-38+25			-75+50,-50+38,-38+25		
Time (min)	Wet mass (kg)	Dry mass (kg)	Time (min)	Wet mass (kg)	Dry mass (kg)
5	44.2	0.55	5	37.42	0.61
10	47.12	0.27	10	40.72	0.30
15	46.72	0.31	15	40.94	0.35
20	47.18	0.27	20	41.44	0.30
25	46.64	0.32	25	41.62	0.35
30	47.46	0.24	30	40.8	0.26
35	47.74	0.22	35	41.06	0.24
40	47.36	0.25	40	40.1	0.28
45	46.98	0.29	45	40.6	0.31
50	47.1	0.28	50	40.84	0.30

Table B.23: Cumulative size distribution data batch 1 Target Gold Torque mill

Size (µm)	5min	10min	15min	20min	25min	30min	35min	40min	45min	50min
1700	100	100	100	100	100	100	100	100	100	100
1180	100	100	100	100	100	100	100	100	100	100
850	100	100	100	99.24	100	100	100	100	100	100
600	98.93	99.31	99.90	98.84	99.90	99.94	99.92	99.84	99.57	99.89
425	98.69	99.10	99.72	98.65	99.87	99.87	99.92	99.77	99.44	99.79
300	98.10	98.62	99.55	98.25	99.67	99.66	99.44	99.51	99.28	99.54
212	96.86	97.30	98.93	97.23	99.11	99.00	97.99	98.75	98.59	98.84
150	93.61	94.02	97.10	94.62	97.26	97.06	93.74	96.68	96.65	97.19
106	88.70	89.15	93.86	90.89	94.03	94.12	86.84	93.53	93.18	94.38
75	80.37	81.82	88.54	85.21	89.19	89.67	76.08	88.34	88.82	89.95
53	70.73	73.05	82.26	78.18	83.32	84.01	63.56	81.94	83.31	84.36
38	60.61	63.61	74.77	70.20	76.69	77.97	48.72	74.91	77.37	77.97
-38	49.41	52.63	66.14	61.16	68.68	70.39	33.79	66.21	69.79	70.24

Table B.24: Cumulative size distribution data batch 2 Target Gold Torque mill

Size (µm)	5min	10min	15min	20min	25min	30min	35min	40min	45min	50min
1700	100	100	100	100	100	100	100	100	100	100
1180	100	100	100	100	100	100	100	100	100	100
850	100	100	100	100	100	100	100	100	100	100
600	99.95	99.85	99.45	99.94	99.78	99.86	99.88	99.73	99.75	99.81
425	99.89	99.75	99.33	99.88	99.66	99.72	99.78	99.65	99.64	99.71
300	99.73	99.57	98.96	99.71	99.35	99.35	99.50	99.44	99.24	99.32
212	99.01	99.01	97.68	99.21	98.55	97.93	98.78	98.85	97.97	98.35
150	97.35	97.38	95.07	97.79	96.52	95.14	96.88	97.24	95.10	96.17
106	95.21	94.64	91.56	95.38	93.35	91.56	93.83	94.67	91.25	93.02
75	91.92	90.11	86.23	91.23	88.29	86.22	88.81	90.78	85.40	87.99
53	87.72	84.53	80.11	86.17	81.82	79.63	82.57	86.04	78.39	81.15
38	82.40	78.22	72.83	80.43	74.31	71.85	75.27	80.76	70.40	74.14
-38	76.09	70.24	64.22	73.04	65.59	62.34	66.57	74.48	61.21	65.28

APPENDIX C HPGR DATA

Table C.1: Cumulative size distribution data for the UG2 ore

		Specific press force (N/mm^2)
Size (µm)	**Feed**	**4.49**
13200	100	100
9500	100	100
6700	82.04	100
4750	54.01	99.71
3350	40.65	97.44
2360	30.81	90.59
1700	25.99	83.19
1180	22.98	77.04
850	21.26	72.42
600	19.78	68.75
425	18.43	65.48
300	16.94	61.94
212	14.33	55.34
150	11.67	47.44
106	7.64	33.85
75	5.48	25.29
53	3.63	17.87
38	2.57	12.83
-38	1.93	9.69

Table C.2: Cumulative size distribution data for the Merensky ore

		Specific press force of Procuct N/mm^2					
Size (µm)	**Feed**	**1.50**	**2.39**	**2.99**	**4.49**	**5.99**	**7.48**
9500	100	100	100	100	100	100	100
6700	82.02	100	100	100	100	100	100
4750	59.16	97.97	99.06	99.16	99.58	99.28	99.53
3350	47.60	90.23	94.54	95.28	96.72	95.82	96.70
2360	37.30	77.24	84.68	86.09	89.39	85.67	88.53
1700	29.47	64.74	73.44	75.39	79.69	73.39	78.02
1180	24.48	55.76	65.04	66.90	72.39	63.83	69.04
850	19.67	46.37	55.36	57.16	63.15	54.43	59.89
600	16.09	39.00	47.61	49.47	55.88	47.64	52.29
425	12.94	31.82	39.84	41.45	48.41	40.44	44.55
300	10.67	26.30	33.59	34.94	42.26	34.94	38.24
212	8.80	21.35	27.81	28.97	35.84	29.38	32.31
150	7.07	16.90	22.36	23.17	30.22	24.55	26.89
106	5.66	13.11	17.54	18.10	24.61	19.85	21.69
75	4.54	10.22	13.58	13.94	20.45	16.39	18.00
53	3.58	7.66	10.07	10.27	16.71	13.28	14.53
38	2.84	5.72	7.30	7.36	13.45	10.62	11.67
-38	2.28	4.25	5.08	5.06	11.34	8.69	9.62

C.1 No-load power

The net energy consumption during the grinding process is calculated by subtracting the no-load energy consumption from the gross energy consumption. The no-load energy consumption is determined by recording the energy consumed by both motors as a function of time without feeding ore to the HPGR.

Figure C.1 shows the no-load energy consumption in kWh as a function of time in hours for of the motor. A linear trend is observed as indicated in Figure C.1. The slope of the graph is the no-load power consumption which is equal to 1.14 kW.

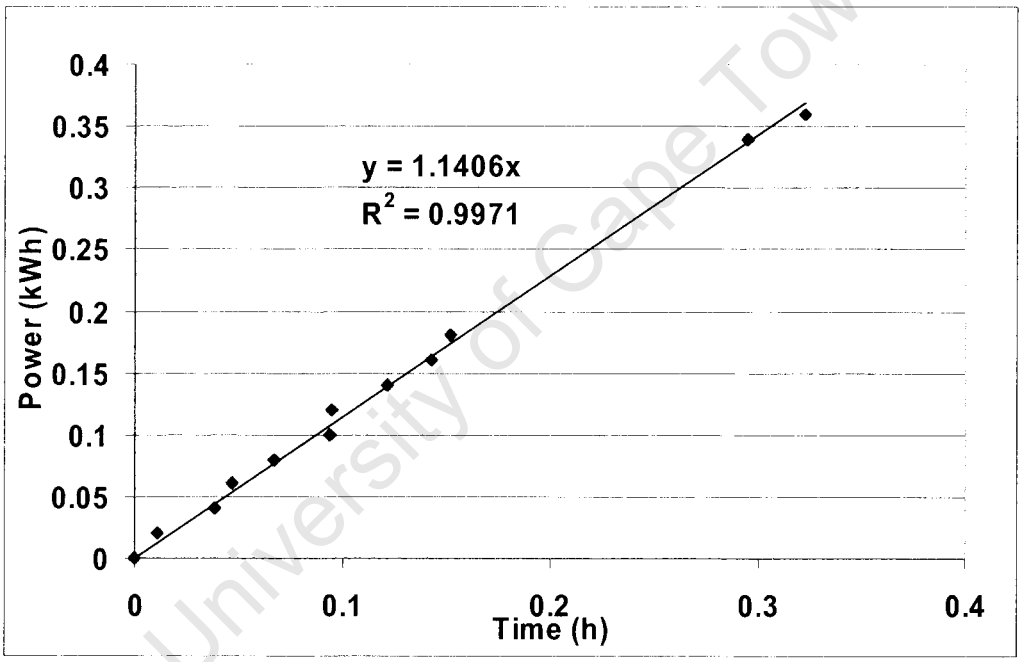

Figure C.1: No-load energy consumption as a function of time

C.2 Conversion from hydraulic pressure to specific press force

The specific press force is defined as the total hydraulic force exerted on the rolls divided by the projected area of the rolls. This form is useful for comparing pressures on different sizes of HPGR units (Klymowsky et al, 2006).

$F(sp) = F/(L * D)$

F(sp) = specific grinding force in N/mm2

F = force in N

L = roll width in mm

D = roll diameter in mm

Figure C.2 shows the relationship between hydraulic pressure in bar to specific press force in N/mm^2.

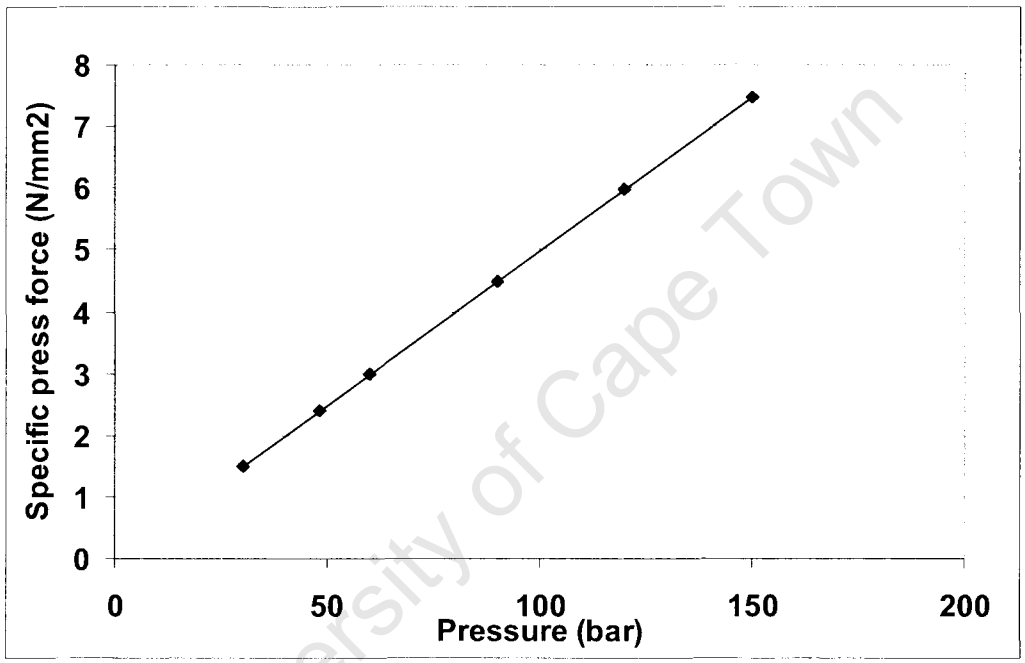

Figure C.2: Conversion from hydraulic pressure to specific press force

APPENDIX D MINERALOGY DATA

Table D.1: UG2 ICP 1 data for impact & abrasion and bed breakage

Bed breakage	Mg (%)	Al (%)	Si (%)	Ca (%)	Ti (%)	V (%)	Cr (%)	Mn (%)	Fe (%)	Co (%)	Ni (%)	Cu (%)	Zn (%)	Pb (%)
300 µm	8.21	6.76	11.80	2.33	0.39	0.16	14.75	0.18	14.40	0.14	0.10	<0.05	0.07	<0.05
212 µm	6.79	7.69	7.20	1.60	0.46	0.20	20.50	0.17	16.70	0.19	0.10	<0.05	0.09	<0.05
150 µm	6.68	7.84	7.52	1.74	0.45	0.19	20.20	0.17	16.40	0.14	0.10	<0.05	0.09	<0.05
106 µm	7.24	7.79	9.30	2.08	0.39	0.18	18.35	0.14	14.45	<0.05	0.07	<0.05	<0.05	<0.05
75 µm	7.45	7.92	12.0	2.93	0.34	0.16	14.6	0.13	12.4	<0.05	0.073	<0.05	<0.05	<0.05
53 µm	7.25	8.16	13.2	3.49	0.33	0.15	13.2	0.12	11.3	<0.05	0.078	<0.05	<0.05	<0.05
38 µm	7.11	8.24	13.2	3.62	0.34	0.14	12.8	0.12	11.2	<0.05	0.091	<0.05	<0.05	<0.05
Impact & Abrasion	Mg (%)	Al (%)	Si (%)	Ca (%)	Ti (%)	V (%)	Cr (%)	Mn (%)	Fe (%)	Co (%)	Ni (%)	Cu (%)	Zn (%)	Pb (%)
300 µm	6.78	7.59	9.75	2.36	0.41	0.17	17.00	0.16	14.50	0.23	0.09	<0.05	0.09	<0.05
212 µm	6.08	8.04	6.96	1.82	0.46	0.19	20.40	0.17	16.40	0.25	0.09	<0.05	0.09	<0.05
150 µm	6.18	8.15	7.03	1.88	0.46	0.20	21.00	0.17	16.60	0.15	0.09	<0.05	0.10	<0.05
106 µm	6.77	8.13	9.28	2.23	0.40	0.18	18.5	0.14	14.3	<0.05	0.085	<0.05	<0.05	<0.05
75 µm	7.10	8.00	10.8	2.67	0.38	0.15	16.3	0.13	13.2	<0.05	0.095	<0.05	<0.05	<0.05
53 µm	7.28	8.01	12.3	3.08	0.36	0.14	14.5	0.13	12.2	<0.05	0.10	<0.05	<0.05	<0.05
38 µm	7.17	7.97	12.25	3.15	0.38	0.13	14.35	0.14	12.25	<0.05	0.12	<0.05	<0.05	<0.05

Table D.2: Merensky Fire assay for PGM data for bed breakage at different pressures

PGM + Au g/t									
Size (µm)	30 PGM	48 PGM	60 PGM	90 r PGM	90 PGM	120 r PGM	120 PGM	150 r PGM	150 PGM
10000	100.0	100.0	100.0	100.0	100.0	100.0	100.0	100.0	100.0
1000	84.0	90.4	89.2	89.7	89.8	85.7	74.7	85.6	87.8
425	65.8	78.0	78.0	76.0	72.2	72.6	64.4	72.4	74.2
212	48.6	64.7	64.8	65.0	57.0	56.5	54.4	58.8	62.2
150	33.6	47.3	48.7	53.5	38.8	44.4	40.4	48.6	50.5
75	19.6	**35.0**	36.3	34.0	25.8	32.8	20.6	**35.8**	**38.3**
38	0.0	**20.2**	21.2	19.5	14.6	17.8	10.6	**20.8**	**22.0**
mass (g)									
Size (µm)	30(g)	48 (g)	60 (g)	90 r (g)	90 (g)	120 r (g)	120 (g)	150 r (g)	150 (g)
10000	100	100	100	100	100	100	100	100	100
1000	61.56	69.75	73.66	70.85	66.82	74.56	71.95	73.95	68.52
425	42.47	48.43	50.52	46.64	46.95	49.59	49.16	47.90	55.35
212	28.22	31.38	32.22	27.82	33.94	30.13	32.69	29.03	32.10
150	22.30	24.50	24.67	20.31	25.38	22.50	24.74	21.93	24.53
75	13.26	14.20	13.14	7.51	15.14	9.63	14.73	10.97	14.19
38	4.61	3.50	2.69	1.20	7.35	1.58	7.74	2.06	5.73

Table D.3: Merensky feed fire assay and size distribution data

Size (µm)	Feed 1 PGM	Feed 2 PGM	Feed 3 PGM	Feed 1 (m)	Feed 2 (m)	Feed 3 (m)
10000	100	100	100	100	100	100
9500	97.2	92.9	87.7	65.2	73.3	61.8
4750	89.5	82.8	80.0	33.5	45.8	30.3
2360	81.1	75.0	73.1	18.9	29.7	17.6
1180	74.5	68.4	66.3	11.4	19.8	11.5
425	65.0	59.3	56.5	6.3	11.5	7.0
212	52.3	50.5	46.2	4.3	7.8	5.0
150	41.8	41.0	37.8	3.5	6.3	4.2
75	29.6	30.3	28.9	2.4	4.4	2.9
38	14.5	15.3	14.3	1.7	2.8	2.1

Table D.4: PGM volume % and number of grains for the HPGR and AG mill product samples of UG2 ore

Liberation Class	PGM Volume %		No of Number of PGM grains	
	HPGR	AG Mill	HPGR	AG Mill
L	70.3	62.6	46	35
SL	16.0	31.3	29	50
AG	8.8	3.3	14	7
SAG	1.9	2.4	7	6
SG	-	0.3	0	1
G	3.0	0.1	4	1

Table D.5: PGM volume % and number of grains for the HPGR Lower and Higher Specific Press Force of Merensky ore in the size class – 38μm

Liberation Class	PGM Volume %		No of Number of PGM grains	
	Low Pressure (48 bar)	High Pressure (150 bar)	Low Pressure (48 bar)	High Pressure (150 bar)
L	46.7	49.3	43	36
SL	4.8	21.1	17	24
AG	47.1	21.2	24	25
SAG	0.1	1.9	1	4
SG	0.4	3.1	1	3
G	0.8	3.5	14	8

Table D.6: PGM volume % and number of grains for the HPGR Lower and Higher Specific Press Force of Merensky ore in the size class – 75+38μm

Liberation Class	PGM Volume %		No of Number of PGM grains	
	Low Pressure (48 bar)	High Pressure (150 bar)	Low Pressure (48 bar)	High Pressure (150 bar)
L	23.3	23.7	30	35
SL	29.0	22.1	18	8
AG	27.7	25.4	19	16
SAG	4.2	21.4	11	6
SG	0.3	0.9	1	3
G	15.5	6.5	21	32